REGULATION OF CORNEAL SCAR FORMATION BY TRANSFORMING GROWTH FACTOR BETA AND CONNECTIVE TISSUE GROWTH FACTOR: ROLES OF PROTEOLYTIC PROCESSING AND DEVELOPMENT OF A GENE SILENCING TECHNIQUE

By

PAULETTE MARIE ROBINSON

A DISSERTATION PRESENTED TO THE GRADUATE SCHOOL
OF THE UNIVERSITY OF FLORIDA IN PARTIAL FULFILLMENT
OF THE REQUIREMENTS FOR THE DEGREE OF
DOCTOR OF PHILOSOPHY

UNIVERSITY OF FLORIDA

2012

To my amazing husband Bently Robinson and adorable son, Orion John Robinson

ACKNOWLEDGMENTS

I would like to thank my loving husband, Bently Robinson, for all of his love and support throughout this journey. Also, I thank my son, Orion John, for being the light of my life. I look forward to watching you grow and develop. My parents, Paul and Jacqueline Kuznia, have supported me throughout all of the endeavors of my life and I am forever grateful. I thank my sister, brothers, and their significant others for their constant encouragement. I also would like to thanks my friends for keeping me sane by providing me hours of entertainment when I wasn't in the lab. I am extremely fortunate that they are there to always make me laugh.

I thank my mentors, Dr. Gregory Schultz and Dr. Alfred Lewin, for their guidance and allowing me to work in their laboratories. I have enjoyed working with both of you and learning life and laboratory lessons. My experience in their labs was very fulfilling and I am very appreciative. I also thank my other committee members, Dr. Clay Smith, Dr. Henry Baker, and Dr. William Hauswirth, for taking the time to meet with me to discuss my findings and help me troubleshoot any problems that had arisen. I thank all of my lab mates both past and present in both the Schultz and Lewin labs for the countless hours of camaraderie. You made coming into work in the lab enjoyable and your assistance with my experiments was priceless. I have had the opportunity to mentor several undergraduates, medical students and master's students. I have learned that by teaching someone, you learn more yourself. I thank all of them (Craig Levoy, Dilan Patel, Joshua Vickers, Sara Rodriguez, Meera Dave, Tyler Smith, and Sriniwas Sriram) for working with me. I truly enjoyed working with each of them and they were a key component to acquiring all of the data that is in this dissertation.

TABLE OF CONTENTS

page

LIST OF TABLES

LIST OF FIGURES

LIST OF ABBREVIATIONS

AAV	Adeno-associated virus
AEBSF	4-(2-Aminoethyl) benzenesulfonyl fluoride hydrochloride
ANOVA	analysis of variance
α-sma	alpha smooth muscle actin
bp	base pairs
CCN	cyr61, ctgf, nov proteins
CTGF	connective tissue growth factor
D	Diopter
DNA	Deoxyribonucleic acid
dsRNA	double stranded RNA
g	gram
GFP	green fluorescent protein
HCF	human corneal fibroblast
IGF	insulin-like growth factor
IgG	Immunoglobulin G
IL-1	Interluekin-1
kDa	kilodalton
L	Liter
LASEK	laser subepithelial keratomileusis
LASIK	laser in situ keratomileusis
ml	milliliters
MMP	matrix metalloproteinases
ng	nanogram
PRK	photorefractive keratectomy

rAAV	recombinant adeno-associated virus
RISC	RNA-induced silencing complex
RNA	Ribonucleic acid
RNAi	RNA interference
sAP	secreted alkaline phosphatase
scAAV	self complementary adeno-associated virus
siRNA	small interfering RNA
TGF-β	transforming growth factor- beta
TIMPs	tissue inhibitors of metalloproteinases
ug	microgram
ul	microliter

Abstract of Dissertation Presented to the Graduate School
of the University of Florida in Partial Fulfillment of the
Requirements for the Degree of Doctor of Philosophy

REGULATION OF CORNEAL SCAR FORMATION BY TRANSFORMING GROWTH FACTOR BETA AND CONNECTIVE TISSUE GROWTH FACTOR: ROLES OF PROTEOLYTIC PROCESSING AND DEVELOPMENT OF A GENE SILENCING TECHNIQUE

By

Paulette Marie Robinson

May 2012

Chair: Gregory Schultz
Co-Chair: Alfred Lewin
Major: Medical Sciences–Genetics

Previous research has demonstrated that corneal scarring following trauma, infection, or refractive surgery is the result of a complex cascade of multiple growth factors, cytokines, chemokines, and proteases that interact in multiple pathways to regulate key processes such as proliferation, migration, differentiation and synthesis of extracellular matrix by corneal cells. The transforming growth factor-beta (TGF-β) system has been shown to play a key role in the formation of scar tissue in the cornea and in other tissues in the body. Furthermore, connective tissue growth factor (CTGF) is a fibrogenic cytokine that is upregulated by TGF-β and serves as a downstream mediator of many of the fibrotic actions of TGF-β, including stimulation of synthesis of extracellular matrix and differentiation of fibroblasts into myofibroblasts. Previous studies suggest that CTGF is proteolytically processed by cultured skin fibroblasts and by some tissues into fragments that have different agonist and antagonist effects. To examine the role of proteolytic processing of CTGF in wound healing of the cornea, we

analyzed both *in vitro* and *in vivo* models. To simulate corneal wound healing *in vitro*, human corneal fibroblasts (HCF) were stimulated with TGF-β1, and the production of CTGF was analyzed. In the conditioned media, two expected forms of CTGF were detected, the full-length 38 kDa protein and a 21 kDa fragment of CTGF. An unexpected immunoreactive 50 kDa protein was also detected in the media. In the cell extract, four forms of CTGF were detected, the full-length 38 kDa protein, 21 kDa, 18 kDa, and 13 kDa fragments. The 21 kDa fragment was identified as CTGF using tandem mass spectrometry. Based on this finding, we analyzed homogenates of unwounded whole eyes from mouse, rat and rabbit and individual eye structures from the rabbit using Western blots and found that the C-terminal 21 kDa and 25 kDa fragments were the dominant forms of CTGF. We next analyzed the expression of CTGF over the complete time course of corneal wound healing in the rat, and found at 12 hours after ablation, all CTGF forms (38 kDa, 25 kDa, and 21 kDa) were at their lowest concentration. At 11 days post ablation when corneal scarring is actively increasing, all three forms of CTGF (38 kDa, 25 kDa, and 21 kDa) were in the highest abundance. For example, at day 11, the 21 kDa CTGF fragment was 32.5-times higher abundance than it was at 12 hours after injury. These data suggest that the CTGF plays important role(s) in regulating corneal wound healing and understanding the production and biological role of the 21 kDa fragment of CTGF will be an important component of the CTGF system during early phases of corneal wound healing.

Ribozymes and siRNAs can be used to selectively reduce the expression of target genes such as the profibrotic genes TGF-β1 and CTGF that cause corneal scarring and haze. Using a secreted alkaline phosphatase reporter assay, we identified two siRNAs

that selectively targeted rat TGF-β1 or CTGF mRNAs which each produced a relative knockdown of at least 50% of the sAP reporter protein. We also tested ribozymes targeting either TGF-β1 or CTGF mRNAs, and found that both ribozymes produced at least a 25% knockdown of the target mRNAs when compared to the vector control.

Since a long term goal of this research is develop a clinically useful therapy to reduce corneal scarring, we also tested the ability of these ribozymes to reduce target gene expression and corneal scarring in excimer laser-injured animal models. A key component of this therapeutic approach is to develop an effective method to deliver the ribozymes to corneal cells. The adeno-associated virus (AAV) vector has been successfully used to deliver genes and ribozymes to retinal cells of patients with selected forms of retinitis pigmentosa and to restore vision in those patients. However, recombinant single stranded AAV vectors usually take four to five days to express the transgenes. Therefore, we generated a self-complementary adeno-associated virus (scAAV) vector expressing the ribozyme and analyzed the efficiency and time course of transduction of rabbit corneal cells following excimer laser ablation. Using a scAAV vector expressing green fluorescent protein (scAAV-GFP), we found all cells types of the cornea (epithelial cells, stroma fibroblasts and endothelial cells) were transduced by the scAAV-GFP vector, with the greatest expression of GFP occurring at day 7. Finally, we applied the a scAAV vector expressing the CTGF ribozyme (scAAV-CTGF-Active-Rz) to the rat cornea after laser-ablation of the corneal epithelium, and we observed a 19% knockdown of CTGF protein on day 14. These findings support the concept that scAAV vector expressing ribozymes or other gene silencing molecules that target either TGF-β1 or CTGF could be used to therapeutically reduce corneal scar formation.

CHAPTER 1
INTRODUCTION

The Eye

More than 80% of the information we obtain from the external world is visually acquired[1]. There are multiple components required for a clear complete picture to be produced. The cornea and lens refract the light onto the retina, the receptor that converts the light into chemical and electric energy. This signal is then transmitted from the optic nerve to the brain and processed into a final visual image by the visual cortex. If any of these parts are damaged or fail to be in good working order, then the image will be distorted, and we will not be able to obtain the complete picture of all the information.

The Cornea

The cornea is a transparent, avascular tissue that functions as the gateway into the eye for external images. The cornea is an effective mechanical barrier that, in conjunction with tear films and the conjunctiva, protect against potential pathological agents. Corneal transparency and shape are critical for refraction. The cornea and tear film account for more than two-thirds of the total refractive power of the eye [2]. Any changes in the contour, smoothness, or total thickness of the cornea may result in a distorted image. The majority of corneal medical and surgical treatments are geared towards restoration of corneal transparency, but recently, the abundance of refractive corrective surgeries have increased [3].

The cornea consists of three cellular layers and two interfaces: epithelium, Bowman's layer, stroma, Descemet's membrane, and the endothelium (Figure1-1.). The epithelium is the outermost barrier layer that is composed of non-keratinized, stratified squamous epithelia cells. It is able to prevent entry of pathogens but permits

diffusion of oxygen and solutes. Bowman's layer is an acellular, basement membrane-like zone consisting of a random arrangement of collagen fibers and proteoglycans located at the interface of the epithelium and stroma in humans and some other mammals. The stroma, consisting of extracellular matrix, keratocytes (quiescent corneal fibroblast) and nerve fibers, accounts for more than 90% of the cornea. Only 2 to 3% of the total volume of the stroma is comprised of cellular components; the remaining portion consists of mostly extracellular matrix components collagen and glycosaminoglycans [4]. Descemet's membrane is a true basement membrane that is composed mostly of collagen IV and laminin [5, 6] and also contains fibronectin [7] to which the corneal endothelial cells are attached. The endothelium is made up of a single layer of mostly hexagonal endothelial cells that regulate the hydration of the cornea. The tight junctions of the corneal endothelium are known to be "leaky" because they permit diffusion of most nutrients into the stroma from the aqueous humor [8, 9]. Metabolic pump sites (Na^+, K^+-ATPase) are found on the basal-lateral membrane regions between adjacent endothelial cells which transport Na^+ ions from the stroma to the aqueous humor[10]. Thus, the capacity of a sheet of endothelial cells to pump ions is directly related to the size (density of cells) and shape (hexagonality) of the cells in an area[11]. This "leaky" tight junction/metabolic pump system allows for sufficient nutrient delivery into the stroma and epithelium. Damage and disruption of the corneal endothelial cell layer typically results in corneal edema, swelling and opacity[9]. The endothelial cells are metabolically active and secretory, but they do not normally proliferate in humans [1]. Thus, when damage occurs to the corneal endothelial layer, "healing" occurs by migration and enlargement of endothelial cells adjacent to the injury. However, as the

cells enlarge to cover the injured area, the amount of basal-lateral membrane area between adjacent cells decreases, which results in dramatically reduced density of pumps sites over an area of the cornea. When the density of endothelial cells decline, the endothelial cell's inability to remove ions using the active ion pumps results in corneal swelling [11]. This swelling distorts the highly ordered orthogonal arrangement of the collagen lamellae and interferes with light waves passing through the cornea and causes the cornea to become opaque.

Refractive Surgery Techniques

The three most common causes of a distorted visual image are myopia, hyperopia and astigmatism. Myopia, also known as nearsightedness, is caused by the cornea being too curved, the lens being too powerful or the eye is too long. Myopia causes the light to focus anterior (inside) to the surface of the retina. Hyperopia, also known as farsightedness, is caused by the cornea being too flat, the lens being too weak or the eye being too short. Hyperopia causes the light to focus posterior (outside) the eye, past the retina. Finally, astigmatism is caused by a cornea that is irregular in shape. The different curvatures of the cornea cause the light rays to have different focal points on different axes. For centuries, many people have used glasses and contact lens to reduce the level of ametropia, which is an inability for an image to focus on the retina.

Recently, excimer laser surgery has been developed to alleviate the need for glasses and contacts to correct the level of ametropia. A survey of the members of the American Society of Cataract and Refractive Surgery reported on the Society's web site that approximately 948,266 refractive surgery procedures were performed in the United States during 2004 and 928,737 in 2005. The three most common excimer laser

surgeries which modify the corneal curvature are photorefractive keratectomy (PRK), laser in situ keratomileusis(LASIK), and laser subepithelial keratomileusis (LASEK).

PRK is a surface ablation procedure that first employs the mechanical removal of the central epithelium followed by excimer ablation of the exposed Bowman's layer and a predetermined depth of the stromal matrix and keratocytes. The wound is allowed to re-epithelialize under the protective cover of a soft contact lens[12]. PRK has been associated with postoperative pain which has been postulated to be due to the loss of the epithelial layer [13]. Corneal haze is a frequent complication due to PRK, with approximately 3% of patients undergoing treatment for minimal to moderately high myopia experiencing corneal haze. Patients with high levels of myopia that require deeper ablation of the stromal layer are at increased risk of developing clinically significant levels of corneal haze, which was reported to approach 15% by Seiler *et al*.[14] In a long term study of 10 years, Alio *et al.*, recently found that 1.7% of patients who underwent PRK for myopia of less than 6 D had clinically significant corneal haze after 10 years, whereas 8.6% of eyes that underwent PRK for myopia of more than 6 D were found to have haze [15]. A diopter (D) is the reciprocal of the focal length measured in meters and is used to describe optical power of the cornea. The lack of a Bowman's layer also contributes to the activation of the epithelial cells and secretion of collagen, which contributes to the scattering of light that is visualized as haze.

LASIK is an intrastromal ablation procedure that uses a microkeratome to create a hinged corneal flap that is lifted and the underlying stromal cells are ablated. After the stromal matrix and cells are ablated, the flap is replaced. LASIK is technically more challenging, but has become more popular, because vision usually returns within one

day and there is minimal pain, because the nerve endings are less disrupted [16, 17, 18]. The creation of a flap allows for maintenance of a central zone of normal cornea between the epithelium and the stromal bed. At the flap margin where Bowman's layer is incised and disrupted, there is direct contact between epithelial cells and stromal matrix, which leads to synthesis and secretion of collagen by the activated epithelial cells. As a result, a circumferential thin ring of haze is noted in LASIK patients at the edge of the corneal flap [19]. Other flap-related complications include free caps, incomplete pass of the microkeratome, flap wrinkles, epithelial in-growth, flap melt, interface debris and diffuse lamellar keratitis[20, 21, 22]. When equal levels of correction are being performed, PRK stimulates a stronger fibrotic response compared to LASIK[23].

The newest approach to refractive surgery is LASEK, which is a modified PRK technique that uses dilute alcohol (usually 18-20%) to loosen the epithelial adhesion of the corneal stroma creating a flap, and then the stromal cells are ablated[22]. After the stromal cells are ablated, the corneal flap is replaced. LASEK is used when a patient has a low corneal thickness indicating that they are not a good candidate for LASIK. The use of ethanol eliminates the need for a microkeratome, which decreases the cost and eliminates the risk of surgical complications.

Whether the flap epithelial tissue is viable and able to reintegrate into the surface epithelium, or if it is simply a nonviable biological "bandage", is a source of substantial debate. In cell culture, Chen *et al*. found a dose- and time-dependent effect of alcohol on survival of epithelial cells with a concentration of 25% ethanol being the inflection point of epithelial survival. They found that the viability of human corneal epithelial cells dropped from 94.47% following a 20 second exposures to 20% ethanol, to only 33.86%

viability following a 20 second exposure to 25% ethanol [24]. *In vivo* experiments showed that the epithelial cells of rabbit corneas exposed to 20% ethanol for 30 seconds had morphologic changes in cytoplasm and surface damage such as alterations of microvilli structure and focal disruption of intercellular junctions that was restricted to the superficial corneal epithelium [25]. Determination of the effects of ethanol on human epithelial cells is difficult because the assessment of cell viability cannot be achieved merely by morphology. Therefore, the effect of 20% ethanol on corneal epithelium has not been fully resolved.

Several comparative studies between the different refractive techniques have been done. Alio [26] compared PRK and LASIK outcomes in a ten year study and found that PRK patients developed haze during the first three months that usually subsides, although, 2.9% of patients had minor haze even after 10 years. Patients who received LASIK never had worse than mild haze throughout the follow-up. A meta-analysis of PRK versus LASEK by Zhao [27], found that there were different degrees of corneal haze after LASEK and PRK but there was no significant difference in visual acuity after the procedures. The severity of corneal haze was similar when comparing PRK and LASEK.

Corneal Wound Healing

After corneal trauma, stromal wound healing is the result a complex cascade of multiple growth factors, cytokines, chemokines and proteases. Directly after epithelial damage, the process of healing is initiated by multiple cytokines and growth factors including, but not limited to, interleukin-1 (IL-1)[28], tumor necrosis factor alpha[29], bone morphogenic proteins 2 and 4[30], epidermal growth factor[31], platelet-derived growth

factor [32], and transforming growth factor- beta (TGF-β)[33]. These wound healing mediators are released by the epithelial cells and/or the lacrimal gland.

Keratocytes in normal, non-injured corneal stromal tissue are often described as being quiescent because synthesis of proteins, DNA and RNA is very low. Following injury, quiescent keratocytes rapidly transform and become “activated keratocytes” (also termed activated fibroblasts), which increase DNA, RNA and protein synthesis. For example, microarray analysis of rat corneas following PRK found that levels of 5,885 genes changed during the first 12 days of healing [11].

Activated keratocytes play major roles in repairing corneal tissue after injury. Keratocytes adjacent to the injury undergo programmed cell death, termed apoptosis, creating a hypocellular zone adjacent to the edge of the wound. The apoptosis of keratocytes peaks at four hours but may last up to one week or more after trauma[34, 35]. The two cytokine systems that induce corneal keratocyte apoptosis are the Fas receptor/Fas ligand system and the IL-1/ IL-1 receptor system[36]. After the initial wave of keratocyte apoptosis, an increased number of cells die from necrosis, which is characterized by the loss of plasma membrane integrity and random DNA degradation [36]. Beyond the zone of keratolysis, quiescent keratocytes become activated in response to growth factors and cytokines. Activated keratocytes are identified about 6 hours post injury by their increases of cell size and organelle content. Proliferation and migration of the activated keratocytes begins 12 to 24 hours after epithelial injury [37]. The proliferating keratocytes give rise to activated keratocytes, fibroblasts, and myofibroblasts that repopulate the depleted stroma [38, 39, 40, 41, 42].

At 8 to 24 hours after injury, chemokines stimulate the attraction of inflammatory cells, such as macrophages/monocytes, T cells and polymorphonuclear cells[35, 43] . These cells begin removing remnants of damaged cells and extracellular matrix by phagocytosis and secretion of protease. Degradation and removal of damaged tissue is orchestrated by the plasminogen-activator/plasmin system, matrix metalloproteinases (MMPs), and other enzymes [44, 45].

One to two weeks after injury, myofibroblasts appear in the anterior stroma [36]. Keratocytes transform into myofibroblasts under the influence of TGF-β[46]. Myofibroblasts are characterized by their high concentration of alpha smooth muscle actin (α-SMA) and by elevated expression of cadherins and TGF-β receptors[47]. Myofibroblasts secrete many growth factors, including TGF-β. Tissue repair remodeling of collagen stromal fibrils into a more normal, orderly arrangement are mediated by MMPs[48]. Return of normal structure and function may take months, or even years, in some eyes depending on the individual's wound healing response.

Corneal Scarring

Corneal scarring, which is described clinically as corneal haze, is a major cause of impaired vision. It was previously thought that corneal haze was caused by the irregular arrangement of large collagen fibers in the stromal layer, which is different than the normal precise, repeating orthogonal orientation of collagen fibers that allows light rays to pass through the ECM without being scattered. Recently, the use of *in vivo* confocal microscopy revealed that the major reflective (light scattering) structures were actually activated fibroblasts and myofibroblast in the wound area [49, 50, 51, 52, 53]. Furthermore, the highly reflective property of the activated fibroblasts was shown to be due to the loss of

corneal crystallin proteins[50] that are present in high levels in the cytoplasm of quiescent, transparent keratocytes.

Roles of TGF- β

TGF-β is a 25kDa, disulfide linked, homodimeric protein that is secreted from almost all nucleated cells. In mammals, TGF-β is present in three isoforms, TGF-β1, TGF-β2, and TGF-β3. TGF-β is a pleiotropic cytokine that regulates apoptosis, angiogenesis, wound healing, the immune response and tumor growth. TGF-β induces a wide variety of biochemical and biological responses depending on the target tissue. Normally, TGF-β is produced in the latent form consisting of TGF-β and a non-covalently bound latency-associated peptide (LAP) that must be released for activation [54]. Several activators have been identified to activate latent TGF-β, such as, proteases, thrombospondin-1, integrin $\alpha_v\beta_6$, and acidification. One of multiple ways that plasmin, MMP-2 and MMP-9 has been identified as an activator of TGF-β is by cleavage of the protease sensitive hinge region of the latent TGF-β binding protein(LTBP), liberating the large latent complex (LLC) from the ECM that then allows another protease to disrupt the TGF-β –LAP complex[55]. Thrombospondin-1 activates TGF-β by direct cleavage of the LAP-TGF-β complex[56]. Conditioned medium that contains latent TGF-β can be activated by mild acid treatment (pH4.5) that is thought to denature LAP that results in disruption of the LAP-TGF-β complex[57].

TGF-β is an important regulator of the immune response, having an inhibitory effect on many types of cells including Th1 cells, Th2 cells, cytotoxic T-lymphocytes, macrophages, natural killer cells, B cells and polymorphonuclear leukocytes [58]. Conversely, TGF-β has potent chemoattractive properties that lead to rapid

accumulation of macrophages, granuloctyes and other cells at the site of inflammation [59, 60.] TGF-β1 knockout mice died within 3-4 weeks of birth of multiple organ inflammatory syndrome involving the heart, skeletal muscle, lungs, liver, stomach, pancreas, brain, eyes, salivary glands and other tissues[61, 62]. Studies of knockout mice clearly establishe TGF-β1 as an integral cytokine involved in the anti-inflammatory pathway.

As with the immune response, TGF-β is bifunctional in cancer with the ability to suppress or promote tumor formation [63, 64, 65]. The tumor suppressive activity comes from TGF-β's ability to inhibit growth of epithelial and lymphoid cells from which most cancers arise[64]. TGF-β has also is needed for maintenance of genomic stability, and suppression of telomerase [66, 67]. As a tumor progresses, TGF-β promotes tumorigenesis by inducing epithelial-to-mesenchymal transition using Smad-dependent and –independent pathways [68, 69]. In carcinoma cells, invasiveness and metastasis in late-stage tumorigenesis appears to require TGF-β signaling[70]. TGF-β stimulates the production of VEGF, which promotes the formation of vasculature to the tumor [71].

During wound healing, TGF-β is a chemoattractant for monocytes, macrophages, and fibroblasts and contributes to the inflammatory phase of wound healing [59, 72]. In fibrotic tissues, TGF-β has been shown to increase fibroblast proliferation [73, 74, 75, 76, 77,] amplify production of extracellular matrix components including fibronectin, type I collagen, integrins, laminin, and glycosaminoglycans [78, 79, 80, 81, 82] and inhibit protease activity, resulting in decreased extracellular matrix degradation[83, 84, 85]. TGF-β decreased synthesis of MMPs and increased synthesis of tissue inhibitors of metalloproteinases (TIMPs) by fibroblasts. Rapid induction of both TGF-β1, and TGF-β2

was observed, but an increase in TGF-β3 was seen at later stages of repair[86]. The TGF-β system is an extremely powerful scar-promoting system in the eye.

Increased levels of TGF-β in tears[87] was found in patients following PRK, and TGF-β proteins were immunolocalized in corneal and lacrimal gland cells[88]. Ninety days following PRK ablation, levels of mRNA precursors for all three isoforms of TGF- β and TGF-β receptors increased and remained elevated in scars in rat corneas[89]. The addition of TGF-β1 to bovine corneas after LASIK flap creation was able to increase the adhesion of the stromal flap but caused the cornea to become opaque[90]. In human corneal fibroblast (HCF), concentrations of 0.1ng/ml or higher significantly reduced cell migration and increased myofibroblast differentiation [91]. Jester *et al.* [92] found that the topical application of a neutralizing antibody to TGF- β1 reduced levels of corneal haze in rabbits following lamellar keratectomy. Thus, TGF-β is a prime target for regulation of ocular scar formation.

Roles of CTGF

Connective tissue growth factor (CTGF) is a 38kDa, single chain, cysteine rich protein that is secreted through the Golgi apparatus[93]. As shown in Figure 1-2, the overall structure of CTGF can be grouped into three major segments: the N-terminal domain, the hinge region, and the C-terminal domain. Furthermore, the structures of the N-terminal and C-terminal domains can be separated into four modules that have conserved amino acid sequences that are similar to other protein in the CCN super-family. The N-terminal domain contains an insulin-like growth factor (IGFBP) binding module that is predicted to bind IGF, a von Willebrand factor type C repeat, which has been implicated as a binding site for TGF-β family members modulating their activity[94]. The C-terminal domain contains a thrombospondin type 1 module that is likely involved

in binding to sulfated glycoconjugates[95] and the CT module, which is similar to that found in TGF-β, platelet-derived growth factor, and nerve growth factor and allows dimerization of these proteins [96,98.] Although hCTGF is glycosylated, the function of this modification has yet to be determined [93]. These glycosylation sites are absent from all other orthologs, which suggests that the conserved function among species are independent of carbohydrate modifications of the protein.

The hCTGF gene map spans approximately 3 kb and is organized into five exons and four introns [100, 101]. The 5' untranslated region consists of many regulatory elements, including a unique TGF-β response element [100, 101]. Previous studies demonstrated the CTGF mRNA expression and protein levels were increased after treatment with TGF-β[102, 103, 104].

CTGF has been implicated in numerous biological activities, including stimulation of cell migration, proliferation, extracellular matrix synthesis, adhesion, survival, differentiation, and apoptosis [105, 106, 107, 108]. CTGF was originally identified as a mitogen for fibroblasts that was present in conditioned media derived from cultures from human umbilical vein endothelial cells [109, 110, 111]. Recent data also showed that CTGF is a key chemokine in development. The mRNA expression pattern of CTGF suggests that CTGF continually functions in the cardiovascular system, bone- and cartilage-associated mesenchyme and maturing layer VII neurons, but CTGF also produces a more transient function associated with the formation of cartilage, bone, tooth and cerebral nerve cells[112, 113, 114, 115, 116, 117]. CTGF knockout animals have interesting pathologies, including a failure of the rib cage to ossify which was due to a failure of the embryo to produce a specific bone-inducing matrix and a failure of the chondrocytes to

proliferate [118]. Thus, during chondrogenesis, CTGF is important for cell proliferation and matrix remodeling.

The initial evidence for important actions of CTGF in wound healing was shown in a study of cutaneous wound repair by Igarashi *et al.* [119]. They found CTGF mRNA was expressed in wounded skin but was absent in unwounded skin. Since that discovery, CTGF has been shown to dramatically increase synthesis of collagen, integrin, and fibronectin, when added to cultures of human skin fibroblasts, and to be highly elevated in biopsies and samples of numerous fibrotic human tissues, including lung, kidney and skin. In mice, subcutaneous injection of CTGF stimulates fibrosis and granulation [111]. In addition, expression of CTGF increased significantly during corneal wound healing, and CTGF mediated the effect of TGF-β induction of collagen synthesis by corneal fibroblasts [104] .

Proteolytic processing of CTGF was first reported from Brigstock *et al.* [120] in pig uterine flushings. Since this discovery, 10-, 12-, 16-, 18-, 19-, 20-,24 and 31-kDa fragments have been identified in different cell types, tissues and body fluids [121, 122, 123, 124, 125, 115, 126]. A 31-kDa fragment was found when HCF were grown on collagen coated plates and stimulated with TGF-β1[126]. *In vivo*, the proteases that cleave CTGF and their cleavage sites are currently unknown. *In vitro* testing has shown that MMP-1, 3, 7, and 13 are able to cleave CTGF into smaller fragments, but none of these have been shown to cleave CTGF *in vivo.* [127]. Most recently, a family of serine proteases, the Kallikrein-related peptidases, have been shown to be able to proteolytically process the CCN protein family members. Specifically, KLK12 and KLK14 were able to process CTGF into lower molecular weight forms[128].

Grotendorst and Duncan [129] found that the two individual domains of CTGF stimulate opposing biological functions, proliferation and differentiation. They used a baculovirus system to express either an N-terminal (20 kDa) or a C-terminal (18kDa) proteins, which were then added to fibroblast cultures. They found that the C-terminal fragment increased DNA synthesis, whereas the N-terminal fragment had no effect on DNA synthesis. In contrast, N-terminal fragment increased differentiation of fibroblasts to myofibroblasts, but the C-terminal had no effect on myofibroblast induction [129]. Thus, the N-terminal and C-terminal fragments had distinct and mutually opposing effects on cells, either stimulating proliferation (C-terminal) or stimulating differentiation (N-terminal). In the first clinical study to determine that the CTGF fragments induce different biological functions, Dziadzio *et al.* [130] found that the N-terminal fragment of CTGF serves as a fibrotic marker for patients that have scleroderma. Understanding what regulates the proteolytic processing of 38 kDa CTGF are important unanswered questions of the CTGF biological system

Proteolytic processing of protein precursors to generate multiple proteins with different biological activities has been shown for several neuropeptides. For example, proopiomelanocortin precursor (POMC) can be proteolytically processed into three different endocrine hormones. Cleavage of POMC precursor in the anterior pituitary generates adrenal corticotrophin hormone (ACTH), which is the major hormone involved in regulation of steroid production. In the intermediate lobe of the pituitary, POMC is proteolytically cleaved into α-melanocyte-stimulating hormones (α–MSH), which regulates skin pigmentation and appetite, and β-endorphin, which is involved in regulation of pain relief[112]. Thus, proteolytic processing of proteins into multiple domains

that have dramatically different biological effects (often mutually exclusive) is a well-established biological phenomenon that adds another level of regulating cell response.

Reduction of Corneal Scar Formation

Scarring of the corneal may be due to many factors such as trauma, infection, and surgical procedures. Currently, no drugs are approved by the FDA with the clinical claim (or intended use) to reduce corneal scarring. After photorefractive keratectomy, the anti-inflammatory corticosteroid, dexamethasone, is often prescribed with the intent to reduce the formation of corneal haze. However, in a randomized, double-blind clinical study, topical use of dexamethasone was found to have no significant reduction of corneal haze after three months of treatment [131]. Mitomycin-C is a nonspecific anticancer drug that is often used interoperatively to reduce corneal haze. The rationale for using mitomycin-C relies on its potent cytostatic effects that arise from blocking DNA and RNA replication and protein synthesis. Although this treatment has been shown to reduce corneal fibrosis after glaucoma surgery, pterygia excision, treatment of conjunctival and corneal intraepithelial neoplasia, it also may have some very damaging side effects. These side effects may include epithelial defects, stromal melting, and endothelial damage [132, 133]. Late side effect of mitomycin-C have been reported, with some occurring as late as five years after treatment [134]. Netto *et al*. [135] reported that treatment of rabbit corneas following PRK with mitomycin-C caused a 20% decrease in cellularity of the anterior stroma at one month after PRK, which continued for the 6 months duration of the study. In a 6 month study of patients receiving PRK**,** Nassiri *et al*. found the postoperative prophylactic use of diluted intraoperative mitomycin-C 0.02% solution caused substantial (9% decrease) corneal endothelial cell loss and the rate of cell loss was correlated with the duration of mitomycin-C exposure [136]. As previously

mentioned, the endothelial cells migrate and enlarge to compensate for cell death, and the loss of cells decreases the ability of the endothelial cells to maintain homeostasis in the stroma due to a loss of ion pumps. Stromal swelling and opacity are some of the side effects of a loss of homeostasis between the stroma and endothelium. Further long term studies are necessary to determine the effects of mitomycin C on corneal wound healing. In summary, there is a major unmet clinical need for a drug treatment that can safely and consistently reduce the risk of vision-degrading corneal scarring after refractive surgery or after other types of corneal injuries.

Gene Therapy

The lack of an effective anti-scarring drug that does not also have potentially serious side effects justifies the development of drugs that specifically target either or both TGF-β or CTGF at the molecular level. The utility of using a nucleic acid to modulate gene expression was first demonstrated by Paterson *et al*. approximately 30 years ago [137]. Multiple strategies have arisen to attenuate gene expression by interfering with cytosolic mRNA or translated protein.

RNA interference (RNAi) uses nucleic acids to modulate gene expression. RNAi, a double-stranded mRNA able to degrade a target mRNA, was first described in *Caenorhadbitis elegans* in 1998 by Andrew [138] and Craig Mello. The RNAi pathway begins with exogenous double stranded RNA (dsRNA) being processed by the RNAse III family member Dicer into small interfering RNA (siRNA) molecules that are 20-25 nucleotides long [139]. The resulting siRNA is incorporated into the multi-protein complex called RNA-induced silencing complex (RISC). The incorporation of the siRNA into the RISC complex causes the sense strand of the double-stranded siRNA to be cleaved [140]. Once the sense strand is cleaved, the siRNA recognizes mRNAs with sequence

complementarity [141]. The target mRNA is then cleaved by a protein, Argonaute 2, within the RISC complex (Figure 1-3A). This allows for silencing of the gene with sequence homology to the siRNA.

Although siRNA is a relatively recent discovery, numerous *in vitro* and *in vivo* studies have been performed to assess the potential viability of RNAi as treatment. Several RNAi therapies have been tested in clinical trials. Currently in Phase II clinical trials, ALN-RSV01 developed by Alnylam Pharmaceuticals Inc., uses an siRNA that targets the nucleocapsid encoding gene of the respiratory syncytial virus and therefore inhibits viral replication in the lungs. Another siRNA based treatment, Bevasiramb which was developed by Acuity Pharmaceuticals, targeted VEGF in treatment of age-related macular degeneration[142]. Bevasiramb reached Phase III clinical trial but the trials were discontinued in 2009 because the results were unlikely to meet their end point goal. Ribozymes are another method to selectively target genes to therapeutically reduce the gene expression.

Hammerhead ribozymes are small self-cleaving RNAs fewer than 40 nucleotides long and consists of two substrate-binding arms and a conserved catalytic core which cleaves the site-specific target mRNA [143, 144, 145]. Ribozymes hybridize to a complementary target sequence, cleave a site-specific substrate and release the cleavage product (Figure 1-3B). A hammerhead ribozyme cleaves best after a NUX triplet where N can be any ribonucleotide, and X can be any ribonucleotide except guanosine (typically GUC, CUC or UUC)[146]. It has been shown hammerhead ribozymes use Mg^{2+} in a direct role during catalysis of the target mRNA [147]. The chemical cleavage step is rapid. However, the rate limiting step is the release step,

which can be accelerated if the hybridization arms of the ribozyme are relatively short (five to six nucleotides)[146].

Clinically, ribozymes have been explored in multiple small trials. Heptazyme™ targeted the highly conserved 5'-untranslated region of hepatitis C virus and was found to inhibit viral replication up to 90% in cell culture [148]. Phase I and II clinical trials of Heptazyme™ showed promise, but unfortunately, toxicological concerns were raised and the study was suspended [149]. Several clinical trials utilizing ribozymes against HIV, specifically targeting the CD4+ T cells or CD34+ hematopoietic cells, have been completed or are underway [150,151-154]. These trials have established the safety and feasibility of ribozyme based therapy, but, unfortunately, they have not been able to show an advantage for the protected cells. These clinical trials suggest that ribozymes are an effective way to specifically reduce target gene expression *in vitro* and *in vivo*.

Ribozymes are excellent candidates for a gene therapy technique that targets TGF-β or CTGF because they exhibit site specific cleavage of target RNA. They also are catalytic, allowing ribozymes to rapidly cleave multiple copies of the target RNA, thereby requiring lower concentrations. Ribozymes are able to target both nuclear and cytoplasmic RNAs and also can discriminate against single base polymorphisms [155]. A major obstacle to overcome when using ribozymes is that naked RNA has a half-life of seconds in bodily fluids following injections or topical applications. Therefore, application of naked RNA ribozymes is not practical *in vivo*. There are several techniques that may be used to overcome this obstacle. Modifying the nucleotides, specifically by blocking the 3' end of the molecule and the 2' positions of pyrimidines, stabilizes the ribozyme, increasing the half-life from minutes to hours yet does not

severely compromise the catalytic activity[156]. Another way to circumvent the short half-life of a ribozyme is to transduce cells with the gene encoding a ribozyme using a viral vector, which will continuously generate new ribozyme molecules in the cell. This is an approach we have taken as described in more detail in the Methods and Results sections.

The use of siRNA holds great promise as a therapeutic treatment to target both TGF-β and CTGF because siRNAs tend to be effective at low concentrations[155] and can specifically target those genes. A major concern about the use of both siRNA and ribozymes is the possibility of off target, non-sequence-specific effects. Recent data suggest that the majority of experimentally verified off target effects are due to the matching of an off-target mRNA to the 6-7 nucleotides in the so-called "seed" region of the siRNA [157, 158]. In contrast, ribozymes are much more sensitive to polymorphisms at the cleavage site (though relatively less so in the hybridizing arms, depending upon position) and have been used for discriminating between single nucleotide polymorphisms [159]. Two other major concerns facing the use of siRNAs or ribozymes *in vivo* are tissue specificity and the ability to withstand degradation by nucleases. The use of viral vectors expressing the siRNA or ribozyme can overcome these issues. Rapid expression of one or both of these types silencing RNA is a key component of our strategy to reduce the formation of corneal fibrosis. The process of wound healing begins as soon as the injury occurs. Therefore, it is paramount to have the knockdown of TGF-β and CTGF as quickly as possible.

Adeno-associated Viral Vectors

Adeno-associated virus (AAV) is a a non-pathogenic, non-enveloped, single stranded, parvovirus. The DNA genome of AAV is 4.7 kb and contains two main open-reading frames, *rep* and *cap* that are sandwiched between 145 base long inverted terminal repeats located at the 5' and 3' ends [160]. The *rep* gene encodes for four different proteins, two of which, rep68 and rep78 are required for viral DNA replication and transcriptional regulation [161]. Wild-type AAV is able to integrate into the host genome on chromosome 19; this is mediated by both rep40 and rep52 proteins [161]. The *cap* gene encodes for three viral capsid proteins, VP1, VP2, and VP3. Recently, the *cap* gene was discovered to encode a short reading frame designated AAP that is required for the assembly of capsids [162]. Wild-type AAV replication depends on the presence of co-infection with either adenovirus or herpes simplex virus. The mechanism by which AAV2 enters the cells is by binding to cell surface heparin sulfate proteoglycans (HSPGs) as its primary receptor and uses integrin, $\alpha_v\beta_5$, or basic fibroblast growth factor as co-receptors for internalization and endocytosis[163, 164, 165]. AAV2 has the capacity to infect a broad range of cells, because most cells express HSPGs. Other serotypes of AAV lack HSPG binding sites on their capsids and bind to other cell surface receptors. The virus particles are released from the endosome at a low pH [166, 167]. The released single-stranded DNA is converted to a double-stranded template by host machinery.

Recombinant AAV (rAAV) is made by replacing the *rep* and *cap* genes with the gene of interest. In order to avoid contamination with wild-type adenovirus, a helper-virus-free method is used to produce rAAV. This method entails cloning E4 and E2A genes from adenovirus into an adeno-virus helper plasmid. This plasmid along with an

AAV helper plasmid containing the *rep* and *cap* genes and a viral vector containing the gene of interest surrounded by the AAV terminal repeat elements are all transfected into HEK293 cells. The cell line provides the E1 protein which is another adenoviral protein essential for AAV replication [168, 169].

AAV is capable of infecting both dividing and non-dividing cells and can produce long-term gene expression. Mohan *et al.* [170] showed selective *in vivo* gene delivery into rabbit keratocytes using rAAV with a lamellar flap technique. They compared the expression of two different genes, β-galatosidase and chloramphenicol acetyltransferase , using two different delivery techniques, plasmid transfection and AAV. They concluded from this study that rAAV is capable of delivering foreign genes into the cornea *in vivo* and the potency and duration of the transgene expression was greater using the AAV vector compared to a transfected plasmid. Finally, they found that rAAV was safe in the cornea, as no toxicity was noted. Liu *et al*. found that rAAV1 transduce all cell types of the cornea and produced the most robust expression of GFP compared to AAV 2, 5, 7, and 8 [171].

Self-complementary AAV (scAAV) uses the same viral capsid and proteins but during replication scAAV generates a double stranded DNA template by intramolecular base pairing as the result of a deletion to terminal resolutions sites from one terminal repeat (TR). Palindromic TRs serve as primers for host cell-mediated synthesis of a dsDNA template that induces gene expression from the single-stranded genome of the rAAV. scAAV have been shown to have a faster onset of gene expression because the scAAV DNA is transcribed rapidly[172, 173]. In the retina, scAAV expressing GFP had quicker expression (2 days) when compared to the rAAV (5 days)[173]. In addition,

scAAV generally have higher transduction efficiency than conventional rAAV vectors[174]. For all these reasons we chose to construct scAAV expressing ribozymes targeting TGFβ1 and CTGF and assess the effectiveness in reducing target gene expression in cell cultures and in animal models of corneal scarring.

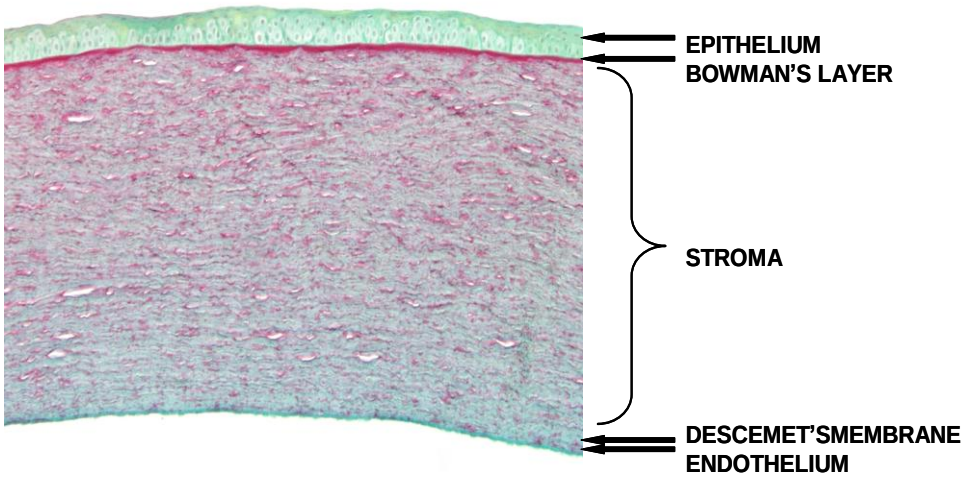

Figure 1-1. The Three Cellular Layers and Two Interfaces of the Cornea. The epithelium is the outermost corneal layer (green) which allows for diffusion of oxygen and solutes but inhibits pathogens. Bowman's layer is an acellular, basement membrane-like zone in between the epithelium and stroma. The stroma is the middle cornea cellular layer (purple) that contains mainly extracellular matrix components with minimal cells. Descemet's membrane is a true basement membrane between the stroma and endothelium The endothelium is the inner most corneal layer (blue) that contains a single layer of cells that regulate corneal hydration. (unpublished Blalock)

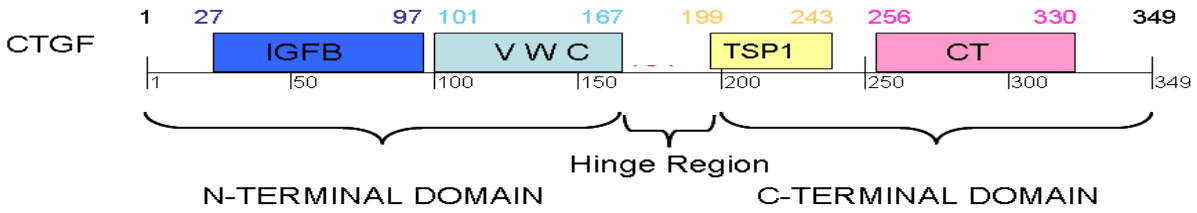

Figure. 1-2. Demonstrates the Different CTGF Protein Modules and Domains of CTGF. IGFB-insulin-like growth factor binding protein-like module; VWC-von Willebrand factor type-C repeat module; TSP1-thrombospondin type 1 repeat module, and C-terminal cystine knot module.

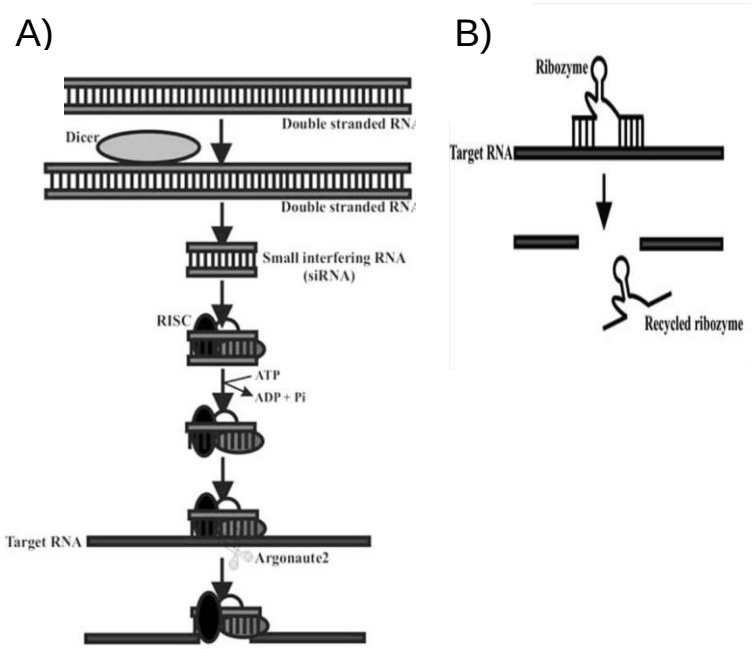

Figure 1-3. Schematic Diagram Illustrating the Degradation of Target RNA by a Ribozyme and siRNA[175]. (A) Model for degradation by the RNAi pathway. Double-stranded RNA is cleaved by the endoribonuclease Dicer into siRNA, which is then recognized and unwound by RNA-induced silencing complex (RISC). The complementary strand of siRNA is delivered to its target RNA by RISC. The hybridized region of target RNA is then endonucleolytically cleaved by Argonaute 2[175]. (B) Model for direct degradation of target RNA by a ribozyme [175]

CHAPTER 2
MATERIALS AND METHODS

Antibody Sensitivity and Detection

Sources of Growth Factors and Antibodies

Recombinant human (rh)CTGF was prepared by the Grotendorst laboratory using a baculovirus expression system [111]. Antibodies were either purchased from US Biological (Swampscott, MA) and Santa Cruz Biotechnology (Santa Cruz, CA) or produced from the University of Florida ICBR Monoclonal Core (Table 2-1). Donkey-anti rabbit, donkey-anti goat and donkey-anti mouse secondary antibodies labeled with an infrared dye were purchased from Li-cor Biosciences(Lincoln, NE). Strepavidin labeled with an infrared dye was also purchased from Li-cor Biosciences.

SDS-PAGE and Western Blots

Sensitivity of the different antibody detection during western blot was measured by making serial dilutions of the rhCTGF from 150 ng/well to 0 ng/well. The sample volume of the rhCTGF was 6.5ul. NuPAGE LDS sample buffer (Invitrogen, Carlsbad, CA) and NuPAGE reducing agent were added to the sample, 2.5ul and 1ul respectively. LDS can be prepared by combining the following: 4.3 M Glycerol, 0.6 M Tris Base, 0.4 M Tris HCl, 0.3 M LDS, 2 mM EDTA, 0.075% of Serva Blue G250, 0.025% of Phenol Red in ultrapure water. Samples were then boiled for 3 minutes. Samples were applied directly to 12% NuPAGE bis-Tris gels (Invitrogen, Carlsbad, CA). To detect CTGF, gels were blotted onto polyvinylidene difluoride (PVDF) membranes using iBlot transfer system (Invitrogen) following the manufacturer's guidelines. Blots were incubated overnight at room temperature while shaking in Odyssey Blocking Buffer (Li-cor Biosciences). Blots were incubated with primary antibody for 2 hours while shaking at

room temperature. Antibodies were used at concentrations of 1.0ug IgG/ml for the US-Biological and Santa Cruz polyclonal antibodies and 5.0ug IgG/ml for Hinge Region, C-terminal and N-terminal monoclonal antibodies in Odyssey Blocking Buffer containing 0.1% Tween 20 (Fisher Scientific, Pittsburg, PA). Blots were then washed 4 times with 0.1% Tween 20 in phosphate buffered saline (PBS) for 5 minutes at room temperature while shaking. PBS can be made by combining the following: 0.2 M NaCl, 3 mM KCl, 12.6 mM Na_2HPO_4, 2 mM KH_2PO_4 in 800ml ultrapure water and adjusted to a pH 7.4. Blots were incubated for 2 hours in infrared labeled secondary antibody from Li-cor Biosciences diluted 1:10000 in Odyssey Blocking Buffer with 0.2% Tween 20 and 0.01% SDS. Blots were then washed 4 times with 0.1% Tween 20 in PBS for 5 minutes at room temperature while shaking. Band detection was performed using the Odyssey Infrared Imaging System (Li-cor Biosciences). C-terminal monoclonal and hinge region monoclonals antibodies were tested for specificity by using CTGF knockout and heterozygous CTGF mice embryo homogenates obtained from Dr. Leask . CTGF Time Course from Human Corneal Fibroblasts Stimulated with TGF-β1

Human Corneal Fibroblast Cell Culture

Cultures of human corneal fibroblasts (HCF) were established by outgrowth from corneal explants, as described previously [176]. Briefly, epithelial and endothelial cells were removed from corneas, the stroma was cut into cubes of approximately 1 mm^3, placed in culture medium consisting of equal parts Dulbecco's Modified Eagle Medium (DMEM), with 4.5g/L Glucose and 1g/L L-glutamine (Gibco BRL, Grand Island, NY) Medium was supplemented with 10% heat-inactivated normal calf serum and 1×

antibiotic-antimycotic (Gibco BRL). Cells from cultures between passages 2 and 5 were used for all experiments.

TGF-β1 Stimulation of CTGF

To stimulate the expression CTGF, HCF were place in serum-free medium for 48 hours. After 48 hours, the medium was replaced by 5ng/ml of TGF-β1 (Sigma, St. Louis, MO) in DMEM. At various time points (0, 1, 6, 12, 18, 24, 48 and 72 hrs) protein samples were collected from the medium, and a protease inhibitor cocktail (cocktail III from Calbiochem, Darmstadt, Germany) and 0.5mM EDTA were added to the medium. Cell lysates were collected with the addition of PBS supplemented with 0.1% TritonX-100 and the previously mentioned protease inhibitors cocktail. Samples were concentrated down using Centriprep Centrifugal Filter Unit with Ultracel-10 membrane (Millipore, Billerica, MA). Concentrated media and extracts were stored at -20^{o}C until further analysis. Three biological replicates were performed per time point.

SDS-PAGE and Western Blots

Polyacrylamide gel electrophoresis in the presence of sodium dodecyl sulfate (SDS-PAGE) was performed as described above. Detection for CTGF was performed as described above with the US Biological polyclonal antibody. The intensity of each band was determined using the area under the curve function in the ImageJ software (U.S. National Institute of Health). A recombinant CTGF standard (concentration of 300 ng) was run on each gel, and the band intensity produced by that rCTGF was used to normalize the different western blots. The relative band intensities were compared for statistical significance using Analysis of Variance (ANOVA) followed by Tukey's Post-

hoc using GraphPad Prism (GraphPad, La Jolla, CA). A p value of <0.05 was considered significant.

Immunoprecipitation and Identification of 21kDa CTGF Band

Immunoprecipitation of CTGF was conducted using Direct Immunoprecipitation Kit (Thermo Scientific, Rockford, IL). Briefly, the US Biological polyclonal antibody was coupled to AminoLink Plus Coupling Resin following manufacturer's instructions. Five aliquots of same sample were applied over the column to purify the CTGF from the cell culture extract. The five elutions were combined and then were concentrated using DNA 110 Speed Vac (Thermo Scientific). The concentrated immunoprecipited CTGF samples were rehydrated in 35ul of dH_2O. The sample was run on SDS-PAGE as previously described. Silver staining was performed using SilverQuest Silver Stain (Invitrogen) following the manufacturer's instructions. SilverQuest Silver Stain was specifically chosen because it was compatible with mass spectroscopy. The 38 and 21 kDa bands were cut out of the gel and then they were destained following manufacturer's instructions. Samples were sent to ProtTech. Inc (Norristown, PA) to perform tandem mass spectroscopy (NanoLC-MS/MS).

Identification of the Protease Class that Cleaves CTGF from HCF Extracts

To stimulate the expression CTGF and proteolysis, HCF were place in serum-free medium for 48 hours. After 48 hours, the medium was replaced by 10 ng/ml of TGF-β in DMEM for 24 hours. Medium was removed and discarded. The HCF were rinsed three times with PBS. The HCF were then scraped off the flask and collected in 1.5ml PBS. The collected cells were pelleted by centrifugation at 14,000 rpm for 10 minutes. Supernatant was collected and pellet was solubilized 0.1% TritonX-100. Stock concentrations of the following protease inhibitors were made as follows :

AEBSF(100mM in water), Aprotinin (80uM in water), Bestatin (5mM in DMSO), E-64 (1.5mM in DMSO), Leupeptin (2mM in water), EDTA (0.5M in water) and Pepstatin (1mM in DMSO). The proteases inhibitors were diluted to the above concentration to model the concentrations used in the protease inhibitor cocktail (cocktail III) from Calbiochem. When the assay was performed these stock solutions were diluted 1:1000. Recombinant CTGF (US Biological, Swampscott, MA) was combined with the supernatant and incubated for 0 or 1 hour at 37 ^{o}C. Proteolysis was stopped by the addition of a protease inhibitor cocktail (Calbiochem) and 0.5mM EDTA. SDS-PAGE and western was performed as previously described. Band detection was performed using the Odyssey Infrared Imaging System. Band intensity was determined using the area under the curve function from ImageJ software(U.S. National Institute of Health). A recombinant CTGF standard (concentration of 300 ng) was run on each gel and the band intensity produced by that rCTGF was used to normalize the different western blots. Three biological replicates were performed. The relative band intensities were compared using student t-test using GraphPad Prism. A p value of <0.05 was considered significant. The differences between the 0 hour and 1 hour of the normalized band intensities were assessed. Then the differences from different treatment groups were compared to the untreated by using student t-test using GraphPad Prism. A p value of <0.05 was considered significant.

CTGF Proteolytic Processing *In Vivo*

Mouse, Rat, and Rabbit Eye Homogenates

Frozen whole mouse, rat, and rabbit eyes were purchased from Pel-Freeze Biologicals (Rogers, AR). Ten mouse eyes were frozen in liquid nitrogen and combined into a steel piston homogenizer. The eyes were shattered by the force placed on the

piston. The eye homogenates were collected by placing 0.1% TritonX-100 in PBS and a protease inhibitor cocktail III and 0.5 mM EDTA to the homogenizer and collecting all of the sample. Samples were centrifuged at 4000 rpm for 10 minutes to extract any pieces of tissue that were not homogenized. Each species had 10 different eyes homogenized together to produce whole eye homogenates. The eye structures (cornea, retina, iris, sclerea, lens and vitreous) of the rabbit eye were individually dissected out of the eye. Ten of each of the eye structures were processed as described above.

SDS-PAGE and Western Blots of Whole Eye Homogenates

SDS-PAGE was performed as described above. To detect CTGF, gels were blotted onto polyvinylidene difluoride (PVDF) membranes using iBlot transfer system (Invitrogen) following the manufacturer's guidelines. Blots were incubated overnight at room temperature while shaking in Odyssey Blocking buffer. Blots were incubated with primary antibody, biotinylated US Biological rabbit anti-CTGFfor 2 hours while shaking at room temperature. The biotinylated antibody was used because the Li-Cor secondary antibodies had been shown to have some off target secondary binding when working with animal samples. The biotinylated US Biological rabbit anti-CTGF, biotinylated hinge region monoclonal, and biotinylated C-terminal monoclonal were diluted to a concentration of 10ug/ml in Odyssey Blocking Buffer containing 0.1% Tween 20. Blots were then washed 4 times with 0.1% Tween 20in PBS for 5 minutes at room temperature while shaking. Blots were incubated for 20 minutes in infrared-labeled streptavidin diluted 1:5,000 in Odyssey Blocking Buffer with 0.2% Tween 20 and 0.01% SDS. Blots were then washed 4 times with 0.1% Tween 20 in PBS for 5 minutes

at room temperature while shaking. Band detection was performed using the Odyssey Infrared Imaging System.

5' Rapid Amplification of cDNA Ends of Mouse and Rat RNA

Total RNA was extracted from mouse and rat whole eyes using the RNA-Bee Reagent (Tel INC, Lake Forest, CA) following manufacturer's instructions and was performed by Liya Pi. The mRNA was purified from the total RNA by using the MicroPoly(A)Purist™ Kit (Ambion,) following the manufacturer's instructions. The 5' RACE was performed using the SMARTer RACE cDNA Amplification Kit (Clonetech, Mountain View, CA) following the manufacturer's instructions. The primers were as follows : Mouse CTGF 5' race primer: 5' GGC TTG GCA ATT TTA GGC GTC CGG AT 3' and Rat CTGF 5' race primer: 5' GGC TTG GCG ATT TTA GGT GTC CGG AT 3'. Bands were identified on a 1% agarose gel.

Rat Corneal Ablation

Adult male Sprague Dawley rats were used for this study, and the procedure was performed in accordance to the animal care guidelines published by the Institute for Laboratory Animal Research (Guide for the Care and Use of Laboratory Animals)[178]. Using the technique that we previously described[104], precise, reproducible, central corneal ablations were created in rat corneas using a Nidek EC-5000 Eximer laser (Nidek, Fremont, CA). Briefly, rats were anesthetized with isofluorane/oxygen inhalation, proparacaine eye drops were applied to achieve local anesthesia of corneas, and both eyes of each rat were ablated to a depth of 80 μm with creating a 4.4mm diameter central epithelium to stroma injury. The ablation conditions were specifically designed to remove all of the corneal epithelial cell layers and some of the stroma to simulate PRK. Both eyes of each rat were ablated. The animals were sacrificed at 0, 1,

6, 12, 18, 24 hours and 4, 7, 11, and 21 days after ablation. Four rat corneas per time point were collected. At the various time points after excimer laser ablation, the animals were euthanized, and the corneas were then excised. Corneas were homogenized using 1mL glass homogenizers in 0.1% TritonX-100 in PBS and a protease inhibitor cocktail III and 0.5mM EDTA was added to each sample. SDS-PAGE and western analysis were performed as described above. Each band intensity was determined by using the area under the curve function in ImageJ software(U.S. National Institute of Health). A recombinant CTGF standard (concentration of 300 ng) was run on each gel, and the band intensity produced by that rCTGF was used to normalize the separate western blots. The relative band intensities were compared for statistical significance using ANOVA followed by Tukey's Post-hoc using GraphPad Prism . A p value of <0.05 was considered significant.

In vitro Analysis of siRNAs

Production of Secreted Alkaline Phosphatase Target Expression Plasmid

We have previously reported using the secreted alkaline phosphatase (sAP) reporter system to test a ribozyme [177]. The sAP reporter gene driven by an hEF1-HTLV promoter was cloned into pBluescript and contained a multiple cloning site located upstream of the sAP reporter gene (Figure 2-1). Six siRNAs targeting rat TGF-β1 and five siRNAs targeting rat CTGF were purchased from Ambion (Ambion, Carlsbad, CA)(Table 2-2). A target sequence, approximately 300 bp or less, containing the siRNA target sequence was cloned into a *Nco*I and *Nsi*I restriction site downstream of the sAP reporter gene. Sanger sequencing by UF Core was performed to confirm the insertion of the correctly oriented 300bp target sequence.

Human Embryonic Kidney 293 Cell Culture and Transfection of a Plasmid and siRNA

Dulbecco's Modified Eagle Medium (DMEM), with 4.5g/L Glucose and 1g/L L- was supplemented with 10% heat-inactivated normal calf serum and an antibiotic-antimycotic and exponentially growing human embryonic kidney 293 (HEK 293) cells were transfected with both the pBluescript sAP target plasmid and either an off target siRNA or a targeted siRNA. Turbofect reagent (Fermentas Inc.; Glen Burnie,MD, USA) was used for the dual transfection following the manufacturer's protocol. The concentration of the pBluescript sAP plasmid was held constant but three different concentrations of each siRNA (8, 20, and 40 nM) were tested. At three different time points (24, 48 and 72 hours) after transfection, level of secreted alkaline phosphatase sAP activity was assessed using a colorometric assay, Quanti-Blue^{TM} (InvivoGen, San Diego, CA, USA). Activity levels of the siRNAs were expressed as relative expression of secreted alkaline phosphatase compared to a off- target controls siRNA. Three replicates were performed for each time point and concentration of siRNA. Relative secreted alkaline phosphatase expression levels were analyzed for statistical significance by student t-test using Graphpad. A p value of <0.05 was considered significant.

In vitro Analysis of scAAV Ribozyme Vectors

scAAV-TGF-β1-Rz Plasmids Construction

Single-stranded synthetic DNA oligonucleotides encoding ribozymes were chemically synthesized. The sequences were, TGF-β1 Rz sense: 5'AGCTTGTTTGCTGATGAGTCCTTCGGGACGAAACAGGA3', TGF-β1 Rz antisense: 5'CTAGTGTTTCGTCCCGAAGGACTCATAGCAAACA3' (Table 2-3). Underlined

nucleotides were replaced (C→G, G→C) to create inactive control ribozyme plasmid. The active and inactive ribozymes were annealed into scAAV plasmid backbone (Figure 2-2) using the *SpeI* and *HindIII* restriction sites. Ligated scAAV-TGF-β1-Active-Rz and scAAV-TGF-β1-inactive-Rz vectors were transformed into *E. coli* SURE™ cells (Agilent Technologies, Inc, Santa Clara, CA). The plasmid DNA was extracted from single colonies and the correct orientation of the insertion was verified by DNA sequencing by the University of Florida sequencing core. To assure that the TRs were still in the vector, the vector was digested with *SmaI* and then run on a 0.6% agarose gel.

scAAV-CTGF-Rz Plasmids Construction

The scAAV-CTGF-Rz was cloned into the scAAV vector as described above. The sequences were, CTGF sense: 5**'**AGCTTGTCTGCTGATGAGCGCTTCGGCGCGAAACCAGGA3', CTGF antisense: 5' CTAGTTTCGCGCCGAAGCGCTCATCAGCAGACAAGCT3'.
Underlined nucleotides were replaced (C→G, G→C) to create inactive control ribozyme plasmid.

Human Embryonic Kidney 293 Cell Culture and Dual Transfection

Dulbecco's Modified Eagle Medium (DMEM), with 4.5g/L Glucose and 1g/L L- was supplemented with 10% heat-inactivated normal calf serum and an antibiotic-antimycotic mixture and exponentially growing HEK293 cells were transfected with both the pBluscript sAP target plasmid and either a GFP control or the active or inactive ribozyme plasmid. Turbofect reagent was used for the dual transfection following the manufacturer's protocol. A ratio of 1:1 of the plasmids (ribozyme vector: target vector) was transfected, and three (24, 48 and 72 hours) time points were assessed. Activity

level of the ribozymes in the scAAV vectors were expressed as relative expression of secreted alkaline phosphatase compared to a control GFP plasmid. Three replicates were performed for each time point. Relative secreted alkaline phosphatase expression levels were analyzed for statistical significance by ANOVA with a Tukey's post-hoc using Graphpad . A p value of <0.05 was considered significant.

In vivo Analysis of scAAV-GFP in Rabbit Corneas After Ablation

Delivery of scAAV-GFP to Rabbit Corneas

The delivery efficiency of the green fluorescent protein (GFP) transgene packaged in scAAV serotype 1 was tested in live rabbit corneas. Adult male New Zealand white rabbits were used for this study and the procedure was performed in accordance to the animal care guidelines published by the Institute for Laboratory Animal Research (Guide for the Care and Use of Laboratory Animals)[178]. Briefly, rabbits were anesthetized with isofluorane/oxygen inhalation, proparacaine eye drops were applied to achieve local anesthesia of corneas, and both eyes of each rabbit were ablated to a depth of 125 μm with a Nidek EC-5000 Eximer laser(Nidek, Fremont, CA) creating a 6.0 mm diameter central epithelium to stroma injury. The ablation conditions were specifically designed to remove all of the corneal epithelial cell layers and some of the stroma to simulate PRK. The ablated areas of both eyes of each rabbit were exposed for 2 min with 60ul of $1x10^{10}$ virus particles per milliliter applied on the cornea in phosphate buffered saline in a 10 mm diameter vacuum trephine. The animals were sacrificed at 0, 1, 2, 3, 4, 7, 30 days and 6 months after vector application. Four rabbit corneas per time point were treated with scAAV. At the various time points after excimer laser ablation and transduction by the scAAV vector, the animals were euthanized, and the corneas were then excised.

Direct Fluorescence Microscopy

The corneas were fixed overnight in 4% paraformaldehyde. After overnight fixation, the corneas were bisected and the tissue was embedded in Tissue Tek OCT Compound (Sakura Finetek, Torrance, CA) and frozen by dipping into liquid nitrogen. Tissue sectioning was performed with a Leica CM 1850 cryostat(Leica, Buffalo Grove, IL) and 10 µm sections were mounted on Superfrost/Plus microscope slides (Fisher Scientific) for image analysis. Nucleic acids were stained with DAPI (Vector Laboratories, Burlingame, CA) and direct GFP fluorescence (no immunostaining) in the corneal sections were analyzed by confocal microscopy (Leica TCS SP2 AOBS Spectral Confocal Microscope equipped with LCS Version 2.61, Build 1537 software). All images were taken with identical exposure settings with either 10× or 20× objective.

Image Analysis

Images were analyzed using Optimas (Adept Turnkey, Sydney, Australia) Imaging software. A threshold for a positive cell was selected and all of the images were analyzed for that threshold of fluorescence. Each tissue section was analyzed by outlining the tissue and looking for threshold fluorescence. The area for fluorescence was expressed in percent area of total tissue. After averaging the score from images of each treatment, all samples were normalized to the time point with the highest expression being considered 100%. Levels of immunostaining determined by the Optimas Imaging software were analyzed for statistical significance by ANOVA followed by Dunnett's post-hoc ($p<0.05$) compared to 0 hour by using GraphPad prism.

In vivo Analysis of scAAV-CTGF-Active-Rz in Rat Corneas After Ablation

Rat Corneal Ablation and scAAV-CTGF-Active-Rz Delivery

The rat corneal ablation was performed as previously described. The scAAV-CTGF-Active-Rz vector was packed into AAV serotype 1. Five animals (2 eyes per animal) were ablated. After the ablation, the control eye was treated with 5 ul of PBS for two minutes and the experimental eye was treated with 5 ul of scAAV-CTGF-Active-Rz at a concentration of 1×10^{10} virus particles/ml. After 14 days, the animals were euthanized, and the corneas were then excised. Corneas were homogenized using 1mL glass homogenizers in 0.1% TritonX-100 in PBS and a protease inhibitor cocktail plus 0.5 mM EDTA was added to each sample. Total protein concentration was determined using the Bradford Assay (Bio-Rad Laboratory Inc., Hercules, CA) and CTGF was determined by ELISA.

CTGF Protein Concentration (ELISA)

CTGF was measured in the conditioned medium of cultured cells by capture sandwich ELISA as we reported previously.[104] Briefly, an ELISA plate was coated with rabbit anti-human CTGF antibody(US Biological) at a concentration of 2.0 µg/mL in PBS overnight. Wells were washed four times with wash buffer (0.05% Tween 20 in PBS) and incubated with blocking buffer (5% Tween 20 in PBS) for 1 hour at room temperature. The wells were washed four times with wash buffer. Then standards ranging from 0-2000 ng/uL of CTGF or sample were added and incubated at room temperature for 2 hours. After washing, biotinylated rabbit anti- CTGF at a concentration of 300 ng/mL was added and incubated at room temperature in the dark for 2 hours; then washed with wash buffer, and streptavidin-horseradish peroxidase was added and incubated at room temperature for 20 minutes. The wells were washed again and

incubated with substrate solution (1:1 mixture of H_2O_2 and tetramethylbenzidine). Absorbance at 405 nm was measured with a microplate reader. CTGF expression was expressed as CTGF protein to total protein. CTGF expression was analyzed for statistical significance by comparing the sc-AAV-CTGF-Rz to the PBS controls by using student t-test using GraphPad Prism. A p value of <0.05 was considered significant.

Table 2-1. Primary Antibodies

Supplier	Catalogue #	Clone	Host	Immugen	Target
US Biological	C7978-25C	Polyclonal	Rabbit	Full-length rCTGF	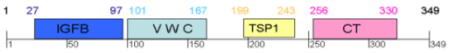
Santa Cruz	CTGF (L-20): sc-14939	Polyclonal	Goat	Human Internal Region	? 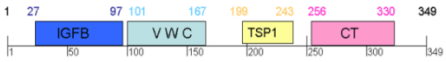
ICBR Core	9-54-A7	Monoclonal	Mouse	Hinge region (181-197)	181-197 
ICBR Core	11-39-1	Monoclonal	Mouse	C-terminus (247-260)	247-260 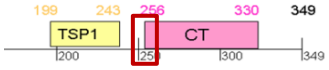
ICBR Core	17-73-F1	Monoclonal	Mouse	N-terminus (81-94)	81-94 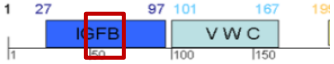

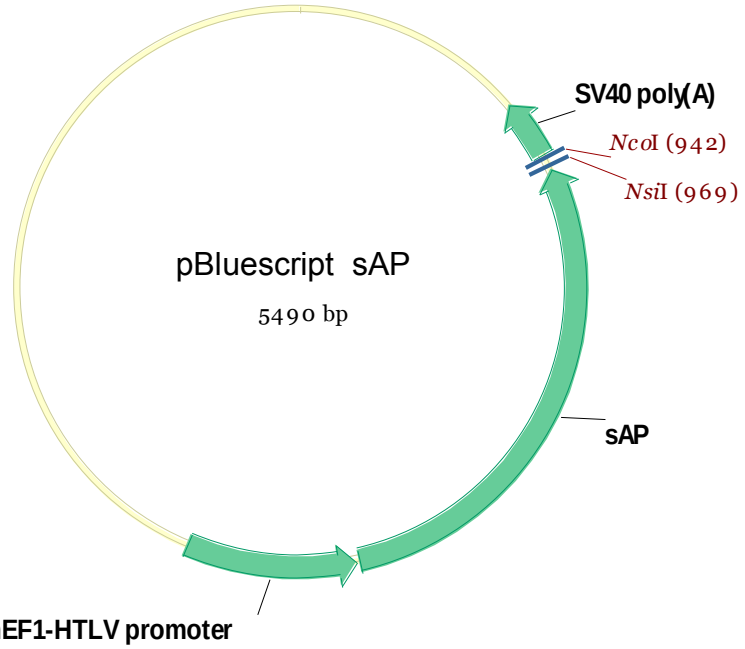

Figure 2-1. Scheme of secreted alkaline phosphatase plasmid before the target gene is added.

Table 2-2. Rat siRNAs

Target Gene	siRNA #	siRNA Target Sequence
TGF-β 1	siRNA 90	gcaacaacgcaatctatg
	siRNA 88	ggagagccctggataccaa
	siRNA 41	gcaacacguagaacucua
	siRNA 92	ggagacggaauacagggcu
	siRNA 86	ggcuaccaugccacuuc
	siRNA 70	gguccuugcccucuacaac
CTGF	siRNA 36	ggcaaaaagtgcatccgga
	siRNA 37	cgggttaccaatgacaat
	siRNA 54	gggacacgaacucauuuag
	siRNA 56	cgaacucauuuagacuaua
	siRNA 83	gcgagaucaugaaaaagaa

Table 2-3. Ribozymes

Ribozyme	Target Sequence	Homolgy		Ribozyme Sequence
CTGF	CCTGGTCCAGAC	Mouse Rat Rabbit Human	Active	AGCTTGTCTGCTGATGAGCGCTTCGGCGCGAAACCAGGA
			Inactive	AGCTTGTCTGCTCATGAGCGCTTCGGCGCGAAACCAGGA
TGF-β1	TCCTGTCCAAAC	Mouse Rat Rabbit Human	Active	AGCTTGTTTGCTGATGAGTCCTTCGGGACGAAACACTAGT
			Inactive	AGCTTGTTTGCTCATGAGTCCTTCGGGACGAAACACTAGT

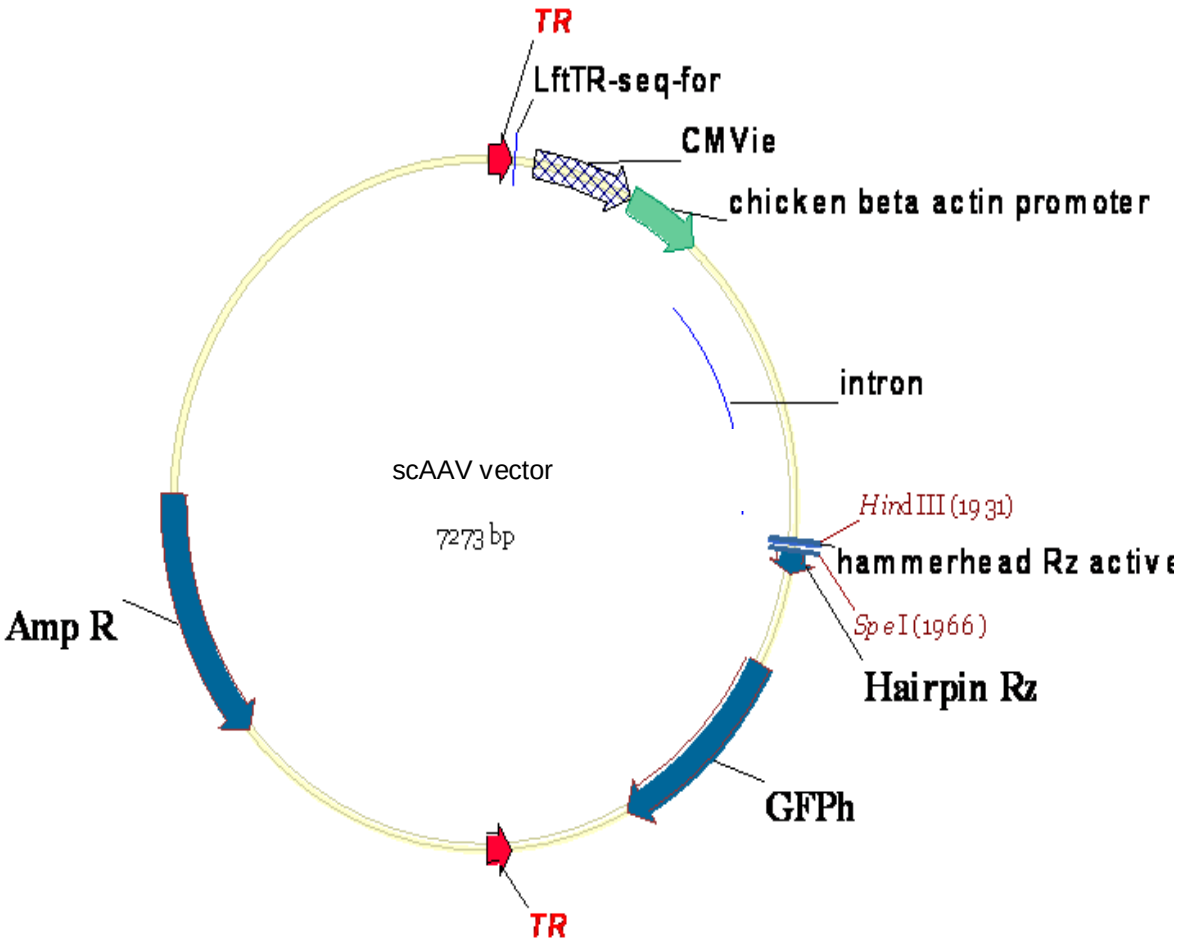

Figure 2-2. Scheme of scAAV vector before the ribozyme is added.

CHAPTER 3
ROLE OF PROTEOLYTIC PROCESSING OF CTGF THROUGHOUT WOUND HEALING

Corneal Scar Formation

Corneal scarring is a major cause of haze and impaired vision. After corneal trauma, stromal scarring is the result a complex cascade of multiple growth factors, cytokines, chemokines, and proteases. Immediately after epithelial damage, the process of healing is initiated by multiple cytokines and growth factors, including interleukin-1 (IL-1), tumor necrosis factor alpha (TNFα), bone morphogenic proteins 2 and 4 (BMP2, BMP4), epidermal growth factor (EGF), platelet derived growth factor (PDGF), transforming growth factor- beta(TGF-β) and connective tissue growth factor (CTGF) [19, 11]. The TGF-β system has been established as a key scar-promoting growth factor system[179, 180]. CTGF, a 38 kDa cysteine rich cytokine, is a downstream mediator of the fibrotic action of TGF-β. The expression level of CTGF was found to be elevated in rat corneas after ablation[104].

Connective Tissue Growth Factor

The structure of CTGF is similar to other CCN proteins in that it contains a C-terminal domain, Hinge region and N-terminal domain. The N-terminal domain contains two modules; the insulin-like growth factor (IGFBP) binding module that is predicted to bind IGF, and the von Willebrand factor type C repeat, which has been implicated as a binding site for TGF-β family members modulating their activity[93]. Within the C-terminal domain, there are two modules; a thrombospondin type 1 module that is likely involved in binding to sulfated glycoconjugates[95] and the CT module, which is similar to that found in TGF-β, platelet-derived growth factor, and nerve growth factor and allows

dimerization of these proteins[96,99]. CTGF has been found in several fragmented forms in several different cell types, tissues and body fluids[121, 122, 123, 124, 125, 115, 126]

We hypothesize that there will be fragmentation of CTGF in both the *in vitro* and *in vivo* corneal wound healing models. We also analyze unwounded whole eye homogenates. We further hypothesize that we will be able to elucidate the class of protease that cleaves CTGF *in vitro*.

Results

Antibody Sensitivity and Detection

Sensitivity of each antibody was determined by running a standard curve of the recombinant CTGF protein. The polyclonal antibodies, Santa Cruz and US Biological had the greatest level of detection at 18.25 ng and 23 ng, respectively, of total CTGF protein. In respect to the monoclonal antibody detection, the hinge region antibody had the greatest level of detection at 50 ng of total CTGF protein, whereas, the C-terminal and N-terminal antibodies had the lowest level of detection at 100 ng of total CTGF protein (Figure 3-1). When the C-terminal monoclonal antibody and the hinge region monoclonal antibodies probed heterozygous CTGF mice homogenates and homozygous CTGF knockout mice homogenates, they detected a 38 kDa band in only the heterozygous CTGF mice homogenates. Neither monoclonal detected a band at 38 kDa for the homozygous CTGF knockout mice homogenates.

TGF-β1 Stimulation of CTGF in HCF

After the antibodies were tested on recombinant CTGF protein for sensitivity and specificity, a time course of CTGF expression from HCF after stimulation with TGF-β1 was performed. HCF cells were serum starved for 48 hours and then stimulated with TGF-β1. At 0, 1, 6, 12, 18, 24, 48, and 72 hours the media and cell extract were

collected and analyzed by western blotting. In the cell extracts(Figure 3-2), the full-length (38 kDa) CTGF protein was detected at all time points from 0 hours to 72 hours with only a slight increase peaking at 18 hours. At 18 hours there was 1.6 times more full-length (38 kDa) CTGF than at 0 hour and was the difference not statistically significant. A 21 kDa CTGF fragment was detected 1 hour post stimulation and peaked 12 hours. The 21 kDa CTGF fragment was statistically significantly different ($p<0.05$) when compared to 0, 1, and 72 hours, with the 12 hour being 37 times greater than the 0 hour time point. At 72 hours after stimulation, the detection level of the 21 kDa fragment returned to the 0 hour level. Finally, two other fragments, 18 kDa and 13 kDa CTGF fragments were detected throughout the treatment times, 0 hours to 72 hours. There was statistically significant change in intensity of these two bands due to the cells being treated with TGF-β1. Therefore, I conclude that these fragments are not produced in response to the addition of TGF-β1.

CTGF is a secreted protein, therefore, the conditioned media from the HCF stimulated with TGF-β1 were analyzed (Figure 3-3). The full-length (38 kDa) fragment protein was initially detected at 6 hours and peaked at 24 hours post stimulation. When compared to 0 and 1 hours, there was a least 17.9 times more full-length (38 kDa) CTGF at 24 hours post stimulation ($p<0.05$). The 21 kDa CTGF fragment was also detected in the conditioned media. The 21 kDa CTGF fragment was detected 6 hours post stimulation and peak at 24 hours. When compared to 0, 1, 6 and 72 hours there was a least 10.3 times more 21 kDa fragment of CTGF at 24 hours post stimulation ($p<0.05$) which was a statistically significantly difference ($p<0.05$). The normalized band intensity of the 21 kDa fragment returned to that of the 0 hour time point at 72 hours.

Finally, an unexpected 50 kDa band was detected in the conditioned media. The greatest detection occurred at the 0 time point and it was at least 2.6 fold higher than any of the other time points($p<0.05$).

Immunoprecipitation and Identification of the 21 kDa CTGF Fragment from HCF

The CTGF from the 24 hour cell extract was purified by immunoprecipitation using the US Biological polyclonal antibody. The sample was analyzed by silver stain and western. The full-length (38kDa) and 21 kDa fragment were detected. The 21 kDa band was identified as CTGF by the sequence, LEDTFGPDPTMIR, using tandem mass spectrometry (Figure 3-4).

Identification of the Protease Class that Cleaves CTGF from HCF Extracts

In order to determine the protease class that cleaves CTGF from the 38 kDa full-length form into the 21 kDa fragment in HCF, a processing assay was conducted. HCF extracts were incubated with rCTGF for 0 or 1 hours with different protease inhibitors and the samples were analyzed by western blot (Figure 3-5). The only protease inhibitor that was able to inhibit the processing of CTGF from the 38 kDa full-length form into the 21 kDa fragment was pepstatin, an aspartic acid protease inhibitor. There was no difference in normalized band intensity between the 0 and 1 hour time points ($p=0.32$). AEBSF, Aprotinin, Bestatin, E-64, Leupeptin, and EDTA were unable to inhibit the processing of full-length (38 kDa) CTGF into the 21 kDa CTGF fragment when comparing the normalized band intensity of the 0 hour time point to the 1 hour time point ($p<0.05$). Also, when the difference in the normalized band intensities of the untreated is compared individually to each treatment group, the group treated with pepstatin was significantly reduced ($p<0.05$).

Identification of a 21 kDa CTGF Fragment in Unwounded Rat, Rabbit, and Mouse Whole Eye Homogenates

To determine if the 21kDa fragment was unique to the HCF culture system, rabbit, rat, and mouse whole eyes were homogenized and analyzed by western blotting using three different antibodies. The US Biological polyclonal, hinge region monoclonal, and C-terminal monoclonal all detected a 25 kDa and 21 kDa fragment in rabbit, rat and mouse unwounded whole eye homogenates(Figure 3-6). Interestingly, there was little 38 kDa full-length CTGF detected in any of homogenates from rats, rabbits or mice. The 150 kDa and 75 kDa bands were due to the streptavidin label Licor dye binding off target.

Identification of a 21 kDa CTGF Fragment in Individual Eye Structures in the Rabbit Eye

To analyze what structure(s) in the eye was producing the 21 kDa CTGF fragment, rabbit eyes were dissected into individual eye structures (cornea, retina, iris, sclerea, lens and vitreous) and homogenized then analyzed by western blot. The cornea, retina, iris, sclerea, lens and vitreous all contained the 21 kDa band and the 25 kDa band (Figure 3-7). These 21 kDa and 25 kDa bands were identified by both the US Biological polyclonal and the C-terminal monoclonal antibodies. The lens had at least 5 times as more 21 kDa CTGF fragment than any of the other structures, because 6 ug of total protein from the lens were added as opposed to 30 ug of total protein from the other structures.

5’ Rapid Amplification of cDNA Ends of Mouse and Rat RNA

To determine if the 21 kDa and 25 kDa CTGF fragments were not attributed to an alternative start site, 5’ Rapid Amplification of cDNA Ends was performed on mouse and rat RNA (Figure 3-8). The only PCR product that was produced was 791 bp

corresponding to full-length CTGF. No other bands were detected. Therefore, I conclude that only major RNA start site exists and that the smaller immune reactive proteins are the result of proteolytic processing.

Immunoprecipitation and Identification of the 21 kDa CTGF Fragment from Rabbit Whole Eye Homogenates

The CTGF from the rabbit whole eye homogenates was purified by immunoprecipitation using the hinge monoclonal antibody. The sample was analyzed by silver stain(Figure 3-9) and coomassie blue staining. The 25 kDa and 21 kDa CTGF fragments were detected. These fragments were sent for analysis by mass spectrometry. We were unable to identify this fragment as CTGF using tandem mass spectrometry.

Detection of CTGF Throughout Corneal Wound Healing in Rats

A time course of CTGF throughout corneal wound healing in rats was performed by ablating normal rat corneas and collecting the corneas at 0, 1, 6, 12, 18, 24 hours and 3, 7, 11, 14 , and 21 days (Figure 3-10). The homogenates of the rat corneas were analyzed by western blot. Low levels of full-length CTGF (38kDa) were detected throughout the wound healing process from 0 hours to 21 days. The normalized band intensity from day 11 post ablation was 1.6 times greater than the 0 hour time point. The lowest normalized band intensity from the 38 kDa full-length CTGF occurred at 12 hours post ablation and was 3.7 times less than the day 11 time point. As previously mentioned, a 25 kDa CTGF fragment was detected in uninjured cornea. The greatest normalized band intensity for the 25 kDa CTGF fragment occurred 11 days post ablation and was 2.5 times($p<0.05$) greater than the 0 hour time point. The 25 kDa

CTGF fragment normalized band intensity at 11 days post ablation was 22.9 times greater than the 12 hour time point which had the lowest band intensity of the 25 kDa CTGF fragment($p<0.0001$). A 21 kDa CTGF fragment was detected at the 0 hour time point and the peak level of detection occurred 11 days post ablation. The normalized band density of the 21 kDa CTGF fragment from day 11 was 32.5 times greater than the 12 hour time point ($p=0.0051$). There were two other bands detected, 18 kDa and 13 kDa, but their signal was not very strong and they did not vary significantly throughout the wound healing process.

Discussion

In this study, we confirmed the presence of several CTGF fragments (21, 18, and 13 kDa fragments) produced in HCF cultures stimulated with TGF-β1. We found that the greatest amount of the 21kDa was found at 12 hours and 24 hours in the cell extract and media, respectively. The 18 kDa fragment and the 13 kDa fragments that were found in the cell extract did not have a significant change in concentration throughout the time course. We unexpectedly found a 50 kDa immunoreactive band that was not due to non-specific binding of the secondary antibody. Steffen *et al.* [125] found in human foreskin fibroblast, there was little to no CTGF found in the conditioned media. They also determined that the full-length 38 kDa CTGF remained cell-associated for at least 5 days after synthesis. This 50 kDa immunoreactive band could be from the CTGF still being associated with some extracellular matrix components.

Several studies have shown processing of CTGF into fragments [115, 121-126, 181]. Most recently, Tall *et al*.[126] analyzed fragmentation patterns of CTGF from HCF grown on different extracellular matrix components (collagen, fibronectin, and vitronectin).

They found a novel 31 kDa CTGF fragment that lacked the N-terminus when cells were grown on collagen. Since our experiments were preformed in plastic cell culture vials that were not treated with collagen, we did not see this same fragmentation pattern. Previously, Ball *et al*. [121] looked at the presence of CTGF fragments during estrous and pregnancy in porcine uterine flushes. They found that in porcine uterine flushes there were four fragments present: 20, 18, 16 and 10 kDa. The full-length CTGF, as well as the processed forms of CTGF, were in higher abundance at day 12 of pregnancy than day 12 of the cycle. These authors were able to perform N-terminal sequencing of the 20, 18, and 16 kDa fragments found in uterine flushings. They found that their 20 kDa fragment was processed at Asp-186. In a later paper, Ball *et al*. [181], were able to model the processing of CTGF *in utero* and identified the processing site of the 20 kDa fragment as being Ala-181. Using tandem mass spectrometry, we identified our 21 kDa fragment from Leu-184 – Arg-196, this area is located in the hinge region of CTGF. Once the 21 kDa fragment from the HCF culture system was identified, we chose to identify the class of protease that cleaves CTGF in this HCF model.

In this study, we were able to identify that a pepstatin sensitive protease from HCF cell extracts was able to process rCTGF into the 21 kDa fragment. Previously, *in vitro* testing has shown that MMP-1, 3, 7, and 13 are able to cleave CTGF into smaller fragments when CTGF was associated with VEGF [127]. Kallikrein-related peptidases, which are secreted serine proteases, specifically, KLK12 and KLK14, have been show to process CTGF into smaller fragments[128]. The MMP and Kallikrein-related peptidases were identified by incubating only the enzyme and substrate together at their optimal conditions. While this could be indicative of the protease in some biological systems,

we were able to identify the protease class that cleaves CTGF in our HCF system as an aspartic acid protease. Further investigation is necessary to identify exactly which aspartic acid protease is responsible for cleaving CTGF but renin, cathepsin D and L have all been localized to the cornea[182 183]. Interestingly, the level of cathepsin D increased in severe burns of the anterior segment of the eye after three weeks [184].

These findings lead us to evaluate the presence of CTGF in whole eye homogenates of mouse, rat and rabbit. In whole eye homogenates of mouse, rat and rabbit, we found that the 21 kDa fragment was present in the highest abundance and this fragment was identified as containing the C-terminal domain of CTGF. We also found that a 25 kDa fragment was present and identified by the C-terminal domain in mouse, rat and rabbit whole eye homogenates. The 75 kDa and 150 kDa bands were found to be due to non-specific binding of the strepavidin conjugated Licor dye. We also examined CTGF expression in the individual eye structures in the rabbit. Once again, we found that the 21 kDa fragment was the pre-dominant form of CTGF in all the structures and this 21 kDa fragment was identified by the C-terminal monoclonal antibody. The lens produces this 21 kDa fragment in abundance because 6 times less total protein was loaded to the gel and there was a distinct band. CTGF expression in the lens was first documented over twenty years ago by Lee *et al.*[185] but there has been very little published since then. Lee *et al.* analyzed the expression of CTGF mRNA from epithelial cells of patients with anterior polar cataracts. They found an increased level of CTGF mRNA in patients who had anterior polar cataracts compared to patients who did not have anterior polar cataracts. In our study, the 25 kDa fragment was also present in all of the individual eye structures, as identified by the C-terminal monoclonal antibody.

Similarly, Ball *et al.* [121] found that the lower molecular weight fragments were the dominant form of CTGF in pig uterine flushings.

CCNs 1, 3, and 4 have been show to have alternate splicing [186]. We were able to determine that the lower molecular weight bands were not due to an alternate start site or splicing of the CTGF gene by performing 5'RACE on rat and mouse RNA. In 1998, Harding *et al*. [187] also found that there were no alternate start site for CTGF in pig endometrium.

Finally, we performed a time course looking at the protein expression and processing of CTGF during wound healing in the rat cornea after ablation. While Blalock *et al*.[104] had previously analyzed the total concentration of CTGF protein using ELISA in the corneas of wounded rats, we are the first to report the processing of CTGF during several time points in wounded rat corneas. Similar to the findings of Blalock *et al*.[104], we found that during the first eighteen hours post wounding, there was very low levels of all forms of CTGF. The peak expression of all three forms of CTGF (38 kDa, 25 kDa, and 21 kDa) was at day 11 post ablation. One to two weeks after injury myofibroblast appear in the anterior stroma [36]. CTGF has been shown to stimulate differentiation of cells into myofibroblast.[105] Our data, taken with these two pieces of knowledge would indicate that the abundance of the 38 kDa, 25 kDa and 21 kDa fragments at day 11 play a role in corneal scar formation. From our data, the significance the proteolytic processing of CTGF throughout wound healing is not yet clear but we can hypothesize the role of the processing. Grotendorst *et al*.[129] found that the C-terminal fragment increased DNA synthesis, whereas the N-terminal fragment had no effect on DNA synthesis. In contrast, N-terminal fragment increased

differentiation of fibroblasts to myofibroblasts, but the C-terminal had no effect on myofibroblast induction.

In summary, these data confirmed the presence of a 21 kDa CTGF fragment produced in HCF cultures stimulated with TGF-β1. Results from studies using protease inhibitors determined that pepstatin was the only protease inhibitor able to reduce the processing of the full-length (38 kDa) CTGF into the 21 kDa fragment, which indicates that the aspartic acid class of proteases is responsible for the cleavage in the HCF cultures. A 21 kDa fragment was found in the highest abundance in whole eye homogenates and this fragment was identified as containing the C-terminal domain of CTGF. These data also indicate the 21 kDa fragment was the dominant form of CTGF found in the whole eye homogenates and individual eye structure homogenates. These fragments were not the product of alternative start sites or splicing. And finally, the highest abundance of all forms of CTGF occurred at day 11 post wound healing.

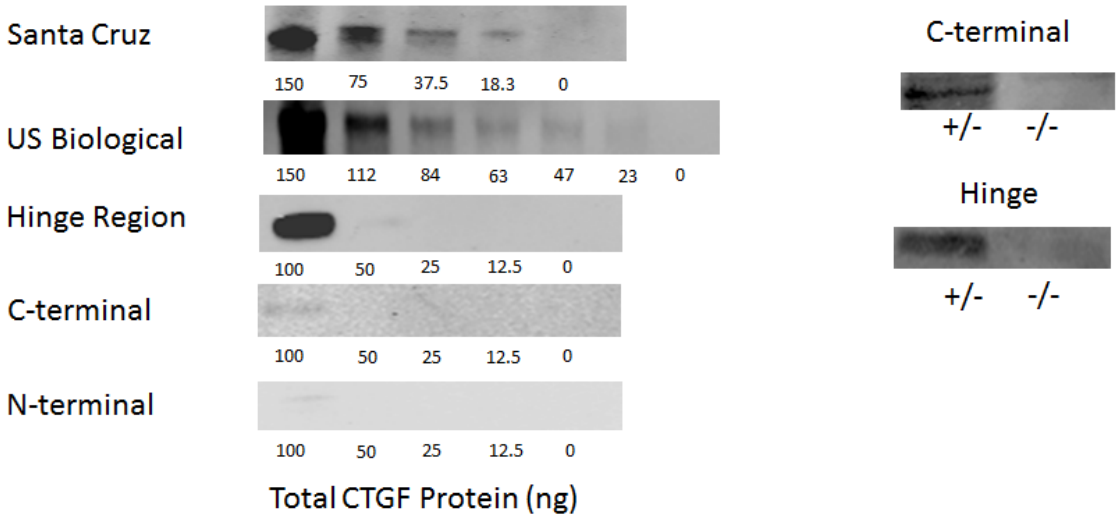

Figure 3-1. Detection of rCTGF using several different antibodies. Santa Cruz polyclonal, US Biological polyclonal, hinge region monoclonal, C-terminal monoclonal, and N-terminal monoclonal were all tested for sensitivity using a rCTGF. Specificity of the hinge region monoclonal and C-terminal monoclonal were tested by analyzing the ability of the antibody to detect CTGF in heterozygous (+/-) and homozygous (-/-) mouse tissue homogenates.

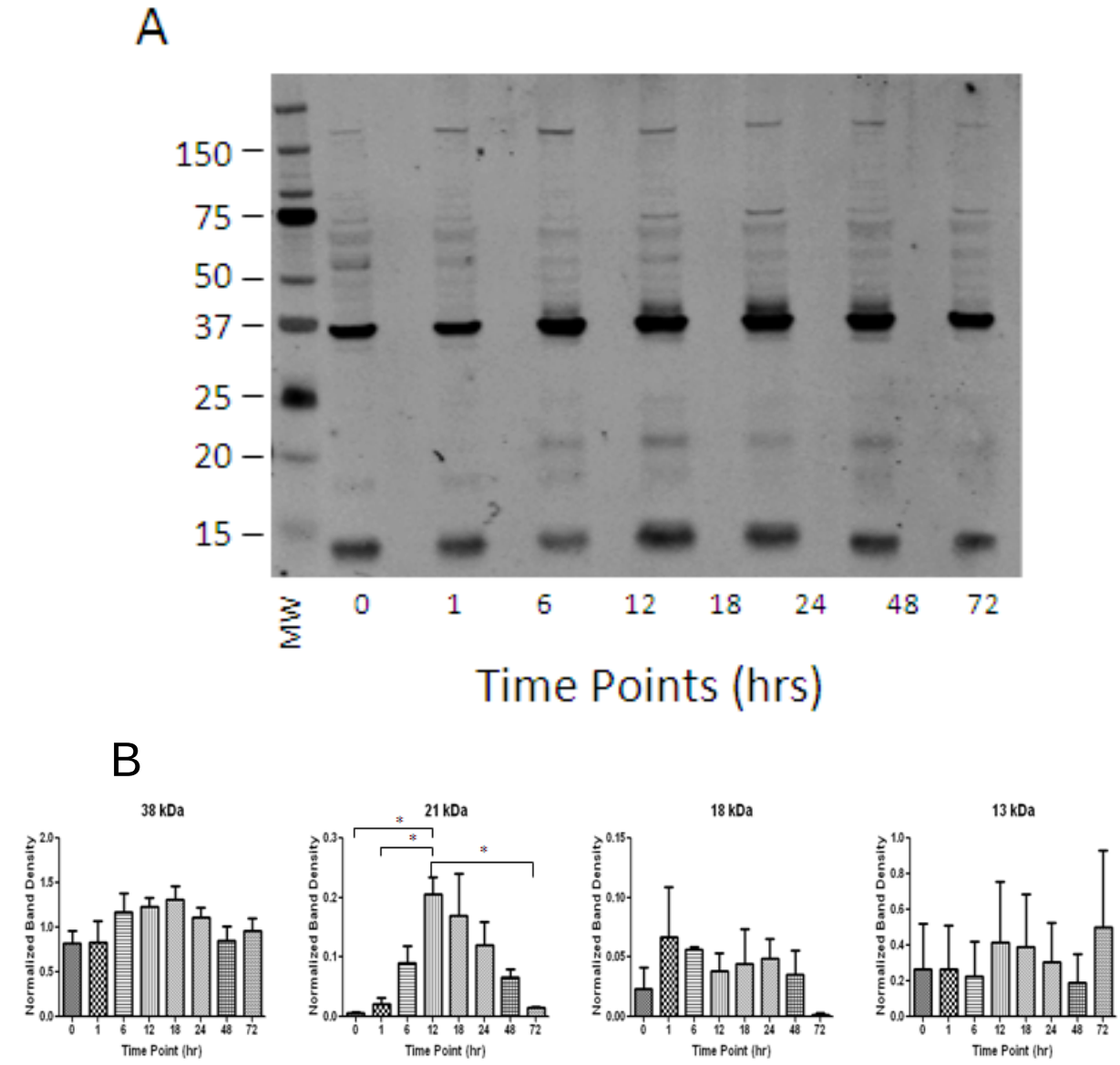

Figure 3-2. Western blot analysis of cell extracts from HCF cells stimulated with TGF-β1. A) Shows a typical western blot of the time course was performed to look at expression of lower molecular weight forms of CTGF using the US Biological polyclonal antibody. B) Quantification of individual CTGF bands (38 kDa, 21 kDa, 18 kDa, and 13 kDa) were performed from replicate blots (n=3). Variation between blots were normalized by comparing each band to a rCTGF standard. Band intensities were compared by analysis of variance (ANOVA) with a Tukey's post-hoc test with significance is indicated by a * ($p<0.05$).

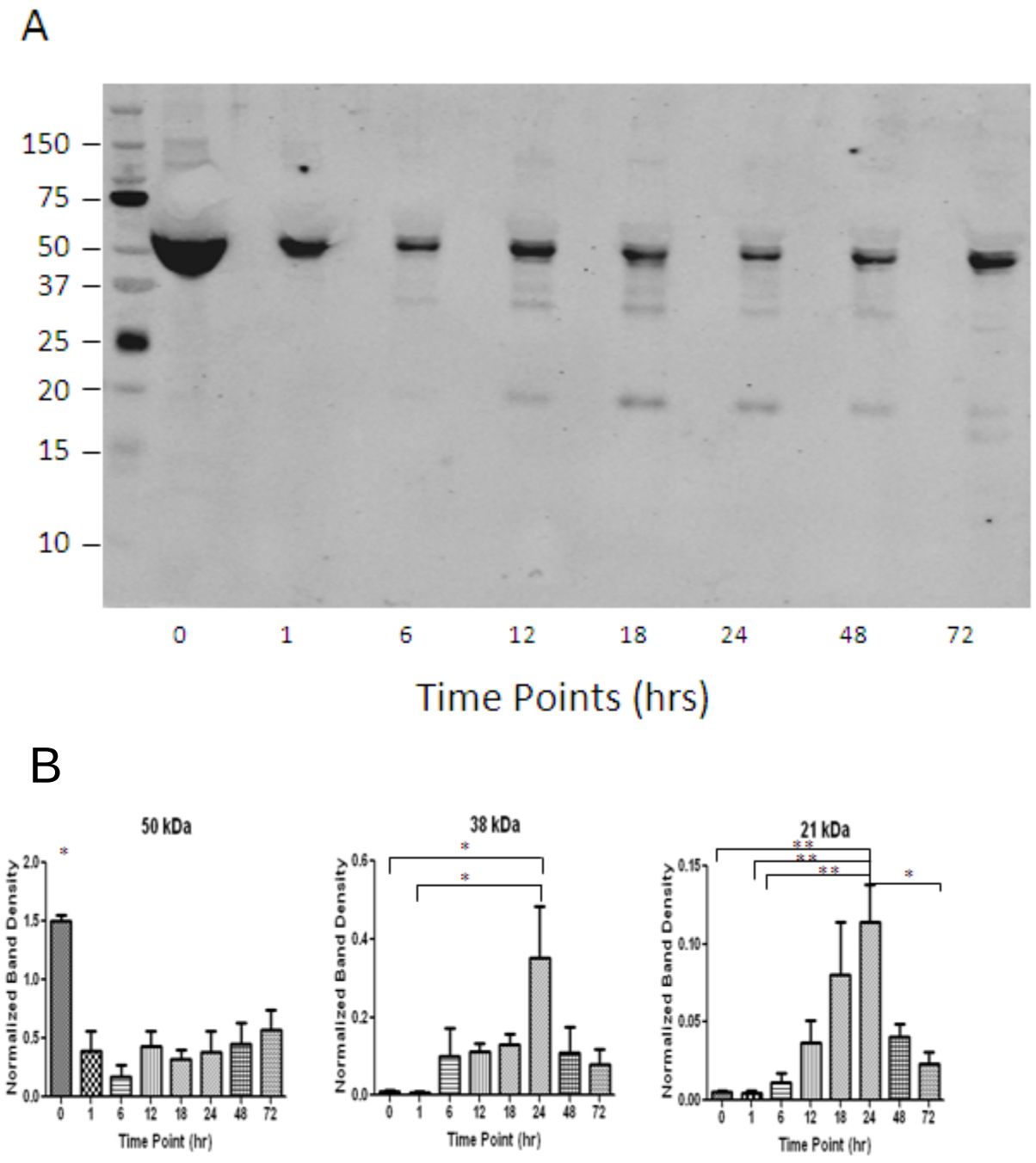

Figure 3-3. Western blot analysis of conditioned media from HCF cells stimulated with TGF-β1. A) Shows a typical western blot of the time course was performed to look at expression of lower molecular weight forms of CTGF using the US Biological polyclonal antibody. B) Quantification of individual CTGF bands (38 kDa, 21 kDa, 18 kDa, and 13 kDa) were performed from replicate blots (n=3). Variation between blots were normalized by comparing each band to a rCTGF standard. Band intensities were compared by analysis of variance (ANOVA) with a Tukey's post-hoc test with significance of $0.01<p<0.05$ indicated by * and $0.001<p<0.0099$ indicated by **.

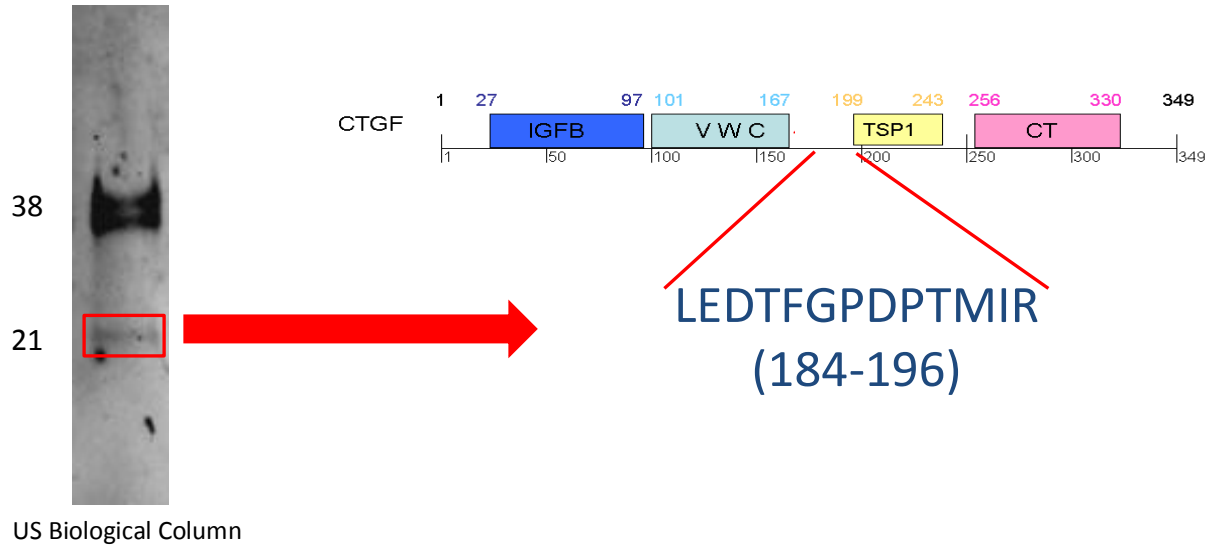

Figure 3-4. Western blot analysis of immunoprecipitated CTGF from HCF cells stimulated with TGF-β1. The 21 kDa fragment (highlighted in the red box) was identified as CTGF from the LEDTFGPDPTMIR sequence located in the hinge region of CTGF.

A

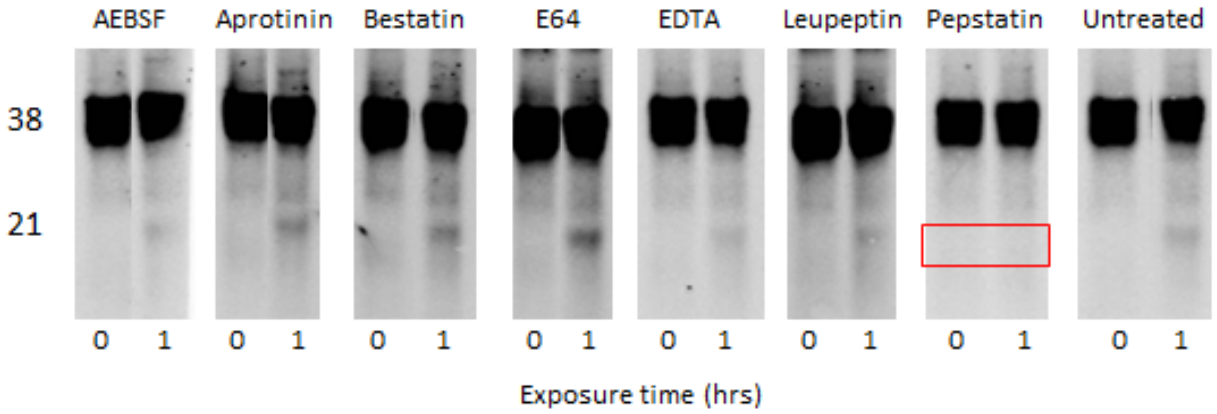
AEBSF
Aprotinin
Bestatin
E64
EDTA
Leupeptin
Pepstatin
Untreated
38
21
0 1 0 1 0 1 0 1 0 1 0 1 0 1 0 1
Exposure time (hrs)

B

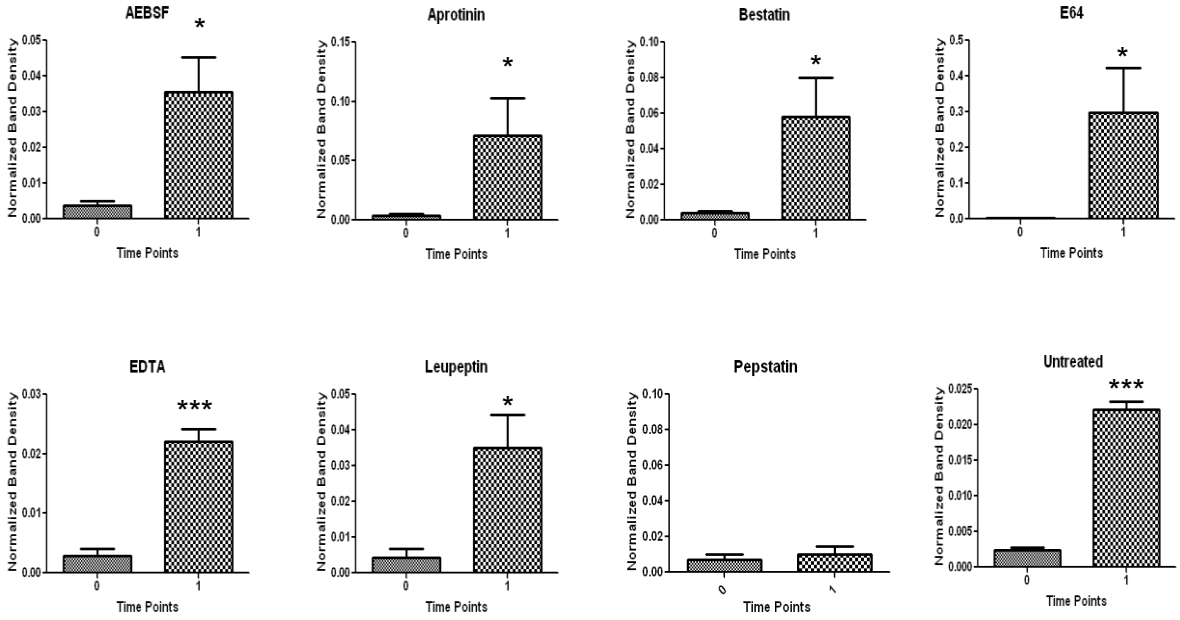
AEBSF
Aprotinin
Bestatin
E64
EDTA
Leupeptin
Pepstatin
Untreated
Normalized Band Density
Time Points
*
***

C

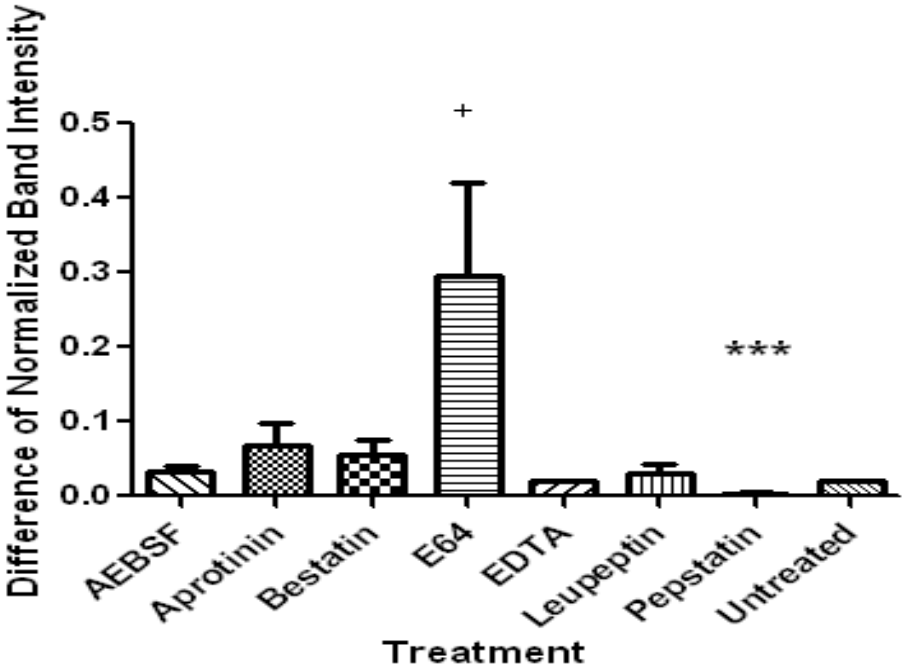

Figure 3-5. Western blot analysis of *in vitro* processing of CTGF into the 21 kDa fragment. A) Briefly, rCTGF was incubated for 0 or 1 hour with the HCF cell extract that was stimulated with TGF-β1. To assess inhibition of processing, the rCTGF protein and cell extract was incubated with different protease inhibitors (Aprotinin, Bestatin, E64, EDTA, Leupeptin, AEBSF or Pepstatin) or no protease inhibitor. B) Relative quantification of the 0 hour and 1 hour time points of the 21 kDa band for each protease inhibitor are shown. Band intensities were compared by student t-test with significance of $0.01<p<0.05$ indicated by * and $p<0.0001$ indicated by ***. C) The average difference between the 0 hour and 1 hour normalized band density for each treatment are shown. Band intensities were compared by student t-test of the treatment compared to the untreated. When compared to the untreated, the pepstatin had a decrease in the 21 kDa band intensity with a significance of $p<0.0001$ indicated by ***. When compared to the untreated, the E64 had an increase in the 21 kDa band intensity with a significance of $0.01<p<0.05$ indicated by +.

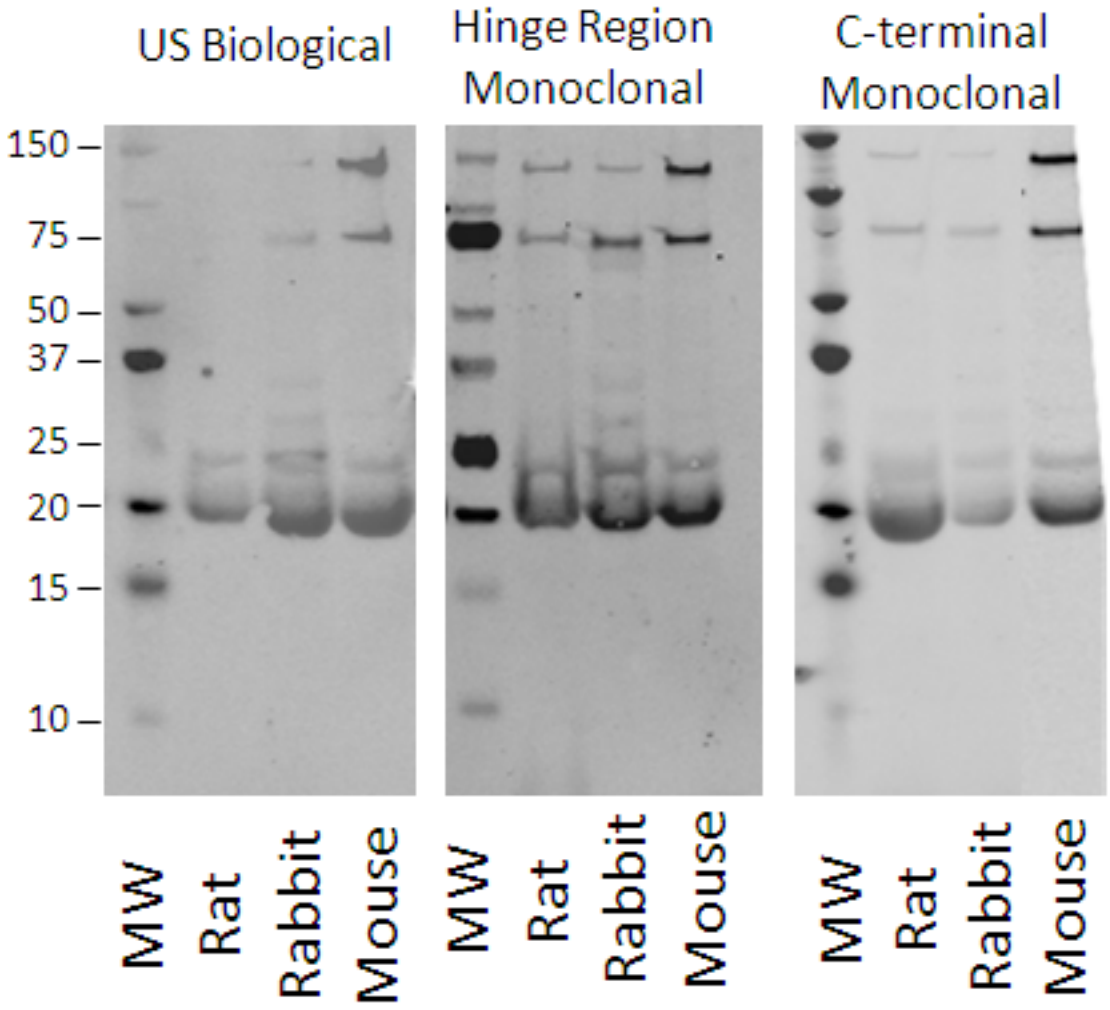

Figure 3-6. Western blot analysis of *in vivo* CTGF from unwounded rabbit, rat and mouse whole eye homogenates. Three different antibodies were used to detect the CTGF. The US Biological polyclonal antibody, the hinge region monoclonal antibody and the C-terminal monoclonal antibody all had similar banding patterns identifying a 21 kDa and 25 kDa band. The upper molecular weight bands (75 kDa and 150 kDa) were due to off target bind of the strepavidin labeled Licor dye.

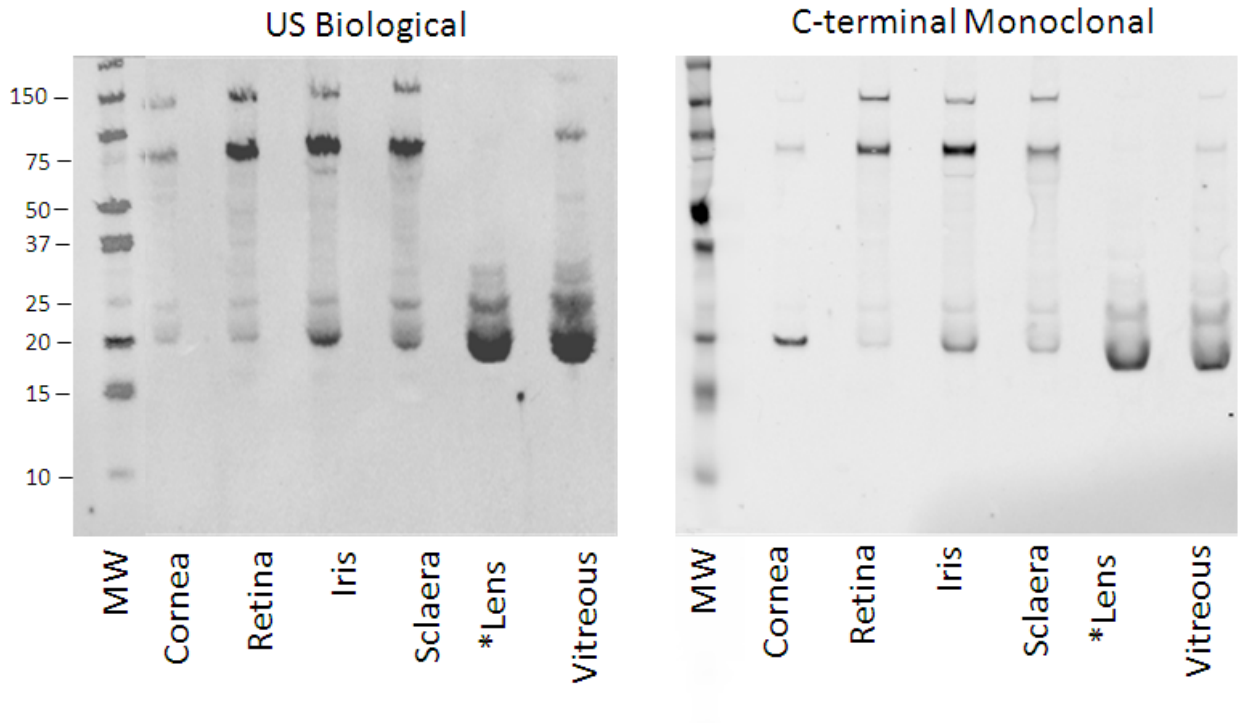

Figure 3-7. Western blot analysis of *in vivo* CTGF from unwounded rabbit eye structures(cornea, retina, iris, sclaera, lens and vitreous). Two different antibodies were used to detect the CTGF. The US Biological polyclonal antibody and the C-terminal monoclonal antibody all had similar banding patterns identifying a 21 kDa and 25 kDa band in all tissue. The upper molecular weight bands (75 kDa and 150 kDa) were due to off target bind of the strepavidin labeled Licor dye. * Indicates that 5 times less total protein from the lens was loaded in the well.

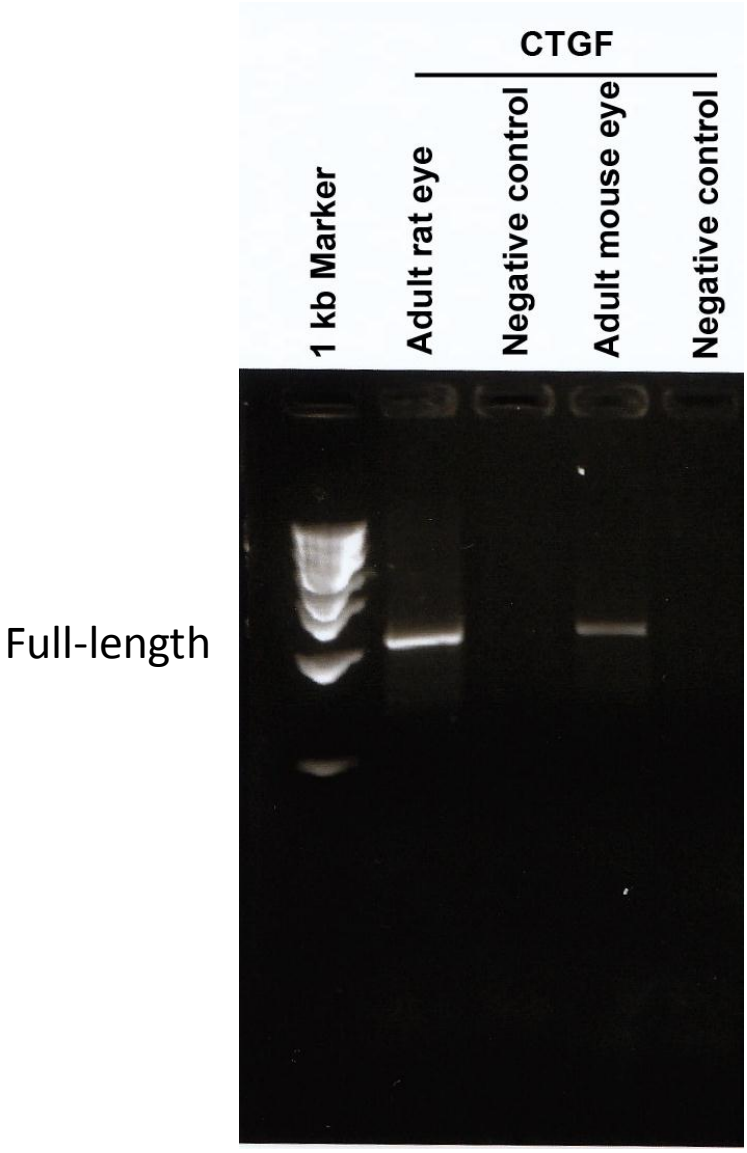

Figure 3-8. Analysis of transcriptional start sites of the CTGF RNA in adult mouse and adult rat eyes using 5' RACE. The full-length transcript is 791bp.

Figure 3-9. Silver stain analysis of a rabbit whole eye homogenates elution from an affinity column containing the hinge region monoclonal antibody.

A

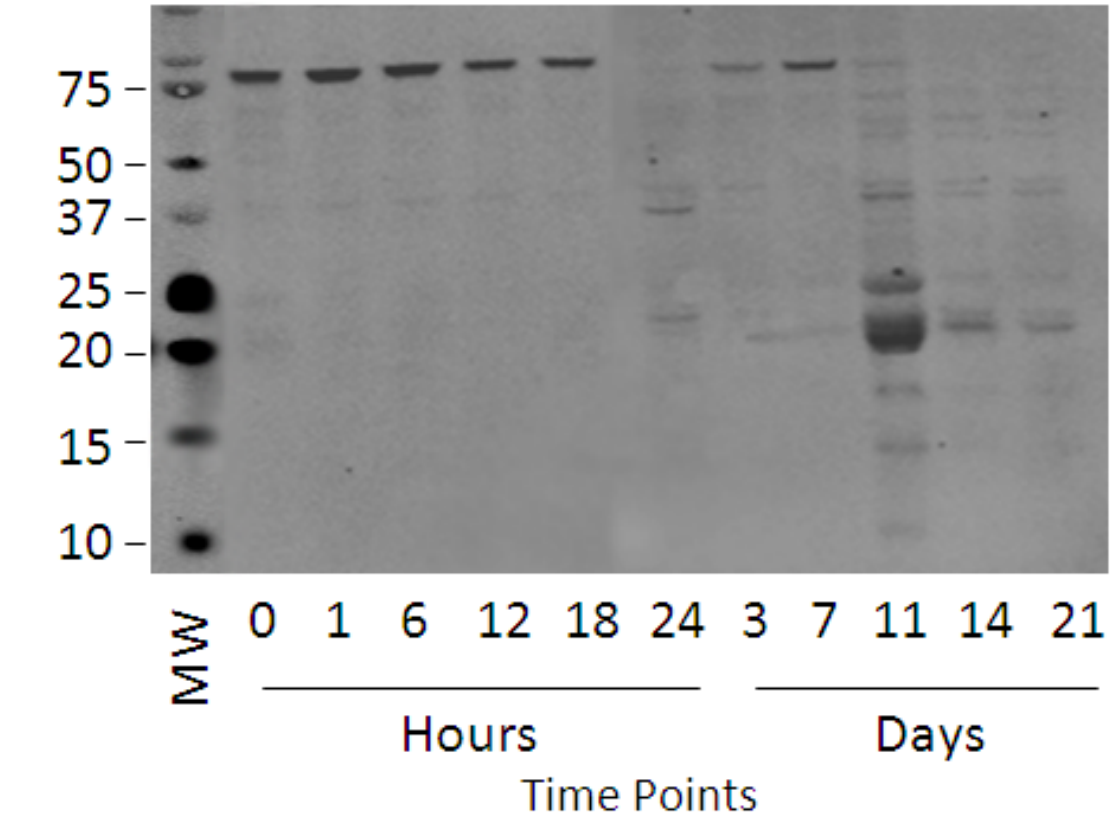
75
50
37
25
20
15
10
MW
0 1 6 12 18 24 3 7 11 14 21
Hours
Days
Time Points

B

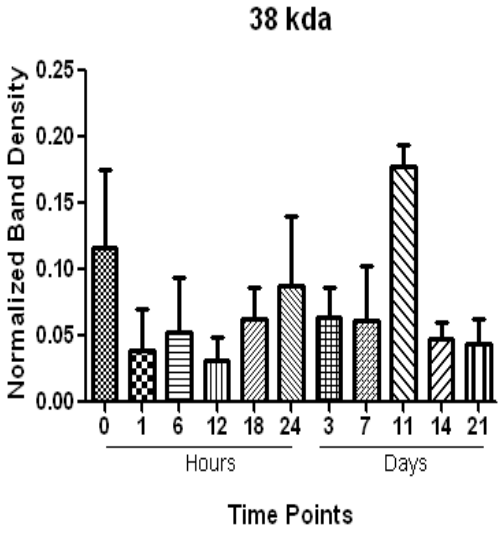
38 kda
Normalized Band Density
0.25
0.20
0.15
0.10
0.05
0.00
0 1 6 12 18 24 3 7 11 14 21
Hours
Days
Time Points

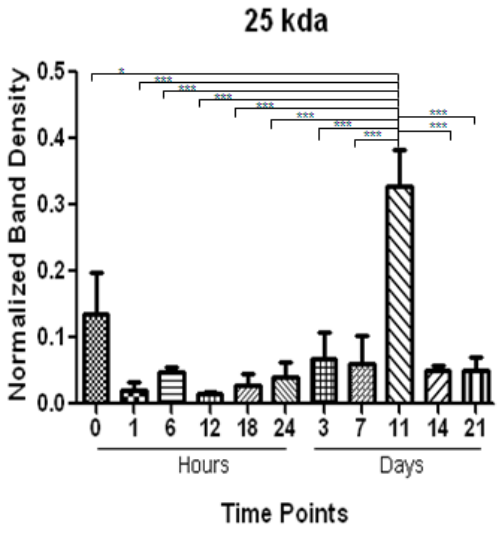
25 kda
Normalized Band Density
0.5
0.4
0.3
0.2
0.1
0.0
0 1 6 12 18 24 3 7 11 14 21
Hours
Days
Time Points

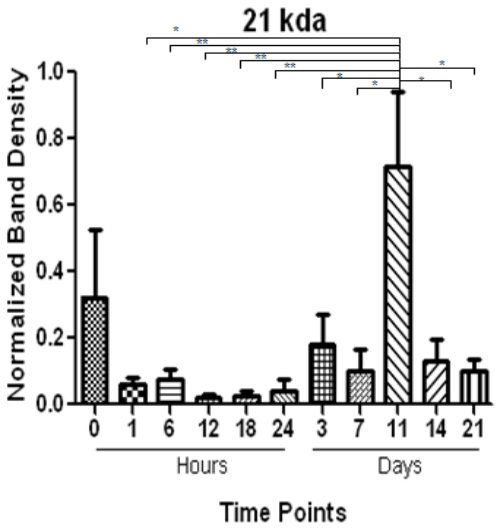

Figure 3-10. Western blot analysis of CTGF throughout a time course of wound healing after ablation from rat corneal homogenates. A) Shows a typical western blot of the time course was performed to look at expression of lower molecular weight forms of CTGF using the US Biological polyclonal antibody. B) Quantification of individual CTGF bands (38 kDa, 25kDa and 21 kDa) were performed from replicate blots (n=4). Variation between blots were normalized by comparing each band to a rCTGF standard. The upper molecular weight band (75 kDa) was due to off target bind of the strepavidin labeled Licor dye. Band intensities were compared by analysis of variance (ANOVA) with a Tukey's post-hoc test with significance of $0.01<p<0.05$ indicated by * , $0.001<p<0.0099$ indicated by **, and $p<0.0001$ indicated by ***.

CHAPTER 4
DEVLEOPMENT OF A THERAPEUTIC GENE SILENCING TECHNIQUE UTILIZING RIBOZYMES AND RNAI IN A SELF COMPLEMENTARY ADENO-ASSOCIATED VIRAL VECTOR

Reduction of Scar Formation

There currently are no approved drugs that selectively reduce the expression of genes causing corneal scarring and haze. Scarring of the cornea can be due to many factors such as trauma, infection and surgical procedures. Mitomycin C is a nonspecific anticancer drug that is used during some ocular surgeries to reduce scarring. Although this treatment has been shown to reduce fibrosis after other ocular treatments, it also may have very damaging side effects. These side effects can include epithelial defects, stromal melting, endothelial damage, and conjunctival thinning[132, 133]. Thus, there is a need for an effective anti-scarring drug that specifically targets fibrotic genes like TGF-β1 and avoids non-specific serious side effects that threaten vision.

Gene Therapy

Hammerhead ribozymes are small, self-cleaving RNAs that contain a conserved catalytic core that cleaves the a specific targeted mRNA[188,143 144]. siRNAs are another very common gene silencing technology. siRNAs are double stranded RNA molecules that are 19-25 nucleotides long [139] and are incorporated into the multi-protein complex called the RNA Induced Silencing Complex or RISC. Within the RISC complex, the sense strand of the siRNA is degraded [140]. Once the sense strand is cleaved, the siRNA recognizes mRNAs by sequence complementarity [141]. The target mRNA is then cleaved which allows for silencing of the gene. We used an adeno-associated virus (AAV) vector, that allows with only a single application, delivery of these gene silencing techniques to the cornea. AAV is a single-stranded DNA virus that non-pathogenic.

Wild-type virus integrates into chromosome 19 of the host genome[161]. The recombinant AAV lacks the *rep gene* necessary for this integration, as well as the *cap gene* that encodes for the viral capsid proteins. The recombinant virus is made by replacing the *rep* and *cap* genes with the gene of interest driven by a promoter sequence. Rapid expression of either a ribozyme or a siRNA, is a key component to reduce the formation of corneal fibrosis because the initiation of wound healing is immediate after an injury. Self-complementary AAV (scAAV), which is double stranded, has been shown to have a faster onset of gene expression because the scAAV DNA is transcribed into RNA rapidly[172, 173]. In addition, scAAV generally has higher transduction efficiency than conventional rAAV vectors[189].

In this study, we investigated the use of gene silencing technologies, ribozymes and siRNAs that target these profibrotic transcripts. We hypothesized that we would be able to identify at least two siRNAs for each rat TGF-β1 or CTGF that had a relative knockdown of at least 50% using a secreted alkaline phosphatase reporter assay. We next hypothesized the ribozymes targeting either TGF-β1 or CTGF would have a significant knockdown when compared to the control vector. The scAAV should have a fast onset; therefore, we suspected that after 2 days GFP expression would be detected in the epithelial and stromal cells of the cornea. Finally, we believed we would see a knockdown of CTGF protein after treating an ablated rat cornea with scAAV-CTGF-Active-Rz.

In vitro Analysis of Gene Silencing Techniques

To quickly test and identify the siRNAs and ribozymes that strongly associate and cleave the target profibrotic factors, TGF-β1 and CTGF, a secreted alkaline

phosphatase (sAP) assay was employed. Briefly, an approximately 300 bp region of the target gene was inserted into the psAP-Bluescript plasmid after the sAP gene (Figure 2-1). In HEK293 cells, a dual transfection was performed with either the siRNA or ribozyme and the target containing psAP-Bluescript plasmid. If the target gene were cleaved, then there would be a reduction in sAP. A control siRNA or plasmid that did not target the 300 bp region of the psAP-Bluescript plasmid was employed as a control and compared to the target siRNAs or ribozyme containing plasmid. The length of transfection and the concentration of the siRNAs and ribozymes(will psAP-Bluescript was held constant) were varied and tested. The relative knockdown was determined by comparing sAP concentration compared to the control plasmid or scrambled siRNA and a student t-test was performed to determine statistical significance.

Analysis of siRNAs targeting rat TGF-β1 Using the Secreted Alkaline Phosphatase Assay

In tissue culture in HEK293 cells, after a 24 hour transfection, at a concentration of 8 nM of siRNA (and the psAP-Bluescript plasmid concentration was held constant), siRNA 90 produced a 47% relative reduction of sAP compared to the control scramble siRNA. When the concentration of the siRNA was increased to 20nM, siRNA 90 and siRNA 86 had 29% and 12% relative knockdowns of sAP, respectively. At the greatest concentration, 40nM, 4 out of 6 siRNAs produced a statistically significant reduction of sAP. At 40 nM, siRNA 86, siRNA 70, siRNA 88 and siRNA 90 had a relative knockdown of sAP greater than 25% and siRNA 86 had the highest level of knockdown at 42 % (Figure 4-1).

After a 48 hour transfection, at concentrations of 8 nM and 20 nM, siRNA 90 was the only siRNA to produce a statistically significant knockdown of 54% and 64%,

respectively. At a concentration of 40 nM, siRNA 70, siRNA 90, and siRNA 92 produced a significant knockdown of at least 16% with siRNA 90 producing the highest level of knockdown at 48%.

After 72hrs and a concentration of 8 nM, siRNA 90, siRNA 70 and siRNA 86 led to 67%, 29% and 40% reductions of sAP expression, respectively. At 20 nM, siRNA 90 and siRNA 86 reduced the expression of sAP by 59% and 38%, respectively. At a concentration of 40 nM, siRNA 70, siRNA 90, and siRNA 92 produced a significant knockdown of at least 25% with siRNA 90 producing the highest level of knockdown of 59%.

Analysis of siRNAs targeting rat CTGF Using the Secreted Alkaline Phosphatase Assay

After a 24 hour transfection, at a concentration of 8 nM, siRNA 36 and siRNA 37 produced 36% and 40% relative knockdowns of sAP compared to the control scrambled siRNA. When the concentration of the siRNA was increased to 20 nM, siRNA 36 and siRNA 37 had 38% and 40% relative knockdowns of sAP, respectively. At the greatest concentration, 40 nM, siRNA 36 and siRNA 37 had relative sAP knockdowns of 41% and 38%, respectively (Figure 4-2).

After a 48 hour transfection, at a concentration of 8 nM, siRNA 36 and siRNA 37 caused relative sAP knockdowns greater than 35%. Both siRNA 36 and siRNA 37 had relative sAP knockdowns of greater than 40% at a concentration of 20 nM of siRNA. At a concentration of 40 nM, siRNA 36 and siRNA 37 produced a significant knockdown of at least 50% with siRNA 37 producing the highest level of knockdown at 52%.

After 72 hrs and a concentration of 8 nM, siRNA 36, and siRNA 37 had a 29% and 31% reduction of sAP expression, respectively. At 20 nM, siRNA 36 and siRNA 37

reduced the expression of sAP by 43% and 46%, respectively. At a concentration of 40 nM, siRNA 36, and siRNA 37 produced a significant knockdown greater than 49%.

Analysis of Ribozymes Targeting TGF-β1 and CTGF Using the Secreted Alkaline Phosphatase Assay

Both ribozymes were cloned into a scAAV vector and were tested using the sAP assay to determine their ability to cleave their specific gene target. When a single nucleotide in the active region of a ribozyme is changed, it will make it inactive [143]. A GFP plasmid that did not contain any sequences that were complementary to the sAP target plasmid was used as a control.

After a 24 hour transfection, the scAAV-TGF-β1-Active-Rz reduced the relative level of sAP by 22% and was statistically significantly different from the control(Figure 4-3). There was a slight decrease of sAP when compared to the scAAV-TGF-β1-Inactive-Rz. After a 48 hours transfection, the scAAV-TGF-β1-Inactive-Rz reduced the relative level of sAP significantly by 15% compared to the control. The scAAV-TGF-β1-Active-Rz significantly reduced the relative sAP by 28% when compared to the control and 13% when controlled to the scAAV-TGF-β1-Inactive-Rz.

After a 24 hour transfection, the scAAV-CTGF-Active-Rz produced a significant knockdown of 9%. After a 48 hour transfection, the scAAV-CTGF-Active-Rz reduced the relative level of sAP significantly by 24% compared to both the control and the scAAV-CTGF-Inactive-Rz. A 30% knockdown compared to control and the scAAV-CTGF-Inactive-Rz was achieved by the scAAV-CTGF-Active-Rz after a 72 hour transfection (Figure 4-4).

Delivery of scAAV-GFP to Rabbit Corneas

In order to determine the ability of a scAAV to infect the cornea, a scAAV expressing GFP was applied to the rabbit cornea after ablation. At several time points, 0, 1, 2, 3, 4, 7, 30 and 6 months, the animals were scarified and corneas were fixed and sectioned. Direct GFP fluorescence was analyzed by confocal microscopy (Figure 4-5).

The GFP fluorescence was first detected 24 hours after application and the peak fluorescence detected occurred at 7 days. Day 7 fluorescence was 22 times greater than day 0 ($p<0.05$). Level of the fluorescence from 6 months was unchanged from day 0 levels of fluorescence(Figure 4-6). The transgene was expressed in all cell types of the cornea: epithelium, keratocytes and endothelium (Figure 4-7).

Delivery of scAAV-CTGF-Active-Rz to Rat Corneas after Ablation

To determine the ability of the scAAV-CTGF-Active-Rz to reduce CTGF *in vivo*, we applied the scAAV-CTGF-Active-Rz to the rat cornea after ablation. At 14 days, the animals were scarified and corneas were homogenized. The CTGF concentration was determined using ELISA and was normalized by the total protein of the sample. After 14 days, the treated corneas had a significant knockdown ($p<0.05$) of 19% when compared to the PBS controls (Figure 4-8).

Discussion

We previously showed the usefulness of using the sAP reporter assay to analyze knockdown by a CTGF ribozyme [177]. Here, we were able to use the sAP reporter assay to identify 2 siRNAs that target either TGF-β1 or CTGF by at least 50%. siRNAs 36 and siRNA 37 targeting CTGF showed the greatest relative knockdown of sAP at all time points (24, 48 and 72 hrs) and at all concentrations(8, 20, and 40 nM). Interestingly, some of the concentration of siRNAs 56 and 83 targeting CTGF had an increase in sAP

when the control siRNA was added. Although the control siRNA was screen for complementarity to the target CTGF region, there may have been some off target antisense affects of the control siRNA reducing concentration of the sAP. For the siRNAs targeting TGF-β1, siRNA 90 had the most significant knockdown at all time points (24, 48 and 72 hours) and at all concentrations (8, 20, and 40 nM). siRNA 70 had the second greatest ability to target the TGF-β1 sequence; its significance was demonstrated at 24 hours for 20 and 40 nM and at 72 hours for 8, 20 and 40 nM. While this reporter system is not perfect, it allows for quick vetting of several siRNAs at different transfection time points and concentrations.

We next used the sAP report assay to assess the relative knockdown of sAP due to the transfection of either the scAAV-CTGF-Active-Rz vector or the scAAV-TGF-β1-Active-Rz vector. As previously mentioned, changing a single nucleotide in the catalytic core of the ribozyme will make it inactive. We also tested the inactive forms of these ribozymes (scAAV-TGF-β1-Inactive-Rz and scAAV-CTGF-Inactive-Rz) and a control plasmid that expressed GFP and not any form of ribozyme. For the ribozymes targeting TGF-β1, we found that the scAAV- TGF-β1-Rz was able to statistically significantly reduce the relative sAP level at all time points (24 and 48 hours) by at least 22% when compared to the GFP control. At 48 hours, the scAAV-TGF-β1-Inactive-Rz had an antisense quality of reducing the sAP relative expression compared to the GFP control. Even with this antisense quality, the scAAV- TGF-β1-Active-Rz statistically significantly reduced the relative sAP expression by 13 % when compared to the scAAV-TGF-Active-β1-Inactive-Rz. For the ribozymes targeting CTGF, we found that the scAAV-CTGF-Active-Rz was able to statistically significantly reduce the relative sAP level at all

time points (24, 48 and 72 hours) by at least 9% when compared to the GFP control at 24 hours and a maximum of 30% at 72 hours. The scAAV-CTGF-Inactive-Rz did not have an antisense quality.

There have been several studies of gene targeting techniques to target CTGF and TGF-β1. The Schultz laboratory has shown the kinetic abilities and *in vitro* knockdown of endogenous mRNA and protein of both the CTGF and the TGF-β1 ribozymes [190,177]. We took these ribozymes and inserted them into a scAAV vector and tested this vector in the sAP reporter assay to confirm that the ability to selectively knockdown the target would not be lost if it was put into a scAAV vector. Jester *et al*.[92] used antibodies targeting TGF-β1 to inhibit corneal fibrosis. They found that the antibodies reduced the expression of fibronectin. This targeted method has not been pursued for two reasons: multiple doses of the antibody needed to be delivered and re-epitheliazation of the cornea (which occurs within days of injury) may block the antibody's ability to penetrate into the cornea. Sugioka *et al.* [191] were able to use siRNAs targeting CTGF to reduce the expression levels of fibronectin in corneal epithelium cells. These experiments were only preformed *in vitro* and not *in vivo*. Chen *et al.* used a pyrrole-imidazole polyamide to target the activator protein-1 binding site of TGF-β1 in a rat alkali burn model. They found that inhibition of this promoter site for TGF-β1 by the pyrrole-imidazole polyamide reduced the haze in the cornea. These data suggest that by using either a ribozyme or a siRNA targeting TGF-β1 or CTGF, we may be able to reduce scar formation in the cornea after ablation.

We next looked at the delivery of the scAAV to the cornea by using the scAAV-GFP virus. AAV has been shown to be able to deliver a transgene to the cornea more

efficiently than the transfection of a plasmid [170]. We found the GFP fluorescence was first detected 24 hours after application and the peak fluorescence detected occurred at 7 days. Day 7 fluorescence was 22 times greater than day 0. Levels of the fluorescence from day 180 were statistically the same as day 0 levels of fluorescence. The transgene was expressed in all cell types of the cornea: epithelium, keratocytes and endothelium. We used the AAV-1 serotype that was shown to have the greatest expression levels of the GFP transgene in all cells in the cornea [192]. In the retina, it was found that scAAV transgene expression was detected at 2 days after injection [173]. We found initial expression of the GFP transgene as early as 24 hours after transduction. We finally analyzed the scAAV-CTGF-Active-Rz ability to knockdown CTGF the rat cornea after ablation. Fourteen days after ablation, we found that the rat corneas treated with the scAAV-CTGF-Active-Rz had a significant knockdown of CTGF at 19% when compared to the control corneas. The rat ablation model does not exhibit a robust scar formation and therefore, this scAAV-CTGF-Active-Rz needs to be tested in the rabbit corneal ablation model to analyze it ability to reduce haze.

In summary, we were able to test two different gene silencing techniques (ribozymes and siRNAs) using the sAP reporter assay. Additionally, we were able to analyze the ability of the scAAV to transduce the cornea. Finally, we were able to show that a scAAV-CTGF-Active-Rz delivered to the cornea after ablation could reduce the level of CTGF. These data taken together show promise for siRNAs and ribozymes to be used to reduce scar formation in the cornea after injury.

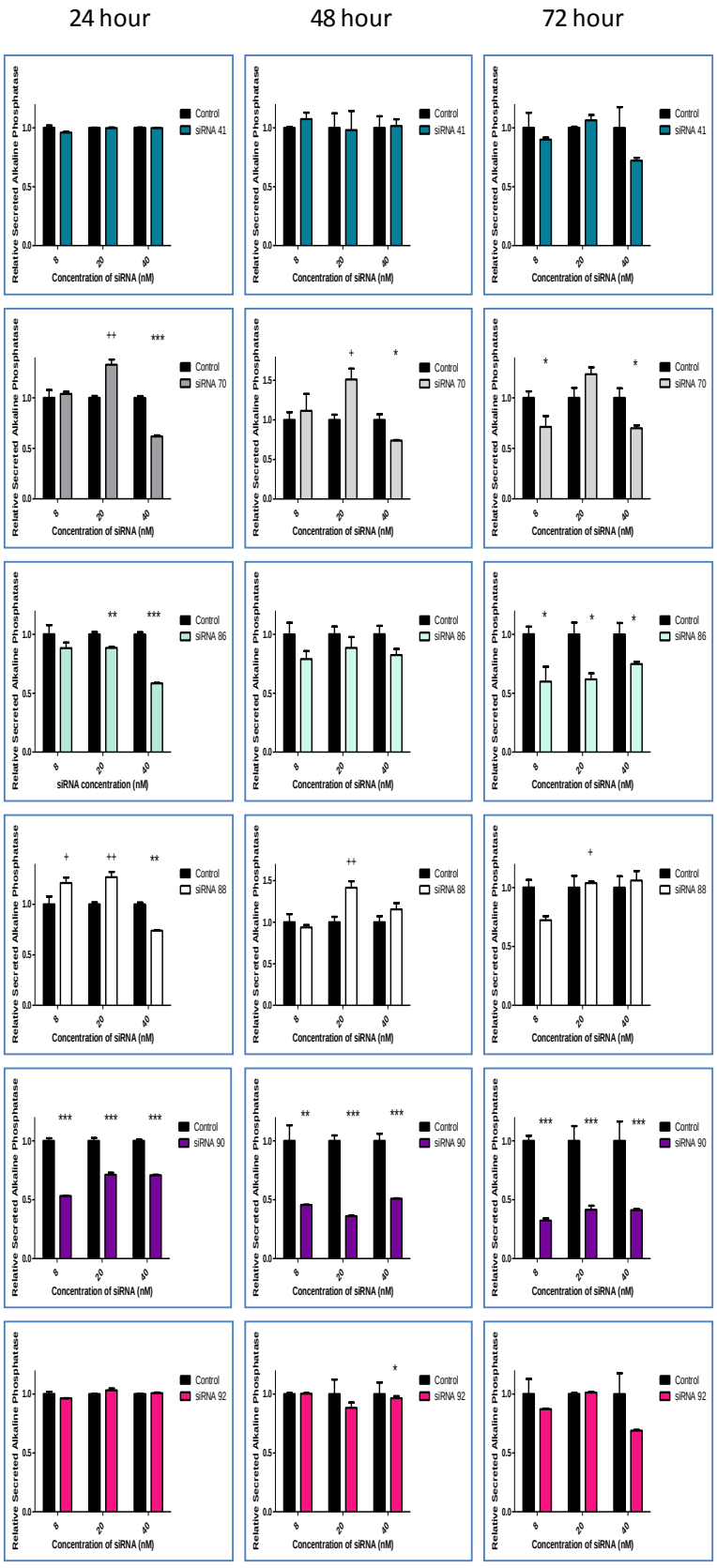
24 hour
48 hour
72 hour
Relative Secreted Alkaline Phosphatase
Concentration of siRNA (nM)
siRNA concentration (nM)
Control
siRNA 41
siRNA 70
siRNA 86
siRNA 88
siRNA 90
siRNA 92

Figure 4-1. Analysis of six siRNAs targeting TGF-β1 using a sAP reporter assay. All of the data is reported as relative knockdown compared to a scramble siRNA. Three different time points after transfection (24, 48 and 72 hrs) were analyzed along with three different concentrations of siRNA (8, 20, and 40 nM). Relative reduction of sAP from the control compared to the siRNA treated group were compared by student t-test with significance of $0.01<p<0.05$ indicated by *, $0.001<p<0.0099$ indicated by **, and $p<0.0001$ indicated by ***. In a few cases, the siRNA caused an increase in sAP and were statistically significant ($0.01<p<0.05$ indicated by + and $0.01<p<0.05$ indicated by ++)

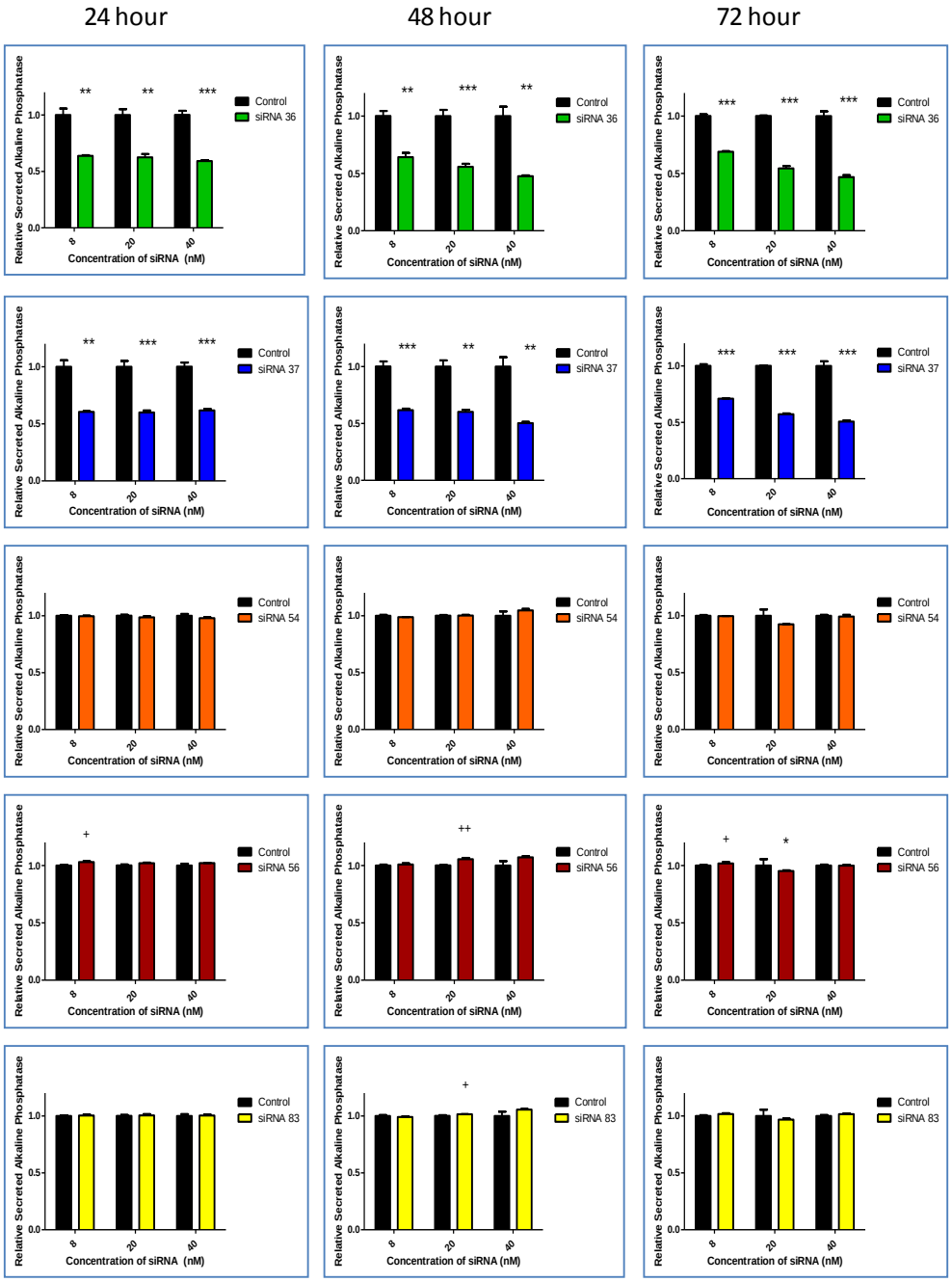

Figure 4-2. Analysis of five siRNAs targeting CTGF using a sAP reporter assay. All of the data is reported as relative knockdown compared to a scrambled siRNA. Three different time points after transfection (24, 48 and 72 hrs) were analyzed along with three different concentrations of siRNA (8, 20, and 40 nM). Relative reduction of sAP from the control compared to the siRNA treated group were compared by student t-test with significance of $0.01<p<0.05$ indicated by *, $0.001<p<0.0099$ indicated by **, and $p<0.0001$

indicated by ***. In a few cases, the siRNA caused an increase in sAP and were statistically significant (0.01<p<0.05 indicated by + and 0.01<p<0.05 indicated by ++)

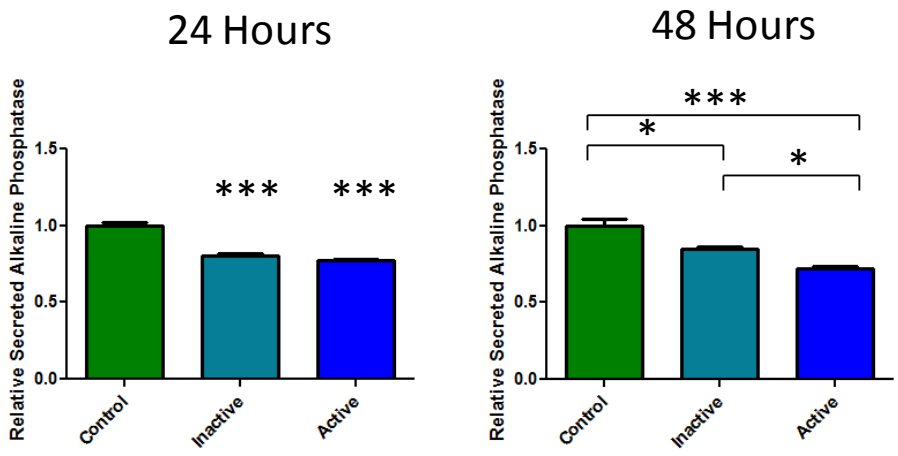

Figure 4-3. Analysis of scAAV-TGF-β1-Active-Rz and scAAV-TGF-β1-Inactive-Rz using a sAP reporter assay. All of the data is reported as relative knockdown compared to a scAAV-GFP. Two different time points after transfection(24 and 48 hours) were analyzed. Relative reduction of sAP from the control compared to the ribozyme treated groups were compared by ANOVA with significance of $0.01<p<0.05$ indicated by *, and $p<0.0001$ indicated by ***.

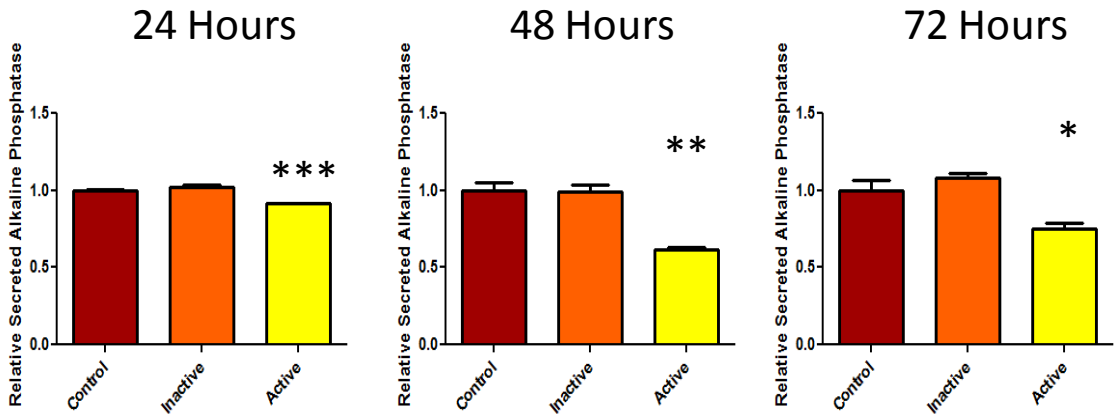

Figure 4-4. Analysis of scAAV-CTGF-Active-Rz and scAAV-CTGF-Inactive-Rz using a sAP reporter assay. All of the data is reported as relative knockdown compared to a scAAV-GFP. Two different time points after transfection(24 and 48 hours) were analyzed. Relative reduction of sAP from the control compared to the ribozyme treated groups were compared by ANOVA with significance of $0.01<p<0.05$ indicated by *, $0.001<p<0.0099$ indicated by **, and $p<0.0001$ indicated by ***.

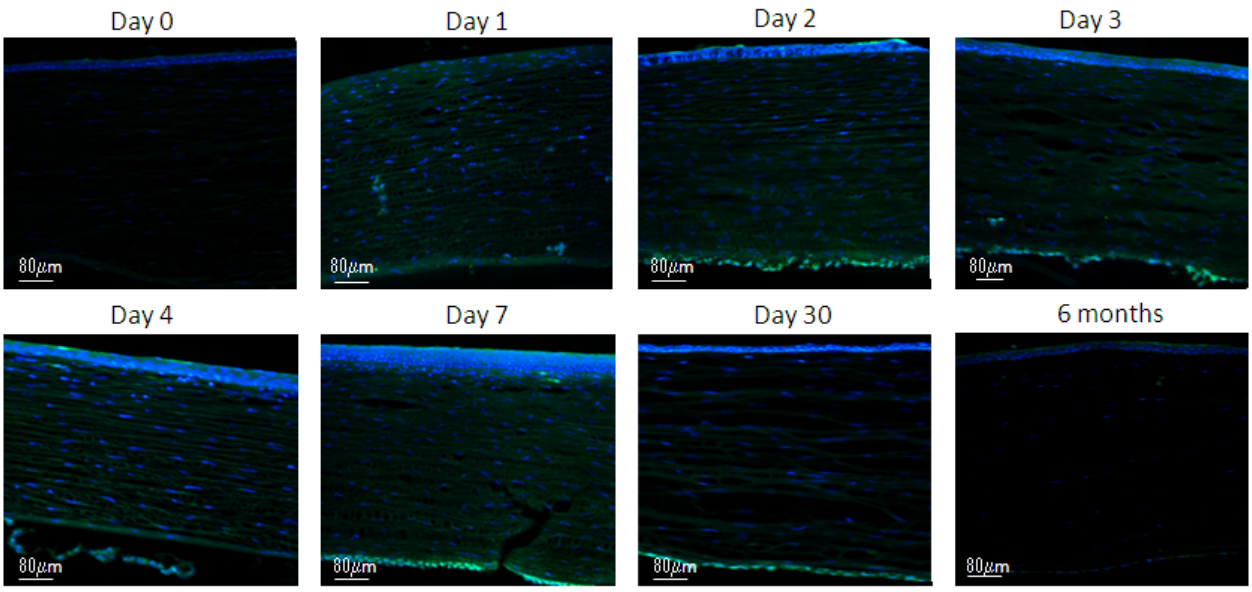

Figure 4-5. Analysis of GFP expression in rabbit corneas treated with scAAV-GFP after ablation using direct fluorescence microscopy.

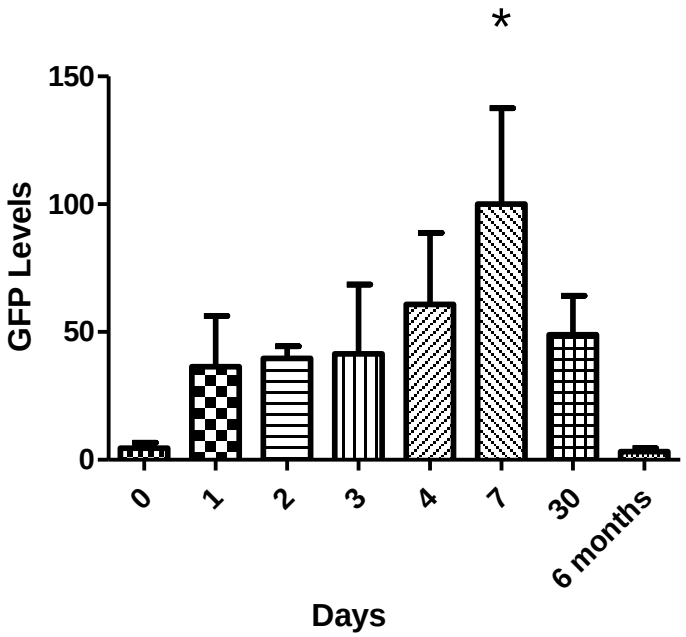

Figure 4-6. Relative levels of GFP fluorescence in rabbit corneas treated with scAAV-GFP after ablation. Statistical significance indicated with a * ($p<0.05$)

A

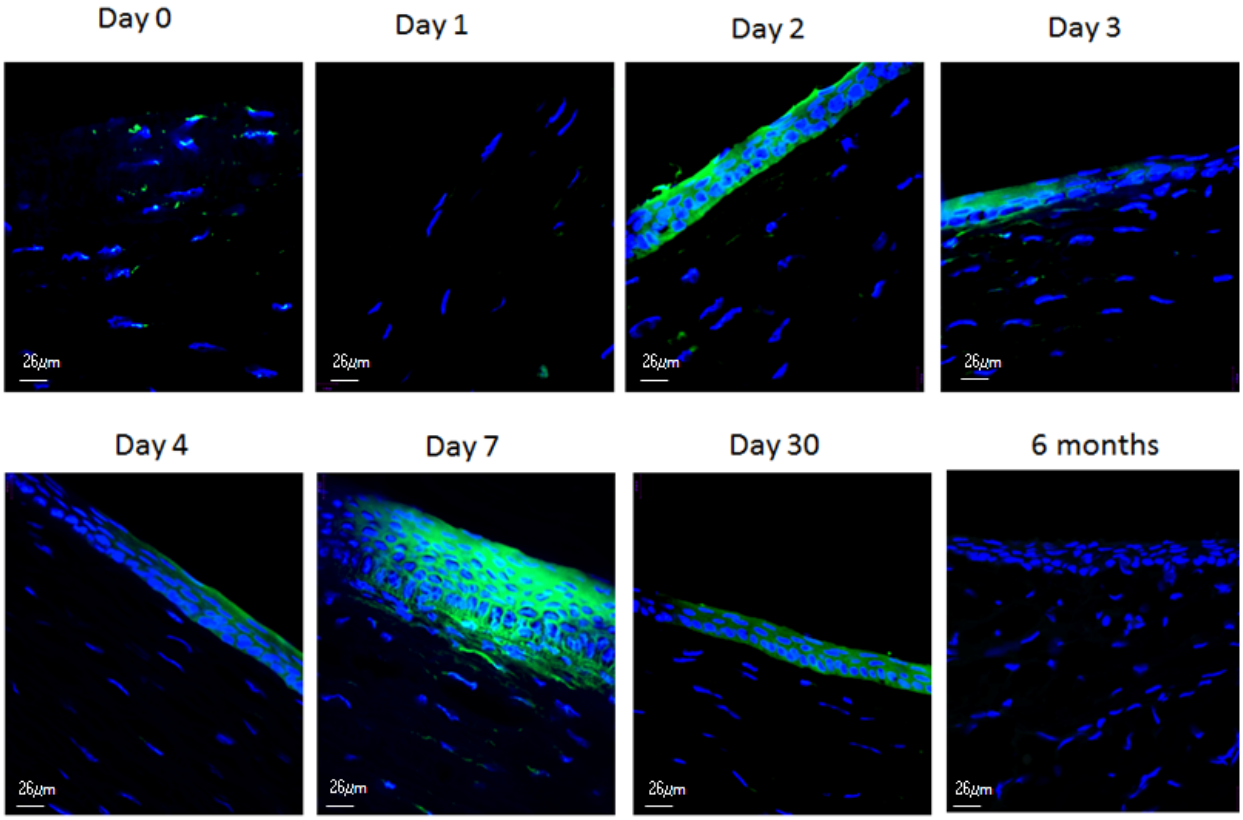

B

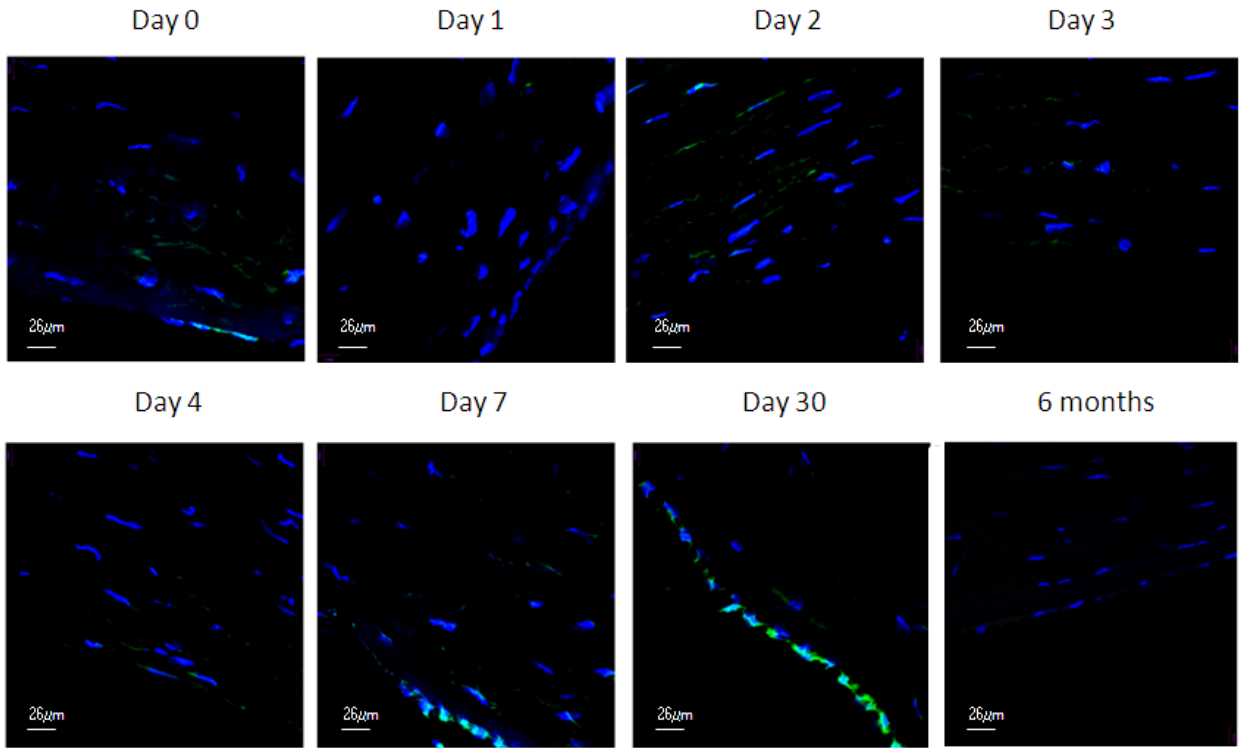

Figure 4-7. Analysis of GFP expression in rabbit corneas treated with scAAV-GFP after ablation using direct fluorescence microscopy. Specifically the A) epithelium and B) endothelium are pictured.

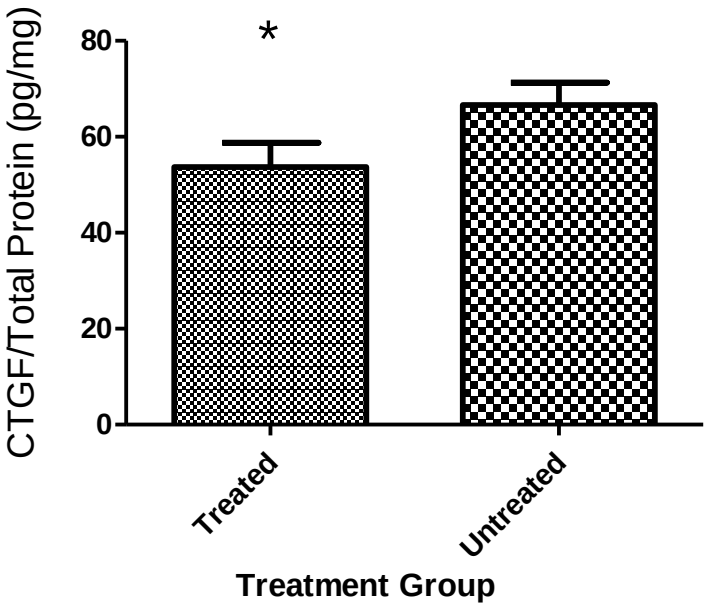

Figure 4-8. Ratio of CTGF to total protein in rat corneas treated with scAAV-CTGF-Active-Rz or PBS control after ablation at day 14. Statistical significance indicated with a * ($p<0.05$).

CHAPTER 5
CONCLUSIONS AND FUTURE DIRECTIONS

CTGF Proteolytic Processing

The proteolytic processing of CTGF into smaller fragments has been well documented, including CTGF being processed in the HCF wound-healing model[126]. While we confirmed processing in the HCF wound-healing model, we also gained a further understanding about the processing of CTGF by elucidating the class of protease that cleaves CTGF into the 21 kDa fragment *in vitro* (Figure 3-5). We were able to identify that the protease was an aspartic acid protease. Our next aim will be to determine the specific protease that cleaves the CTGF *in vivo.*

In unwounded whole eye homogenates (Figure 3-6) and individual structures of the eye (Figure 3-7), we found that CTGF was present primarily as the 21 kDa and 25 kDa fragments. We hypothesize that this 21 kDa fragment is the same fragment that we found in the HCF wound healing model. We would be able to confirm that it is the same fragment by having both peptides (the *in vitro* and *in vivo* 21 kDa fragments) sequenced using Edman degradation. This would not only confirm that the 21 kDa fragment is the same, it would also identify where CTGF is proteolytically processed. We have sent some of the fragments for Edman degradation, but the sequence was not properly identified, possibly because of a low concentration of the fragment when compared to total protein of the sample. If even at high concentrations of the 21 kDa fragment, Edman degradation does not produce a CTGF sequence, then the cleavage site could be determined by using a site directed mutagenesis assay. By altering one amino acid at a time, we could identify which amino acid is necessary in order for CTGF to be proteolytically processed into the 21 kDa form.

We were also able to follow the production of CTGF fragments throughout wound healing in rat corneas after ablation (Figure 3-10). We were able to see fragmentation in the unwounded cornea at day 0, and by day 11 there was an increase in all forms of CTGF (38 kDa, 25 kDa, and 21 kDa). We identified these fragments using the US Biological polyclonal antibody that targets the whole CTGF peptide. Therefore, we are unable to make any conclusions as to which domains were present in the 21 kDa fragment throughout wound healing in the cornea. Previously, the N-terminal of CTGF was shown to be elevated in scleroderma patients[130]. We would also like to analyze the presence of the N-terminal and C-terminal fragments during wound healing. These findings will better define the role of the fragments of CTGF throughout wound healing in the cornea.

We made tremendous progress in analyzing the proteolytic processing of CTGF in both the *in vitro* and *in vivo* corneal wound healing models. These experiments demonstrate the abundance of the processed CTGF 21 kDa form in the unwounded cornea and these findings parallel the findings from Brigstock[120] that showed the lower molecular weight fragment were the primary form in porcine uterine flushings. These findings have great importance for the area of wound healing, not only in the cornea, but throughout the different tissues in the body because CTGF is a major player in the wound healing cascade. It is necessary to identify the role of the fragmentation, in order to gain a better understanding of scar formation in all tissues.

Reduction of Corneal Haze by Targeting Profibrotic Growth Factors

The TGF-β1 system, which includes CTGF as a downstream mediator of TGF-β1, has been shown to play a key role in the formation of haze in the cornea.

Therefore, attenuating the activity of these two profibrotic genes could help reduce scar formation. We were able to quickly and efficiently analyze two forms of gene silencing techniques (siRNAs and ribozymes) for their ability to target TGF-β1 or CTGF using a sAP reporter assay. We had success in finding at least two siRNAs that targeted either TGF-β1 or CTGF, and the ribozymes were able to target and cleave the TGF-β1 or CTGF sequence (Figure 4-1, Figure 4-2, Figure 4-3, and Figure 4-4). Since naked mRNA has a short half-life, an alternate strategy for delivery of these gene silencing techniques is necessary. Encoding these gene silencing techniques in a scAAV would circumvent the problem of half-life. We found that when the cornea is transduced by scAAV-GFP, there was expression of GFP in all the layers of the cornea and the initiation of the expression began within 24 hour (Figure 4-5, Figure 4-6, and Figure 4-7). These findings produce a greater understanding of when and where the scAAV transgenes are expressed. Therefore, we could express any number of small genes (not just ribozymes or siRNAs) in the cornea to evaluate their ability to influence corneal scar formation.

Finally, we were also able to analyze the ability of scAAV-CTGF-Active-Rz to reduce CTGF protein in the rat corneas 14 days after ablation (Figure 4-8). Unfortunately, scar formation in the rat cornea after ablation is not robust. Therefore, we would like to apply this scAAV-CTGF-Active-Rz to the rabbit cornea after ablation, which is a standard model for corneal wound healing. These ribozymes and siRNAs could be used in several different tissues to reduce scar formation because the mRNA sequences of CTGF or TGF-β1 are the same all tissues.

We also would like to analyze the ability of the siRNAs to reduce scar formation in the rabbit model. The siRNAs could be expressed in a scAAV as a short hairpin RNA (shRNA) that would be processed into the siRNA within the cell. We also have experience with iontophoresis of anti-sense oligos into the cornea, therefore, the siRNAs could also be delivered to the cornea using iontohphoresis. These future experiments will help our understanding of the roles of TGF-β1 and CTGF in corneal wound healing. These results indicate that targeting CTGF and TGF-β1 using either a ribozyme or siRNA may help reduce scar formation in the cornea. In conclusion, these findings have made significant progress in understanding the processing of CTGF in corneal wound healing and developing a gene silencing technique to target profibrotic growth factors.

LIST OF REFERENCES

1. Yamada,N., Yanai,R., Inui,M., & Nishida,T. Sensitizing effect of substance P on corneal epithelial migration induced by IGF-1, fibronectin, or interleukin-6. *Invest Ophthalmol. Vis. Sci.* **46**, 833–839 (2005).

2. Chaudhuri,A., Hallett,P.E., & Parker,J.A. Aspheric curvatures, refractive indices and chromatic aberration for the rat eye. *Vision Res.* **23**, 1351–1363 (1983).

3. Choi,D.M., Thompson Jr,R.W., & Price Jr,F.W. Incisional refractive surgery. *Curr. Opin. Ophthalmol.* **13**, 237–241 (2002).

4. Otori,T. Electrolyte content of the rabbit corneal stroma. *Exp. Eye Res.* **6**, 356–367 (1967).

5. Sawada,H., Konomi,H., & Nagai,Y. The basement membrane of bovine corneal endothelial cells in culture with beta-aminopropionitrile: biosynthesis of hexagonal lattices composed of a 160 nm dumbbell-shaped structure. *Eur. J. Cell Biol.* **35**, 226–234 (1984).

6. Grant,D.S. & Leblond,C.P. Immunogold quantitation of laminin, type IV collagen, and heparan sulfate proteoglycan in a variety of basement membranes. *J. Histochem. Cytochem.* **36**, 271–283 (1988).

7. Fujikawa,L.S., Foster,C.S., Harrist,T.J., Lanigan,J.M., & Colvin,R.B. Fibronectin in healing rabbit corneal wounds. *Lab Invest* **45**, 120–129 (1981).

8. Noske,W., Levarlet,B., Kreusel,K.M., Fromm,M., & Hirsch,M. Tight junctions and paracellular permeability in cultured bovine corneal endothelial cells. *Graefes Arch. Clin. Exp. Ophthalmol.* **232**, 608–613 (1994).

9. Dawson,D.G., O'Brien,T.P., & Edelhauser,H.F. Long-term corneal keratocyte deficits after PRK and LASIK: in vivo evidence of stress-induced premature cellular senescence. *Am. J. Ophthalmol.* **141**, 918–920 (2006).

10. Fischbarg,J. & Lim,J.J. Determination of the impedance locus of rabbit corneal endothelium. *Biophys. J.* **13**, 595–599 (1973).

11. Tuli,S., Goldstein,M., & Schultz,G.S. Modulation of Corneal Wound Healing in *Cornea* (eds. Krachmer,J.H., Mannis,J.M. & Holland,E.J.) 133–150 (Elsevier Mosby, Philadelphia, 2005).

12. Barnes,S.D. & Azar,D.T. Laser subepithelial keratomileusis: not just another way to spell PRK. *Int. Ophthalmol. Clin.* **44**, 17–27 (2004).

13. Taneri,S., Zieske,J.D., & Azar,D.T. Evolution, techniques, clinical outcomes, and pathophysiology of LASEK: review of the literature. *Surv. Ophthalmol.* **49**, 576–602 (2004).

14. Seiler,T. & McDonnell,P.J. Excimer laser photorefractive keratectomy. *Surv. Ophthalmol.* **40**, 89–118 (1995).

15. Alio,J.L. *et al.* Ten-year follow-up of photorefractive keratectomy for myopia of more than -6 diopters. *Am. J. Ophthalmol.* **145**, 37–45 (2008).

16. Carones,F., Fiore,T., & Brancato,R. Mechanical vs. alcohol epithelial removal during photorefractive keratectomy. *J. Refract. Surg.* **15**, 556–562 (1999).

17. Shah,S., Sebai Sarhan,A.R., Doyle,S.J., Pillai,C.T., & Dua,H.S. The epithelial flap for photorefractive keratectomy. *Br. J. Ophthalmol.* **85**, 393–396 (2001).

18. Shahinian,L., Jr. Laser-assisted subepithelial keratectomy for low to high myopia and astigmatism. *J. Cataract Refract. Surg.* **28**, 1334–1342 (2002).

19. Netto,M.V. *et al.* Wound healing in the cornea: a review of refractive surgery complications and new prospects for therapy. *Cornea* **24**, 509–522 (2005).

20. Walker,M.B. & Wilson,S.E. Incidence and prevention of epithelial growth within the interface after laser in situ keratomileusis. *Cornea* **19**, 170–173 (2000).

21. Helena,M.C., Baerveldt,F., Kim,W.J., & Wilson,S.E. Keratocyte apoptosis after corneal surgery. *Invest Ophthalmol. Vis. Sci.* **39**, 276–283 (1998).

22. Taneri,S., Feit,R., & Azar,D.T. Safety, efficacy, and stability indices of LASEK correction in moderate myopia and astigmatism. *J. Cataract Refract. Surg.* **30**, 2130–2137 (2004).

23. Nagano,T. *et al.* Stimulatory effect of pseudomonal elastase on collagen degradation by cultured keratocytes. *Invest Ophthalmol. Vis. Sci.* **42**, 1247–1253 (2001).

24. Chen,C.C., Chang,J.H., Lee,J.B., Javier,J., & Azar,D.T. Human corneal epithelial cell viability and morphology after dilute alcohol exposure. *Invest Ophthalmol. Vis. Sci.* **43**, 2593–2602 (2002).

25. Kim,S.Y., Sah,W.J., Lim,Y.W., & Hahn,T.W. Twenty percent alcohol toxicity on rabbit corneal epithelial cells: electron microscopic study. *Cornea* **21**, 388–392 (2002).

26. Alio,J.L., Ortiz,D., Muftuoglu,O., & Garcia,M.J. Ten years after photorefractive keratectomy (PRK) and laser in situ keratomileusis (LASIK) for moderate to high myopia (control-matched study). *Br. J. Ophthalmol.* **93**, 1313–1318 (2009).

27. Freathy,R.M. *et al.* Variants in ADCY5 and near CCNL1 are associated with fetal growth and birth weight. *Nat. Genet.*(2010).

28. Mohan,R.R. *et al.* Apoptosis in the cornea: further characterization of Fas/Fas ligand system. *Exp. Eye Res.* **65**, 575–589 (1997).

29. Mohan,R.R., Mohan,R.R., Kim,W.J., & Wilson,S.E. Modulation of TNF-alpha-induced apoptosis in corneal fibroblasts by transcription factor NF-kappaB [In Process Citation]. *Invest Ophthalmol. Vis. Sci.* **41**, 1327–1336 (2000).

30. Mohan,R.R., Kim,W.J., Mohan,R.R., Chen,L., & Wilson,S.E. Bone morphogenic proteins 2 and 4 and their receptors in the adult human cornea. *Invest Ophthalmol. Vis. Sci.* **39**, 2626–2636 (1998).

31. Wilson,S.E., Chen,L., Mohan,R.R., Liang,Q., & Liu,J. Expression of HGF, KGF, EGF and receptor messenger RNAs following corneal epithelial wounding. *Exp. Eye Res.* **68**, 377–397 (1999).

32. Tuominen,I.S. *et al.* Human tear fluid PDGF-BB, TNF-alpha and TGF-beta1 vs corneal haze and regeneration of corneal epithelium and subbasal nerve plexus after PRK. *Exp. Eye Res.* **72**, 631–641 (2001).

33. Jester,J.V., Huang,J., Petroll,W.M., & Cavanagh,H.D. TGFbeta induced myofibroblast differentiation of rabbit keratocytes requires synergistic TGFbeta, PDGF and integrin signaling. *Exp. Eye Res.* **75**, 645–657 (2002).

34. Wilson,S.E., Liu,J.J., & Mohan,R.R. Stromal-epithelial interactions in the cornea. *Prog. Retin. Eye Res.* **18**, 293–309 (1999).

35. Helena,M.C., Baerveldt,F., Kim,W.J., & Wilson,S.E. Keratocyte apoptosis after corneal surgery. *Invest Ophthalmol. Vis. Sci.* **39**, 276–283 (1998).

36. Wilson,S.E. *et al.* The wound healing response after laser in situ keratomileusis and photorefractive keratectomy: elusive control of biological variability and effect on custom laser vision correction. *Arch. Ophthalmol.* **119**, 889–896 (2001).

37. Netto,M.V. *et al.* Wound healing in the cornea: a review of refractive surgery complications and new prospects for therapy. *Cornea* **24**, 509–522 (2005).

38. Fini,M.E. Keratocyte and fibroblast phenotypes in the repairing cornea. *Prog. Retin. Eye Res.* **18**, 529–551 (1999).

39. Gan,L., Hamberg-Nystrom,H., Fagerholm,P., & Van,S.G. Cellular proliferation and leukocyte infiltration in the rabbit cornea after photorefractive keratectomy. *Acta Ophthalmol. Scand.* **79**, 488–492 (2001).

40. Andresen,J.L. & Ehlers,N. Chemotaxis of human keratocytes is increased by platelet-derived growth factor-BB, epidermal growth factor, transforming growth factor-alpha, acidic fibroblast growth factor, insulin-like growth factor-I, and transforming growth factor-beta. *Curr. Eye Res.* **17**, 79–87 (1998).

41. Denk,P.O. & Knorr,M. The in vitro effect of platelet-derived growth factor isoforms on the proliferation of bovine corneal stromal fibroblasts depends on cell density. *Graefes Arch. Clin. Exp. Ophthalmol.* **235**, 530–534 (1997).

42. Musselmann,K., Kane,B.P., & Hassell,J.R. Isolation of a putative keratocyte activating factor from the corneal stroma. *Exp. Eye Res.* **77**, 273–279 (2003).

43. Wilson,S.E. *et al.* The wound healing response after laser in situ keratomileusis and photorefractive keratectomy: elusive control of biological variability and effect on custom laser vision correction. *Arch. Ophthalmol.* **119**, 889–896 (2001).

44. Woessner,J.F., Jr. Matrix metalloproteinases and their inhibitors in connective tissue remodeling. *FASEB J.* **5**, 2145–2154 (1991).

45. McVicker,B.L. *et al.* The effect of ethanol on asialoglycoprotein receptor-mediated phagocytosis of apoptotic cells by rat hepatocytes. *Hepatology* **36**, 1478–1487 (2002).

46. Desmouliere,A., Geinoz,A., Gabbiani,F., & Gabbiani,G. Transforming growth factor-beta 1 induces alpha-smooth muscle actin expression in granulation tissue myofibroblasts and in quiescent and growing cultured fibroblasts. *J. Cell Biol.* **122**, 103–111 (1993).

47. Jester,J.V., Barry,L.P., Cavanagh,H.D., & Petroll,W.M. Induction of alpha-smooth muscle actin expression and myofibroblast transformation in cultured corneal keratocytes. *Cornea* **15**, 505–516 (1996).

48. Chintala,S.K. *et al.* Matrix metalloproteinase gelatinase B (MMP-9) is associated with leaking glaucoma filtering blebs. *Exp. Eye Res.* **81**, 429–436 (2005).

49. Moller-Pedersen,T., Li,H.F., Petroll,W.M., Cavanagh,H.D., & Jester,J.V. Confocal microscopic characterization of wound repair after photorefractive keratectomy. *Invest Ophthalmol. Vis. Sci.* **39**, 487–501 (1998).

50. Jester,J.V. *et al.* The cellular basis of corneal transparency: evidence for 'corneal crystallins'. *J. Cell Sci.* **112 (Pt 5)**, 613-622 (1999).

51. Moller-Pedersen,T. Keratocyte reflectivity and corneal haze. *Exp. Eye Res.* **78**, 553–560 (2004).

52. Ivarsen,A., Laurberg,T., & Moller-Pedersen,T. Characterisation of corneal fibrotic wound repair at the LASIK flap margin. *Br. J. Ophthalmol.* **87**, 1272–1278 (2003).

53. Piatigorsky,J. Review: A case for corneal crystallins. *J. Ocul. Pharmacol. Ther.* **16**, 173–180 (2000).

54. Annes,J.P., Munger,J.S., & Rifkin,D.B. Making sense of latent TGFbeta activation. *J. Cell Sci.* **116**, 217–224 (2003).

55. Taipale,J., Miyazono,K., Heldin,C.H., & Keski-Oja,J. Latent transforming growth factor-beta 1 associates to fibroblast extracellular matrix via latent TGF-beta binding protein. *J. Cell Biol.* **124**, 171–181 (1994).

56. Schultz-Cherry,S. & Murphy-Ullrich,J.E. Thrombospondin causes activation of latent transforming growth factor-beta secreted by endothelial cells by a novel mechanism. *J. Cell Biol.* **122**, 923–932 (1993).

57. Lyons,R.M., Keski-Oja,J., & Moses,H.L. Proteolytic activation of latent transforming growth factor-beta from fibroblast-conditioned medium. *J. Cell Biol.* **106**, 1659–1665 (1988).

58. Prud'homme,G.J. Pathobiology of transforming growth factor beta in cancer, fibrosis and immunologic disease, and therapeutic considerations. *Lab Invest* **87**, 1077–1091 (2007).

59. Wahl,S.M. *et al.* Transforming growth factor type beta induces monocyte chemotaxis and growth factor production. *Proc. Natl. Acad. Sci. U. S. A* **84**, 5788–5792 (1987).

60. Reibman,J. *et al.* Transforming growth factor beta 1, a potent chemoattractant for human neutrophils, bypasses classic signal-transduction pathways. *Proc. Natl. Acad. Sci. U. S. A* **88**, 6805–6809 (1991).

61. Shull,M.M. *et al.* Targeted disruption of the mouse transforming growth factor-beta 1 gene results in multifocal inflammatory disease. *Nature* **359**, 693–699 (1992).

62. Kulkarni,A.B. & Karlsson,S. Transforming growth factor-beta 1 knockout mice. A mutation in one cytokine gene causes a dramatic inflammatory disease. *Am. J. Pathol.* **143**, 3–9 (1993).

63. Ma,D.H. *et al.* In vitro antiangiogenic activity in ex vivo expanded human limbocorneal epithelial cells cultivated on human amniotic membrane. *Invest Ophthalmol. Vis. Sci.* **45**, 2586–2595 (2004).

64. Wakefield,L.M. & Roberts,A.B. TGF-beta signaling: positive and negative effects on tumorigenesis. *Curr. Opin. Genet. Dev.* **12**, 22–29 (2002).

65. Galliher,A.J., Neil,J.R., & Schiemann,W.P. Role of transforming growth factor-beta in cancer progression. *Future. Oncol.* **2**, 743–763 (2006).

66. Glick,A.B., Weinberg,W.C., Wu,I.H., Quan,W., & Yuspa,S.H. Transforming growth factor beta 1 suppresses genomic instability independent of a G1 arrest, p53, and Rb. *Cancer Res.* **56**, 3645–3650 (1996).

67. Yang,X. *et al.* Synergistic activation of functional estrogen receptor (ER)-alpha by DNA methyltransferase and histone deacetylase inhibition in human ER-alpha-negative breast cancer cells. *Cancer Res.* **61**, 7025–7029 (2001).

68. Zavahir,F. *et al.* A study of the cellular response to orientated fibronectin material in healing extensor rat tendon. *J. Mater. Sci. Mater. Med.* **12**, 1005–1011 (2001).

69. Han,G. *et al.* Distinct mechanisms of TGF-beta1-mediated epithelial-to-mesenchymal transition and metastasis during skin carcinogenesis. *J. Clin. Invest* **115**, 1714–1723 (2005).

70. Oft,M., Heider,K.H., & Beug,H. TGFbeta signaling is necessary for carcinoma cell invasiveness and metastasis. *Curr. Biol.* **8**, 1243–1252 (1998).

71. Benckert,C. *et al.* Transforming growth factor beta 1 stimulates vascular endothelial growth factor gene transcription in human cholangiocellular carcinoma cells. *Cancer Res.* **63**, 1083–1092 (2003).

72. Postlethwaite,A.E., Keski,O.J., Mosses,H.L., & Kang,A.H. Stimulation of the chemotactic migration of human fibroblasts by transforming growth factor β. *J Exper Medicine* **165**, 251–256 (1987).

73. Assoian,R.K., Frolik,C.A., Roberts,A.B., Miller,D.M., & Sporn,M.B. Transforming growth factor-beta controls receptor levels for epidermal growth factor in NRK fibroblasts. *Cell* **36**, 35–41 (1984).

74. Leof,E.B. *et al.* Induction of c-sis mRNA and activity similar to platelet-derived growth factor by transforming growth factor beta: a proposed model for indirect mitogenesis involving autocrine activity. *Proc Natl Acad Sci* **83**, 2453–2457. (1986).

75. Soma,Y. & Grotendorst,G.R. TGF-beta stimulates primary human skin fibroblast DNA synthesis via an autocrine production of PDGF-related peptides. *J. Cell Physiol* **140**, 246–253 (1989).

76. Ishikawa,O., LeRoy,E.C., & Trojanowska,M. Mitogenic effect of transforming growth factor beta 1 on human fibroblasts involves the induction of platelet-derived growth factor alpha receptors. *J. Cell Physiol* **145**, 181–186 (1990).

77. Battegay,E.J., Raines,E.W., Seifert,R.A., Bowen-Pope,D.F., & Ross,R. TGF-beta induces bimodal proliferation of connective tissue cells via complex control of an autocrine PDGF loop. *Cell* **63**, 515–524 (1990).

78. Ignotz,R.A. & Massague,J. Transforming Growth Factor-b Stimulates the Expression of Fibronectin and Collagen and Their Incorporation Into the Extracellular Matrix. *Journal Biological Chemistry* **261**, 4337–4345. (1986).

79. Raghow,R., Postethwaite,A.E., Keski-Oja,S., Moses,H.L., & Kang,A.H. Transforming growth factor-beta increases levels of type I procollagen and fibronectin messenger RNAs posttranscriptionally in cultured human dermal fibroblasts. *J Clin Invest* **79**, 1285–1289. (1987).

80. Roberts,A.B. *et al.* Transforming growth factor type beta: rapid induction of fibrosis and angiogenesis in vivo and stimulation of collagen formation in vitro. *Proc. Natl. Acad. Sci. U. S. A* **83**, 4167–4171 (1986).

81. Varga,J. & Jimenez,S.A. Stimulation of normal human fibroblast collagen production and processing by transforming growth factor-beta. *Biochem. Biophys. Res. Commun.* **138**, 974–980 (1986).

82. Penttinen,R.P., Kobayashi,S., & Bornstein,P. Transforming growth factor beta increases mRNA for matrix proteins both in the presence and in the absence of changes in mRNA stability. *Proc. Natl. Acad. Sci. U. S. A* **85**, 1105–1108 (1988).

83. Laiho,M., Saksela,O., Andreasen,P.A., & Keski Oja,J. Enhanced production and extracellular deposition of the endothelial-type plasminogen activator inhibitor in cultured human lung fibroblasts by transforming growth factor-beta. *J Cell Biol.* **103**, 2403–2410 (1986).

84. Lund,L.R. *et al.* Transforming growth factor-beta is a strong and fast acting positive regulator of the level of type-1 plasminogen activator inhibitor mRNA in WI-38 human lung fibroblasts. *EMBO J.* **6**, 1281–1286 (1987).

85. Kerr,L.D., Olashaw,N.E., & Matrisian,L.M. Transforming growth factor beta 1 and cAMP inhibit transcription of epidermal growth factor- and oncogene-induced transin RNA. *J Biol. Chem.* **263**, 16999–17005 (1988).

86. Werner,S. & Grose,R. Regulation of wound healing by growth factors and cytokines. *Physiol Rev.* **83**, 835–870 (2003).

87. Vesaluoma,M., Teppo,A.M., Gronhagen-Riska,C., & Tervo,T. Release of TGF-beta 1 and VEGF in tears following photorefractive keratectomy. *Curr. Eye Res.* **16**, 19–25 (1997).

88. Yoshino,K., Garg,R., Monroy,D., Ji,Z., & Pflugfelder,S.C. Production and secretion of TGF-B by the human lacrimal gland. *Curr. Eye Res.*615–624 (1996).

89. Chen,C. *et al.* Measurement of mRNAs for TGFbeta and extracellular matrix proteins in corneas of rats after PRK. *Invest Ophthalmol. Vis. Sci.* **41**, 4108–4116 (2000).

90. Mi,S. *et al.* Adhesion of laser in situ keratomileusis-like flaps in the cornea: Effects of crosslinking, stromal fibroblasts, and cytokine treatment. *J. Cataract Refract. Surg.* **37**, 166–172 (2011).

91. Wang,L. *et al.* Concentration-dependent effects of transforming growth factor beta1 on corneal wound healing. *Mol. Vis.* **17**, 2835–2846 (2011).

92. Jester,J.V., Barry-Lane,P.A., Petroll,W.M., Olsen,D.R., & Cavanagh,H.D. Inhibition of corneal fibrosis by topical application of blocking antibodies to TGF beta in the rabbit. *Cornea* **16**, 177–187 (1997).

93. Chen,Y., Segarini,P., Raoufi,F., Bradham,D., & Leask,A. Connective tissue growth factor is secreted through the Golgi and is degraded in the endosome. *Exp. Cell Res.* **271**, 109–117 (2001).

94. Abreu,J.G., Ketpura,N.I., Reversade,B., & De Robertis,E.M. Connective-tissue growth factor (CTGF) modulates cell signalling by BMP and TGF-beta. *Nat. Cell Biol.* **4**, 599–604 (2002).

95. Bork,P. The modular architecture of a new family of growth regulators related to connective tissue growth factor. *FEBS Lett.* **327**, 125–130 (1993).

96. Murray-Rust,J. *et al.* Topological similarities in TGF-beta 2, PDGF-BB and NGF define a superfamily of polypeptide growth factors. *Structure.* **1**, 153–159 (1993).

97. Moussad,E.E. & Brigstock,D.R. Connective tissue growth factor: What's in a name? *Mol. Genet. Metab* **71**, 276–292 (2000).

98. Leask,A. & Abraham,D.J. TGF-beta signaling and the fibrotic response *FASEB J.* **18**, 816–827 (2004).

99. Moussad,E.E. & Brigstock,D.R. Connective tissue growth factor: What's in a name? *Mol. Genet. Metab* **71**, 276–292 (2000).

100. Grotendorst,G.R., Okochi,H., & Hayashi,N. A novel transforming growth factor beta response element controls the expression of the connective tissue growth factor gene. *Cell Growth Differ.* **7**, 469–480 (1996).

101. Xin,L.W., Martinerie,C., Zumkeller,W., Westphal,M., & Perbal,B. Differential expression of novH and CTGF in human glioma cell lines. *Clin. Mol. Pathol.* **49**, M91–M97 (1996).

102. Brunner,A., Chinn,J., Neubauer,M., & Purchio,A.F. Identification of a gene family regulated by transforming growth factor- beta. *DNA Cell Biol.* **10**, 293–300 (1991).

103. Querfeld,C., Sollberg,S., Huerkamp,C., Eckes,B., & Krieg,T. Pseudoscleroderma associated with lung cancer: correlation of collagen type I and connective tissue growth factor gene expression. *Br. J. Dermatol.* **142**, 1228–1233 (2000).

104. Blalock,T.D. *et al.* Connective Tissue Growth Factor Expression and Action in Human Corneal Fibroblast Cultures and in Rat Corneas following Phototherapeutic Keratectomy. *Invest Ophtahlmol Vis Sci* .1879–1887 (2003).

105. Grotendorst,G.R. Connective tissue growth factor: a mediator of TGF-beta action on fibroblasts. *Cytokine Growth Factor Rev.* **8**, 171–179 (1997).

106. Lau,L.F. & Lam,S.C. The CCN family of angiogenic regulators: the integrin connection. *Exp. Cell Res.* **248**, 44–57 (1999).

107. Ayer-Lelievre,C. *et al.* Report and abstracts on the first international workshop on the CCN family of genes. *Mol. Pathol.* **54**, 105–120 (2001).

108. Perbal,B. NOV (nephroblastoma overexpressed) and the CCN family of genes: structural and functional issues. *Mol. Pathol.* **54**, 57–79 (2001).

109. Bradham,D.M., Igarashi,A., Potter,R.L., & Grotendorst,G.R. Connective tissue growth factor: a cysteine-rich mitogen secreted by human vascular endothelial cells is related to the SRC-induced immediate early gene product CEF-10. *J. Cell Biol.* **114**, 1285–1294 (1991).

110. Ryseck,R.P., Macdonald-Bravo,H., Mattei,M.G., & Bravo,R. Structure, mapping, and expression of fisp-12, a growth factor- inducible gene encoding a secreted cysteine-rich protein. *Cell Growth Differ.* **2**, 225–233 (1991).

111. Frazier,K., Williams,S., Kothapalli,D., Klapper,H., & Grotendorst,G.R. Stimulation of fibroblast cell growth, matrix production, and granulation tissue formation by connective tissue growth factor. *J. Invest Dermatol.* **107**, 404–411 (1996).

112. Hook,V. *et al.* Proteases for processing proneuropeptides into peptide neurotransmitters and hormones. *Annu. Rev. Pharmacol. Toxicol.* **48**, 393–423 (2008).

113. Yamamoto,Y. *et al.* Possible roles of CTGF/Hcs24 in the initiation and development of ossification of the posterior longitudinal ligament. *Spine (Phila Pa 1976.)* **27**, 1852–1857 (2002).

114. Friedrichsen,S. *et al.* CTGF expression during mouse embryonic development. *Cell Tissue Res.* **312**, 175–188 (2003).

115. Surveyor,G.A., Wilson,A.K., & Brigstock,D.R. Localization of connective tissue growth factor during the period of embryo implantation in the mouse. *Biol. Reprod.* **59**, 1207–1213 (1998).

116. Slee,R.B. *et al.* Differentiation-dependent expression of connective tissue growth factor and lysyl oxidase messenger ribonucleic acids in rat granulosa cells. *Endocrinology* **142**, 1082–1089 (2001).

117. Leask,A., Holmes,A., Black,C.M., & Abraham,D.J. Connective tissue growth factor gene regulation. Requirements for its induction by transforming growth factor-beta 2 in fibroblasts. *J. Biol. Chem.* **278**, 13008–13015 (2003).

118. Ivkovic,S. *et al.* Connective tissue growth factor coordinates chondrogenesis and angiogenesis during skeletal development. *Development* **130**, 2779–2791 (2003).

119. Igarashi,A., Okochi,H., Bradham,D.M., & Grotendorst,G.R. Regulation of connective tissue growth factor gene expression in human skin fibroblasts and during wound repair. *Mol. Biol. Cell* **4**, 637–645 (1993).

120. Brigstock,D.R. *et al.* Purification and characterization of novel heparin-binding growth factors in uterine secretory fluids. Identification as heparin-regulated Mr 10,000 forms of connective tissue growth factor. *J. Biol. Chem.* **272**, 20275–20282 (1997).

121. Ball,D.K. *et al.* Characterization of 16- to 20-kilodalton (kDa) connective tissue growth factors (CTGFs) and demonstration of proteolytic activity for 38-kDa CTGF in pig uterine luminal flushings [published erratum appears in Biol Reprod 1998 Dec;59(6):1554]. *Biol. Reprod.* **59**, 828–835 (1998).

122. Denham,W. *et al.* Transient human gene therapy: a novel cytokine regulatory strategy for experimental pancreatitis. *Ann. Surg.* **227**, 812–820 (1998).

123. Boes,M. *et al.* Connective tissue growth factor (IGFBP-rP2) expression and regulation in cultured bovine endothelial cells. *Endocrinology* **140**, 1575–1580 (1999).

124. Nishida,T. *et al.* Demonstration of receptors specific for connective tissue growth factor on a human chondrocytic cell line (HCS-2/8). *Biochem. Biophys. Res. Commun.* **247**, 905–909 (1998).

125. Steffen,C.L. *et al.* Characterization of cell-associated and soluble forms of connective tissue growth factor (CTGF) produced by fibroblast cells in vitro. *Growth Factors* **15**, 199–213 (1998).

126. Tall,E.G., Bernstein,A.M., Oliver,N., Gray,J.L., & Masur,S.K. TGF-{beta}-stimulated CTGF Production is Enhanced by Collagen and Associated with Biogenesis of a Novel 31 kDa CTGF Form in Human Corneal Fibroblasts. *Invest Ophthalmol. Vis. Sci,.*5002–5011 (2010).

127. Hashimoto,G. *et al.* Matrix metalloproteinases cleave connective tissue growth factor and reactivate angiogenic activity of vascular endothelial growth factor 165. *J. Biol. Chem.* **277**, 36288–36295 (2002).

128. Guillon-Munos,A. *et al.* Kallikrein-related peptidase 12 hydrolyzes matricellular proteins of the CCN family and modifies interactions of CCN1 and CCN5 with growth factors. *J. Biol. Chem.* **286**, 25505–25518 (2011).

129. Grotendorst,G.R. & Duncan,M.R. Individual domains of connective tissue growth factor regulate fibroblast proliferation and myofibroblast differentiation. *FASEB J.* **19**, 729–738 (2005).

130. Dziadzio,M. *et al.* N-terminal connective tissue growth factor is a marker of the fibrotic phenotype in scleroderma. *QJM.* **98**, 485–492 (2005).

131. Gartry,D.S., Muir,M.G., Lohmann,C.P., & Marshall,J. The effect of topical corticosteroids on refractive outcome and corneal haze after photorefractive keratectomy. A prospective, randomized, double-blind trial. *Arch. Ophthalmol.* **110**, 944–952 (1992).

132. Majmudar,P.A. *et al.* Topical mitomycin-C for subepithelial fibrosis after refractive corneal surgery. *Ophthalmology* **107**, 89–94 (2000).

133. Raviv,T., Majmudar,P.A., Dennis,R.F., & Epstein,R.J. Mytomycin-C for post–PRK corneal haze. *J. Cataract Refract. Surg.* **26**, 1105–1106 (2000).

134. Dougherty,P.J., Hardten,D.R., & Lindstrom,R.L. Corneoscleral melt after pterygium surgery using a single intraoperative application of mitomycin-C. *Cornea* **15**, 537–540 (1996).

135. Netto,M.V. *et al.* Effect of prophylactic and therapeutic mitomycin C on corneal apoptosis, cellular proliferation, haze, and long-term keratocyte density in rabbits. *J. Refract. Surg.* **22**, 562–574 (2006).

136. Nassiri,N., Farahangiz,S., Rahnavardi,M., Rahmani,L., & Nassiri,N. Corneal endothelial cell injury induced by mitomycin-C in photorefractive keratectomy: nonrandomized controlled trial. *J. Cataract Refract. Surg.* **34**, 902–908 (2008).

137. Paterson,B.M., Roberts,B.E., & Kuff,E.L. Structural gene identification and mapping by DNA-mRNA hybrid-arrested cell-free translation. *Proc. Natl. Acad. Sci. U. S. A* **74**, 4370–4374 (1977).

138. Fire,A. *et al.* Potent and specific genetic interference by double-stranded RNA in Caenorhabditis elegans. *Nature* **391**, 806–811 (1998).

139. Bagasra,O. & Prilliman,K.R. RNA interference: the molecular immune system. *J. Mol. Histol.* **35**, 545–553 (2004).

140. Leuschner,P.J., Ameres,S.L., Kueng,S., & Martinez,J. Cleavage of the siRNA passenger strand during RISC assembly in human cells. *EMBO Rep.* **7**, 314–320 (2006).

141. Scherer,L.J. & Rossi,J.J. Approaches for the sequence-specific knockdown of mRNA. *Nat. Biotechnol.* **21**, 1457–1465 (2003).

142. Tiemann,K. & Rossi,J.J. RNAi-based therapeutics-current status, challenges and prospects. *EMBO Mol. Med.* **1**, 142–151 (2009).

143. Ruffner,D.E., Stormo,G.D., & Uhlenbeck,O.C. Sequence requirements of the hammerhead RNA self-cleavage reaction. *Biochemistry* **29**, 10695–10702 (1990).

144. Symons,R.H. Small catalytic RNAs. *Annu. Rev. Biochem.* **61**, 641–671 (1992).

145. Xu,R. *et al.* Activity identification of chimeric anti-caspase-3 mRNA hammerhead ribozyme in vitro and in vivo. *Sci. China C. Life Sci.* **44**, 618–627 (2001).

146. Lewin,A.S. & Hauswirth,W.W. Ribozyme gene therapy: applications for molecular medicine. *Trends Mol. Med.* **7**, 221–228 (2001).

147. Steitz,T.A. & Steitz,J.A. A general two-metal-ion mechanism for catalytic RNA. *Proc. Natl. Acad. Sci. U. S. A* **90**, 6498–6502 (1993).

148. Popescu,F.D. New asthma drugs acting on gene expression. *J. Cell Mol. Med.* **7**, 475–486 (2003).

149. Peracchi,A. Prospects for antiviral ribozymes and deoxyribozymes. *Rev. Med. Virol.* **14**, 47–64 (2004).

150. Amado,R.G. *et al.* Anti-human immunodeficiency virus hematopoietic progenitor cell-delivered ribozyme in a phase I study: myeloid and lymphoid reconstitution in human immunodeficiency virus type-1-infected patients. *Hum. Gene Ther.* **15**, 251–262 (2004).

151. MacPherson,J.L. *et al.* Long-term survival and concomitant gene expression of ribozyme-transduced CD4+ T-lymphocytes in HIV-infected patients. *J. Gene Med.* **7**, 552–564 (2005).

152. Michienzi,A. *et al.* RNA-mediated inhibition of HIV in a gene therapy setting. *Ann. N. Y. Acad. Sci.* **1002**, 63–71 (2003).

153. Wong-Staal,F., Poeschla,E.M., & Looney,D.J. A controlled, Phase 1 clinical trial to evaluate the safety and effects in HIV-1 infected humans of autologous lymphocytes transduced with a ribozyme that cleaves HIV-1 RNA. *Hum. Gene Ther.* **9**, 2407–2425 (1998).

154. Burnett,J.C. *et al.* Combinatorial latency reactivation for HIV-1 subtypes and variants. *J. Virol.* **84**, 5958–5974 (2010).

155. Tafech,A., Bassett,T., Sparanese,D., & Lee,C.H. Destroying RNA as a therapeutic approach. *Curr. Med. Chem.* **13**, 863–881 (2006).

156. Beigelman,L. *et al.* Chemical modification of hammerhead ribozymes. Catalytic activity and nuclease resistance. *J. Biol. Chem.* **270**, 25702–25708 (1995).

157. Han,J. *et al.* Molecular basis for the recognition of primary microRNAs by the Drosha-DGCR8 complex. *Cell* **125**, 887–901 (2006).

158. Kim,H.H. *et al.* Photoprotective and anti-skin-aging effects of eicosapentaenoic acid in human skin in vivo. *J. Lipid Res.* **47**, 921–930 (2006).

159. Millington-Ward,S. *et al.* A mutation-independent therapeutic strategem for osteogenesis imperfecta. *Antisense Nucleic Acid Drug Dev.* **9**, 537–542 (1999).

160. Berns,K.I. & Giraud,C. Biology of adeno-associated virus. *Curr. Top. Microbiol. Immunol.* **218**, 1–23 (1996).

161. Lu,Y. Recombinant adeno-associated virus as delivery vector for gene therapy–-a review. *Stem Cells Dev.* **13**, 133–145 (2004).

162. Sonntag,F., Schmidt,K., & Kleinschmidt,J.A. A viral assembly factor promotes AAV2 capsid formation in the nucleolus. *Proc. Natl. Acad. Sci. U. S. A* **107**, 10220–10225 (2010).

163. Qing,K. *et al.* Human fibroblast growth factor receptor 1 is a co-receptor for infection by adeno-associated virus 2. *Nat. Med.* **5**, 71–77 (1999).

164. Summerford,C. & Samulski,R.J. Membrane-associated heparan sulfate proteoglycan is a receptor for adeno-associated virus type 2 virions. *J. Virol.* **72**, 1438–1445 (1998).

165. Zolotukhin,S. *et al.* Recombinant adeno-associated virus purification using novel methods improves infectious titer and yield. *Gene Ther.* **6**, 973–985 (1999).

166. Bartlett,J.S., Wilcher,R., & Samulski,R.J. Infectious entry pathway of adeno-associated virus and adeno-associated virus vectors. *J. Virol.* **74**, 2777–2785 (2000).

167. Douar,A.M., Poulard,K., Stockholm,D., & Danos,O. Intracellular trafficking of adeno-associated virus vectors: routing to the late endosomal compartment and proteasome degradation. *J. Virol.* **75**, 1824–1833 (2001).

168. Li,J., Samulski,R.J., & Xiao,X. Role for highly regulated rep gene expression in adeno-associated virus vector production. *J. Virol.* **71**, 5236–5243 (1997).

169. Monahan,P.E. *et al.* Direct intramuscular injection with recombinant AAV vectors results in sustained expression in a dog model of hemophilia. *Gene Ther.* **5**, 40–49 (1998).

170. Mohan,R.R., Schultz,G.S., Hong,J.W., Mohan,R.R., & Wilson,S.E. Gene transfer into rabbit keratocytes using AAV and lipid-mediated plasmid DNA vectors with a lamellar flap for stromal access. *Exp. Eye Res.* **76**, 373–383 (2003).

171. Liu,J. *et al.* Different tropism of adenoviruses and adeno-associated viruses to corneal cells: implications for corneal gene therapy. *Mol Vis* **14**, 2087–2096 (2008).

172. McCarty,D.M. *et al.* Adeno-associated virus terminal repeat (TR) mutant generates self-complementary vectors to overcome the rate-limiting step to transduction in vivo. *Gene Ther.* **10**, 2112–2118 (2003).

173. Kong,F. *et al.* Self-complementary AAV5 vector facilitates quicker transgene expression in photoreceptor and retinal pigment epithelial cells of normal mouse. *Exp. Eye Res.* **90**, 546–554 (2010).

174. Natkunarajah,M. *et al.* Assessment of ocular transduction using single-stranded and self-complementary recombinant adeno-associated virus serotype 2/8. *Gene Ther.* **15**, 463–467 (2008).

175. Tafech,A., Bassett,T., Sparanese,D., & Lee,C.H. Destroying RNA as a therapeutic approach. *Curr. Med. Chem.* **13**, 863–881 (2006).

176. Woost,P.G., Jumblatt,M.M., Eiferman,R.A., & Schultz,G.S. Growth factors and corneal endothelial cells: I. Stimulation of bovine corneal endothelial cell DNA synthesis by defined growth factors. *Cornea*. **11**, 1–10. (1992).

177. Robinson,P.M., Blalock,T.D., Yuan,R., Lewin,A.S., & Schultz,G.S. Hammerhead ribozyme-mediated knockdown of mRNA for fibrotic growth factors: transforming growth factor-beta 1 and connective tissue growth factor. *Methods Mol. Biol.* **820**, 117–132 (2012).

178. National Research Council Committee. *Guide for the care and use of laboratory animals*. **8**.1–246, (2011)..

179. Border,W.A. *et al.* Natural inhibitor of transforming growth factor-beta protects against scarring in experimental kidney disease. *Nature* **360**, 361–364 (1992).

180. Border,W.A. & Noble,N.A. Transforming growth factor beta in tissue fibrosis. *N. Engl. J. Med.* **331**, 1286–1292 (1994).

181. Ball,D.K., Rachfal,A.W., Kemper,S.A., & Brigstock,D.R. The heparin-binding 10 kDa fragment of connective tissue growth factor (CTGF) containing module 4 alone stimulates cell adhesion. *J. Endocrinol.* **176**, R1–R7 (2003).

182. Sharma,A., Bettis,D.I., Cowden,J.W., & Mohan,R.R. Localization of angiotensin converting enzyme in rabbit cornea and its role in controlling corneal angiogenesis in vivo. *Mol. Vis.* **16**, 720–728 (2010).

183. Zeeuwen,P.L. *et al.* The cystatin M/E-cathepsin L balance is essential for tissue homeostasis in epidermis, hair follicles, and cornea. *FASEB J.* **24**, 3744–3755 (2010).

184. Reim,M., Bahrke,C., Kuckelkorn,R., & Kuwert,T. Investigation of enzyme activities in severe burns of the anterior eye segment. *Graefes Arch. Clin. Exp. Ophthalmol.* **231**, 308–312 (1993).

185. Lee,E.H. & Joo,C.K. Role of transforming growth factor-beta in transdifferentiation and fibrosis of lens epithelial cells. *Invest Ophthalmol. Vis. Sci.* **40**, 2025–2032 (1999).

186. Perbal,B. Alternative splicing of CCN mRNAs .... it has been upon us. *J. Cell Commun. Signal.* **3**, 153–157 (2009).

187. Harding,P.A., Surveyor,G.A., & Brigstock,D.R. Characterization of pig connective tissue growth factor (CTGF) cDNA, mRNA and protein from uterine tissue. *DNA Seq.* **8**, 385–390 (1998).

188. Uhlenbeck,O.C. A small catalytic oligoribonucleotide. *Nature* **328**, 596–600 (1987).

189. Natkunarajah,J., Osborne,V., & Holden,C. Allergic contact dermatitis to iodopropynyl butylcarbamate found in a cosmetic cleansing wipe. *Contact Dermatitis* **58**, 316–317 (2008).

190. Blalock,T.D., Yuan,R., Lewin,A.S., & Schultz,G.S. Hammerhead ribozyme targeting connective tissue growth factor mRNA blocks transforming growth factor-beta mediated cell proliferation. *Exp. Eye Res.* **78**, 1127–1136 (2004).

191. Sugioka,K. *et al.* Connective tissue growth factor cooperates with fibronectin in enhancing attachment and migration of corneal epithelial cells. *Tohoku J. Exp. Med.* **222**, 45–50 (2010).

192. Liu,J. *et al.* Different tropism of adenoviruses and adeno-associated viruses to corneal cells: implications for corneal gene therapy. *Mol. Vis.* **14**, 2087–2096 (2008).

BIOGRAPHICAL SKETCH

Paulette was born to Paul and Jacqueline Kuznia in Tampa, Florida. She went to high school at Poudre High School in Fort Collins, Colorado. Upon graduation, she chose to return to Florida for college and enrolled at the University of Florida. She majored in microbiology and cell science and obtained a minor in chemistry. After college, she was a research and development laboratory technician at Regeneration Technology Inc. in Alachua, Florida, where she gained experience in working in an industrial biotechnology laboratory. She enjoyed her work there but she was only a temporary employee and she found a more permanent position as a Quality Control Analyst at Oxthera Inc. She realized that in order to succeed in industry she needed to increase her knowledge base by continuing her education. Paulette was accepted to the University of Florida's interdisiplinary research program and began her research in corneal wound healing with her mentors, Dr. Gregory Schultz and Dr. Alfred Lewin. Paulette hopes to return to research and development in industrial biotechnology after obtaining her Ph. D.